Numerical simulation of aerodynamic plasma actuator effects

Vom Fachbereich Maschinenbau
an der Technischen Universität Darmstadt
zur Erlangung des Grades eines

Doktor-Ingenieurs
(Dr.-Ing.).

genehmigte

D i s s e r t a t i o n

vorgelegt von

Débora Gleice da Silva Del Rio Vieira, M.Sc.

aus Ilha Solteira, Brasilien

Berichterstatter:	Prof. Dr. rer. nat. M. Schäfer
Mitberichterstatter:	Prof. Dr-Ing. C. Tropea
Tag der Einreichung:	05.02.2013
Tag der mündlichen Prüfung:	23.04.2013

Darmstadt 2013
D 17

Erklärung

Hiermit versichere ich, die vorliegende Doktorarbeit unter der Betreuung von Prof. Dr. rer. nat. Michael Schäfer nur mit den angegebenen Hilfsmitteln selbständig angefertigt zu haben.

Darmstadt, den 5. Februar 2013.

to my parents Edson and Marlene

Contents

Abstract

The present work used an *in-house* code (FASTEST) for solving the incompressible Navier-Stokes equations with Finite Volume Method applied to the flow over a flat plate influenced by plasma actuators. The actuators were modeled using experimental data (from PIV) for a precise evaluation of the plasma body force and its fluid mechanic effects. This method is proven and found to have a good accuracy suitable for a quantitative analysis of the proposed test cases. Tollmien-Schlichting waves were artificially excited upstream the actuators position. The waves develop downstream of the excitation point and are amplified in certain frequency modes. The use of plasma actuators can attenuate or cancel the Tollmien-Schlichting waves. This process can be used for turbulence delay and reduction of drag coefficients in aircraft wings. Several modes of operation of the plasma actuators were tested in different arrangements and power supply. For cycle operational mode of the plasma actuator, one sensor was used a few millimeters downstream the actuator and the setup parameters are optimized with the help of an optimization algorithm. Linear Stability Analysis was also performed with the data obtained from Direct Numerical Simulations to investigate the influence of the actuator in the flow stability proprieties.

Kurzfassung

In dieser Arbeit wird ein *in-house code* (FASTEST) basierend auf der Finite-Volumen-Methode verwendet, um die inkompressiblen Navier-Stokes-Gleichungen einer Strömung über eine ebene Platte beeinflusst durch Plasma-Aktuatoren zu lösen. Die Aktuatoren wurden mit Hilfe experimenteller Daten (aus PIV Messungen) für eine präzise Auswertung der Plasma-Volumenkraft und ihrer strömungsmechanischen Effekte modelliert. Die Methode wurde überprüft und bietet eine gute Genauigkeit für eine quantitative Analyse der vorgeschlagenen Testfälle. Tollmien-Schlichting-Wellen wurden stromaufwärts der Aktuatoren künstlich angeregt. Die Wellen entstehen stromab des Anregungspunktes und werden in bestimmten Frequenzen verstärkt. Die Verwendung von Plasma-Aktuatoren kann die Tollmien-Schlichting Wellen dämpfen oder auslöschen. Dieser Prozess kann zur Verzögerung der Turbulenz und zur Verringerung des Strömungswiderstandskoeffizienten in Flugzeugtragflächen verwendet werden. Mehrere Betriebsmodi der Plasma-Aktuatoren wurden mit unterschiedlichen Anordnungen und Stromversorgungen getestet. Im amplitudenmodulierten Betriebmodus des Plasma-Aktuators wurde ein Sensor wenige Millimeter hinter dem Aktuator platziert und die Betriebsparameter wurden mit Hilfe eines Optimierungsalgorithmus optimiert. Ebenso wurde mit den Daten aus Direkten Numerischen Simulationen eine lineare Stabilitätsanalyse durchgeführt, um den Einfluss des Aktuators auf die Eigenschaften der Strömungsstabilität zu untersuchen.

Preface

The research work presented in this thesis was carried out from December 2009 to January 2013 during my time as a PhD student at the Institute of Numerical Methods applied to Mechanical Engineering (FNB) at the Technische Universität Darmstadt, Germany. This is a part of an interdisciplinary project hosted at the Graduate School of Computational Engineering (GSC CE) supported by the German Research Foundation (DFG), inside the Excellence Initiative. The experimental contribution to this work and the expertise in plasma actuator technology comes from the cluster of excellence Center of Smart Interfaces (CSI). Financial support from the CSI and GSC CE are gratefully acknowledged.

First of all, I thank God for the gift of having one more step done in my life.

I would like to thank Professor M. Schäfer for supervising my thesis, spending time in helpful discussions, giving me the opportunity to study in Germany and, also for providing a creative and scientifically stimulating atmosphere at the FNB.

I am grateful to Professor C. Tropea, the co-advisor of this work, for his support and motivation at CSI.

My special thanks to S. Grundmann, the research area coordinator at CSI, for his time and patience during very inspiring discussions about plasma actuators.

I thank Prof. S. Ulbrich from the Non-Linear Optimization group from the Mathematics department, for the contribution in the optimization part of this work.

I gratefully appreciated my time sitting at the GSC CE and I want to thank Dr. rer. pol. Markus Lazanowski, for promoting a very inspiring atmosphere for research in there. To all staff and colleagues at the Graduate School I also thank for nice moments we had and a lot of cake on Thursdays afternoon. The news letter team and the students committee are activities which I surely will miss.

Special thanks also for all colleagues and staff members of FNB for creating a high quality research and team work environment. I also thank those who persistently tried to teach me how to ski.

I thank all staff and colleagues from the Wind Channel in Griesheim, also the many office partners at the Mini-max, and the plasma actuator group for sharing their expertise with me, especially A. Duchmann and A. Kurz for our long discussions.

Thanks to J. Ghihlieri for the interdisciplinary view and friendship.

Out of the academic environment, I also would like to thank all friends I've made in Darmstadt and Fulda, my "Brazilian family in Germany", and the Grupo Jabez. I thank my family in Brazil for their comprehension and I thank Kay and his family for their unconditional support.

Débora Vieira

Darmstadt
January, 2013

1. Introduction

1.1. Motivation

Nowadays, there is a worldwide concern regarding environmental issues. Great attention of the scientific community is focused in new technologies which promise lower consumption of the natural resources or less energy expenditure, with a satisfactory performance. From the economical point of view, the need for fewer resources can be even more attractive if it is also followed by measurable cost reductions.

Particularly, the aircraft industry has reached, in the last years, significant improvement in fuel efficiency, CO_2 emission and noise reduction. Each new generation of commercial airplanes deliver about 15 % of improvement in these issues, [Gol11]. Such great progress is obtained due to a massive research effort in this direction. At the moment, for current aircraft configurations, the aerodynamics stands as the key contributor to the forthcoming designs in the near future. The big challenge to be conquered now is the development of new technologies which provide drag reduction at the airplane wings. This aim has been a great motivation for scientists all over the world.

It is well known that a laminar boundary layer provides lower skin friction when compared to a turbulent one. Therefore, drag at the airplane wing can be reduced by delaying turbulence transition by some distance downstream. In this context, the techniques developed for manipulation of the boundary layer flow receive the name of Flow Control Methods.

The use of surface Dielectric Barrier Discharge (DBD), or simple plasma actuators, for flow control is a recently proposed alternative in the scientific community. Some of the innovative and very promising methodologies which use plasma actuators present great advantages when compared to the usual flow control methods. DBD actuators have very low weight and negligible volume. They also have very short time response which enables easy control of operating parameters, such as forcing and frequency, see [Gru08].

Likewise, absence of moving parts, simple construction and easy power manipulation are other very attractive characteristics. Altogether, the plasma actuator features provide this new technology to be of a high interest in fluid dynamics applications for flow control.

1.2. State-of-the-art

The recent advances in flow manipulation techniques promoted the development of higher performance aerodynamic vehicles, turbines, and many other well known applications which involve fluid mechanical problems. With a great scientific interest and a rising popularity, flow control methods search for manners to properly modify the boundary layer flow and consequently manipulate the turbulence transition, or even flow separation.

Within this context, methods which do not need any additional energy input are called passive flow control methods. They include special techniques which apply geometrical modifications, addition of roughness or small surface dispositive for vortex generation. The experimental work in [FB05], investigated the boundary-layer stabilizing effect of moderate amplitude streaks forced by a spanwise array of roughness elements. The authors show that in the presence of those streaks, the most unstable Tollmien-Schlichting waves grow less. The stabilization effects achieved were limited by the streak amplitude, due to the limitations of the disturbance generating devices which were used. Messing and Kloker, [MK10] used Direct Numerical Simulations (DNS) to investigate the stabilizing effects of small wall orifices on a laminar boundary-layer flow. The optimization of such problems is usually based on the assumption of an ideal and homogeneous suction. But real panels with many orifices frequently give rise to local three-dimensional effects. Wassermann and Kloker, [WK02], also used passive control for crossflow-vortex induced transition in a three-dimensional flat-plate boundary-layer using DNS. A significant transition delay was shown for the use of upstream flow modification by appropriate steady nonlinear vortex modes. Although the apparent simplicity of passive methods the success of such techniques indispensably depends on a certain combination of parameters like flow velocity, flow direction, and fluid proprieties. There are only a few possibilities for re-adjustments in passive methods. Additionally, there is

not a general configuration with an optimal performance which works satisfactorily for diverse situations.

On the other hand, flow control techniques which need additional energy input to provide any modification of velocity or pressure fields are called Active Flow Control methods. Though these techniques have some operational costs, the main advantage is the possibility to modify the operational parameters and adjust them according to many distinguished flow scenarios. The use of blowing and suction actuators, also called zero-net-mass actuators, is a well known example of an active flow control technique. These actuators are able to induce certain modifications in the boundary layer velocity profile, or even to produce flow disturbances at some determined frequency and amplitude. Amitay and Glezer, [AG06], used blowing and suction actuators to control the separation region of a flow passing an airfoil. This kind of actuator has the advantage of controlling the operational parameters and the possibility to adjust them for providing a good performance according to several flow situations. Nevertheless, the main problem regarding the application of zero-net-mass actuators lies in the complicated construction of such systems on an airplane wing.

Lorentz force actuators were used by Cierpka et al. in [CWG07]. This sort of actuator has much simpler installation issues and lower weight, when compared to blowing and suction actuators. For most fluid mechanic applications, the absence of moving parts of Lorentz force actuators is a great advantage. These actuators are able to add momentum directly to the flow field, and they are used to manipulate the boundary layer in weakly conducting media, like sea water. The authors in [CWG07] also controlled the separation region with Lorentz force actuators for a periodic excitation of different wave forms. It was proven that a combination of the excitation frequency together with the amount of momentum which is added to the flow, is the most important control parameter. In [AMMGG07] the authors applied Lorentz force actuators in two and three dimensional simulations for Tollmien-Schlichting wave cancellation. Many other researchers have also used Lorentz force actuators. More examples of applications can be found in [WGMLL03], [CWG08], [Hin07], [WSG07], and [WAG11].

Dielectric Barrier Discharge (DBD) actuators provide the same advantages as Lorentz force actuators such as low weight, absence of moving parts and easy installation. But DBD actuators also provide one more benefit: they can be used in air flow. The simplicity of this variety of actuators together with the advantages of power control, are some of the very attractive characteristics which had recently motivated several

researches to apply plasma actuators for aerodynamic flow control. More details about the working principle of plasma actuators are given in Chapter 3.

In the last decades, plasma actuators have been used in different forms for a wide range of applications. Barckmann and Tropea, in [BT10], used plasma actuators in an experimental work to control the separation region of an airfoil flow at higher Mach numbers. Room and Greenblatt, in [RG10], used plasma actuators for promoting subcritical transition in a pipe flow. Huang and Zhang, [HZ08], used plasma actuators oriented in streamwise and spanwise directions for noise control in a flow-induced cavity. Sosa, Adamo and Artana, in [SAA09], used three plasma actuators to decrease drag on a flow passing a circular cylinder. The efficiency of plasma actuators applied on wind turbine blades was investigated in [NCO08]. Furthermore, the review paper [CEW10] presents a variety of possible applications for plasma actuators.

Experimental investigations using plasma actuators were done by Grundmann and Tropea [GT07] on attenuation of Tollmien-Schlichting (TS) waves in a flat plate flow with an adverse pressure gradient. They used two actuators oriented in spanwise direction which forced the flow in downstream direction. They obtained local modifications of the boundary layer with a more stable velocity profile. The authors excited artificial disturbances in the laminar boundary layer flow by using one plasma actuator operating in pulsed mode. Flow disturbances were amplified downstream leading to turbulence transition. Two steady operating actuators, positioned downstream of the excitation point were able to produce a significant damping of the disturbances, resulting in transition delay. In further research of the same authors, [GT08], the artificially excited TS waves were cancelled using one single actuator which operated in pulsed mode, reaching best results with higher efficiency. An actuator which operates in pulsed mode acts directly against the velocity fluctuations and counteract with them by superposition. The authors were able to reduce the energy required to achieve transition delay in a boundary layer flow, having very high wave attenuation rates. In comparison with the previous work of the same authors, the energy consumption for pulsed mode actuators was only about 12 %. They also investigated the influence of other parameters as force intensity and phase shift.

In [GSE10], Grundmann, Sayles and Eaton presented results for an asymmetric diffuser with plasma-actuator induced inlet condition perturbations. The authors investigated the influence of the two operational regimes for the plasma actuator: pulsed and steady, and its influences on the performance of the studied diffuser.

In [Qua09] the author presented results using optimization tools for controlling a plasma actuator and promote cancellation of Tollmien-Schlichting waves on a flat plate with an adverse pressure gradient. Due to the difficulties to evaluate the derivatives for the objective function, Quadros, in [Qua09], preferred to use methods for unconstrained optimization. The two variables submitted to the optimization process were power and phaseshift. The first algorithm used, called Nelmead method, is a pattern search that compares values of a function at three locations (vertices of a triangle). The worst vertex value is rejected and replaced with a new one, generating a sequence of triangles. The second method investigated by Quadros, is called NEWUOA and includes a quadratic model to search for the minimum value of an objective function. The values for the objective function were obtained with two sensors, positioned upstream and downstream the actuator. Results obtained with the NEWUOA method yield a significantly higher precision, due to the use of a second order approximation.

Although the large number of publications on the topic, and the wide range of applications proposed for the use of plasma actuators, the fully understanding of some fundamental questions regarding performance and efficiency of plasma actuators still could not be correctly answered. For numerical simulations, most of the current problems were usually treated by the use of *ad hoc* or empirical models, which are not satisfactorily accurate. There is an immediate need for a more accurate model in order to achieve good results for more effective flow control.

A good numerical representation of a plasma actuator only can be reached by a correct determination of the force which arises from the plasma with a precise magnitude. The force magnitude represents the quantities of momentum which are directly added to the flow field, which is the key feature of the entire procedure of turbulence control. However, some physical aspects represent difficulties in the process of force quantification or evaluation. One of the major problems arises from the fact that the gas-discharge processes occur in scales of time and space which are many orders of magnitude smaller when compared to the scales of the corresponding fluid dynamics problem. The so called phenomenological models try to bypass the huge discrepancy between the temporal and spatial scales with the use of several simplifications. As an example, one can mention the work of Jayaraman and Shy, [JS08]. Nevertheless, the large number of assumptions produced a resulting force with a non-physical shape.

The experimental research work of Kriegseis et al. [KGT11] shows a detailed investigation and quantification of the operational parameters of plasma actuators with

measurements for light emission and thrust production. In the same direction, [KMGT11] also shows a detailed investigation of the plasma actuator capacitance and power. From the analysis of the results obtained from the previous mentioned studies, Kriegseis recently proposed a new and very prominent alternative for plasma actuator body force evaluation, described in [Kri11]. Experimental data obtained with an experimental procedure called Particle Image Velocimetry (PIV) provides measurements of the velocity fields in the small area surrounding the actuators. With an accurate PIV technique, it is possible to precisely evaluate the body force magnitude, and simply apply these values to a CFD calculation.

The numerical work in [MKMJSGT11] recently verified the entire procedure proposed by [Kri11] using simulations in OpenFoam with turbulence modelling and quiescent air tests. The velocity profiles obtained from numerical simulations were compared with the velocity measurement by PIV experiments. These comparisons show a good agreement for quiescent air tests, and prove the reliability of the presented method proposed by Kriegseis.

1.3. Aims and scope

The present work represents one more step in direction to the development of new technologies for flow control. Tollmien-Schlichting (TS) waves are artificially excited and plasma actuators are used to attenuate the amplified disturbances. DNS is used to quantify the plasma actuator's influence on a flat-plate boundary-layer flow. Despite the high computational costs, DNS is chosen to provide a more accurate representation of the TS waves and the development of velocity disturbances on a boundary layer at all length scales. In addition, the correct simulation of the wave amplification phenomenon requires a fine grid resolution, inherent in DNS simulations. To perform a numerical simulation with all turbulence scales was necessary for such very detailed scientific investigation. The use of other methods for turbulence simulation such as Reynolds-Averaged Navier-Stokes equations (RANS) or Large eddy simulations (LES) was avoided to guarantee an exact representation of the forcing field. Thereby, using DNS the body force stabilizing effects can be analyzed without undesired effects arising from the approximations of a turbulence model adopted.

The main objective is to promote a quantitative study of the wave attenuation rates and the boundary-layer stability modifications promoted by different arrangements of actuators with several operational modes. Also the influence of configuration parameters shall be verified, such as the position of the actuator along the boundary layer and force magnitude. A very detailed analysis and quantification of the plasma actuator effects leads to the answer of some basic questions regarding practical applications. The answer for such questions also provides significant improvement of the boundary-layer manipulation techniques using plasma actuators.

Even though the main results presented are obtained with numerical simulations, the chosen approach utilizes an interdisciplinary method, i.e. by a combination with experimental data for modeling purposes. The overall aim of these investigations is to advance one step more inside the turbulence control techniques field and to promote the understanding of plasma actuator stabilizing effects over Tollmien-Schlichting waves.

1.4. Thesis organization

This work is organized as follows:

- Chapter 2 provides a phenomenological background of fluid dynamics, together with a description of the governing equations, and a brief explanation of the important physical parameters applied. The flow passing a boundary layer and the transition process from laminar to turbulent is shortly explained, with an emphasis given on the Tollmien-Schlichting wave transition scenario. A short review on linear stability theory, and how this is applied in this work, is also provided.
- Chapter 3 provides a description of plasma actuators and how they are used in experimental research. It is described how plasma actuators can influence the boundary layer and their advantages compared to other actuators. A description of the new model used in the simulations for numerical representation of the plasma actuator on the flow is given. Two different operational modes are considered: continuous and alternate. These both methods can influence the boundary layer flow in different ways which is also explained.
- Chapter 4 describes the numerical methods which are used, and why they were chosen. Some features of the used numerical solver are highlighted. The excitation

of disturbances is discussed, and a briefly explanation of the optimization scheme is also here provided.

- Chapter 5 provides a description of the numerical procedure including grid convergence, validation and verification tests. A description of the simulation parameters is given together with information about computational resources and simulation setup. Preparation steps for flow control simulations using plasma actuators include a coherent simulation of a flat-plate Blasius base-flow and a correct Tollmien-Schlichting wave amplification. Linear stability theory is used to compare and validate the wave growth. The effects of the plasma actuator are investigated in quiescent air and in non-disturbed flow at several free-stream velocities.
- Chapter 6 provides results for boundary layer stabilization using plasma actuators. The velocity modifications promoted by the actuators which operate in continuous mode are able to attenuate periodic velocity fluctuations by locally changing the stability proprieties of the boundary layer flow. The influence of the power supply applied to the actuator is verified at two different speeds. The influence of the actuator position is also investigated. Arrangements of several actuators are used in several combinations to promote different scenarios for control of the flow disturbances. The averaged profiles were compared with the well known case of a constant suction boundary layer. The stabilizing effect of one single actuator is verified over a multi-frequency disturbed flow.
- Chapter 7 shows results for Tollmien-Schlichting wave cancelation using one single actuator which operates in pulsed mode. The sensibility of the control parameters is verified. An optimization algorithm is used to find the best combination of parameters capable to produce the maximum wave damping. The process of active wave cancellation is compared with the boundary layer stabilization. A quantitative analysis of power consumption for both techniques is presented. The major effects found in these two approaches are combined in arrays of actuators which operate in combined mode. The performance of such arrays is compared with the results for the performance of one single actuator in diverse modes of operation.
- Chapter 8 presents the combination of active wave cancellation with boundary layer stabilization techniques to produce high efficiency results in flow disturbances attenuation. A hypothetical case, which would allow that negative

forcing is produced by the plasma actuator, is used to explain the different effects involved. Further tests use a hybrid approach for the plasma actuator operational mode. The results are compared with the linear stability theory.

- Chapter 9 finally presents the main conclusions and a brief summary of the present work. An outlook is given for future efforts inside the research field.

2. Fluid mechanics background

In the following theoretical review, the description of some important concepts is based on the renowned work of Schlichting [Sch82], which presents the fundamental concepts for fluid mechanics of boundary layer flows. The Laminar Stability Theory is briefly described. More detailed information can be found in [SH01]. Only basic concepts and fundamental aspects are described which are elementary for the comprehension of results which are presented in the following chapters.

2.1. Equations and important parameters

The unsteady flow of an incompressible Newtonian fluid can be mathematically described by the Navier-Stokes equations combined with the continuity equation:

$$\rho\left(\frac{\partial \boldsymbol{u}}{\partial t} + \boldsymbol{u}\cdot\nabla\boldsymbol{u}\right) = -\nabla p + \mu\nabla^2\boldsymbol{u} + \boldsymbol{f} \tag{2.1}$$

$$\nabla\cdot\boldsymbol{u} = 0 \tag{2.2}$$

Therein $\boldsymbol{u}$ is the velocity vector with the components u, v, and w, ρ is the fluid density, p is the pressure, μ is the fluid viscosity, and $\boldsymbol{f}$ is an external body force.

Considering a flow past, for example, a flat plate, Figure 2.1, the velocity of the fluid increases from zero at the wall (no slip), until its complete freestream value; thereby, the influence of viscosity is confined to the layer immediately close to the solid surface. This layer is the so called boundary layer.

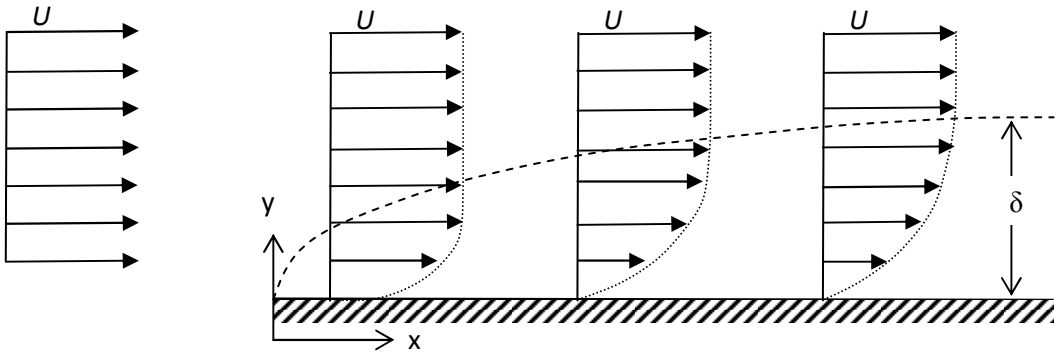

Figure 2.1: Boundary layer along a flat plate at zero incidence. U is the freestream velocity and δ is the thickness of the boundary layer.

Considering an infinitely long flat plate, where $x = 0$ on the edge, U is the freestream velocity, and pressure gradient is negligible. The fluid motion equations (2.1 and 2.2) lead to the steady boundary layer equations:

$$\frac{\partial u}{\partial x} + \frac{\partial v}{\partial y} = 0 \tag{2.3}$$

$$u\frac{\partial u}{\partial x} + v\frac{\partial v}{\partial y} = \frac{\mu}{\rho}\frac{\partial^2 u}{\partial y^2} \tag{2.4}$$

$$y = 0: \quad u = v = 0; \qquad y \to \infty: \quad u = U \tag{2.5}$$

Blasius [Bla08] discussed the previous formulation as a non-dimensional ordinary differential equation called Blasius equation. The simple evaluation of the Blasius equation provides a theoretical solution for the velocity profile of a flat plate boundary layer flow, Figure 2.2. A laminar-boundary layer with a zero pressure gradient is called *Blasius boundary layer*.

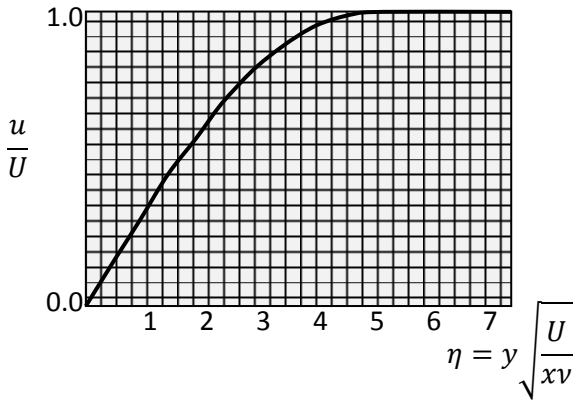

Figure 2.2: Non-dimensional boundary layer velocity profile.

Because the influence of viscosity decreases asymptotically, the value of the parallel velocity component u tends to the value of the potential flow velocity U. An estimation of the boundary layer thickness can be defined as the distance from the wall where $u = 0.99\,U$. From the Blasius solution it follows:

$$u = 0.99U: \quad \eta = 5.0 \quad , \tag{2.6}$$

$$\delta \approx \delta_{99} = 5.0\sqrt{\frac{\nu x}{U}} \quad , \tag{2.7}$$

The distance by which the external flow is displaced as a consequence of the viscous effects present in a boundary layer is called *displacement thickness*, and is defined as:

$$\delta_1 = \int_{y=0}^{\infty} \left(1 - \frac{u}{U}\right) dy. \tag{2.8}$$

Compared with the potential flow, the momentum lost inside the boundary layer can be defined as the *momentum thickness*:

$$\delta_2 = \int_{y=0}^{\infty} \frac{u}{U}\left(1 - \frac{u}{U}\right) dy \tag{2.9}$$

For a flat plate flow at zero incidence, these two quantities become:

$$\delta_1 = 1.7208\sqrt{\frac{\nu x}{U}} \tag{2.10}$$

$$\delta_2 = 0.664\sqrt{\frac{\nu x}{U}} \tag{2.11}$$

At this point, it is useful to define the Reynolds number as a function of the displacement thickness:

$$Re = \frac{U\delta_1}{\nu} \tag{2.12}$$

Using the theoretical solution, the wall shear stress τ_{wall} and the skin-friction coefficient c_f, can be estimated as follows:

$$\tau_{wall}(x) \sim \sqrt{\frac{\mu\rho U^3}{x}} \tag{2.13}$$

$$c_f = \frac{\tau_{wall}(x)}{\frac{\rho}{2}U^2} = \frac{0.664}{\sqrt{Re}}\sqrt{\frac{l}{x}} \tag{2.14}$$

where l is the length of the flat plate. The wall shear stress is inversely proportional to the boundary-layer thickness. That is, a thinner boundary layer produces a higher wall shear stress then compared to a thicker one.

The ratio between the displacement thickness and the momentum thickness is called *shape factor*:

$$H_{12} = \frac{\delta_1}{\delta_2} \tag{2.15}$$

The shape factor can be used for an estimation of the stability of a flat-plate boundary layer. Laminar boundary layers have a shape factor value around $H_{12} = 2.59$ for a zero pressure gradient. At the transition region, the shape factor value decreases. For turbulent boundary layers one has about $H_{12} = 1.4$. The presence of a pressure gradient can modify the shape factor values. Boundary layers with an adverse pressure gradient have higher shape factor values up to $H_{12} = 4.09$, which occurs right before a flow separation. On the other hand, a favorable pressure gradient produces a more stable profile, and lower shape factor values, down to $H_{12} = 2.0$. Therefore, the shape factor is a very sensitive parameter. It is also very useful to determine the flow quality and it is a good indicatory parameter for the boundary layer development.

2.2. Turbulence transition

The dynamic process which occurs when a flat plate flow changes from laminar to turbulent was already exhaustively investigated numerically and experimentally.

In the literature one can find basically two dominant scenarios for turbulence transition on a flat-plate boundary layer flow: Bypass transition and Tollmien-Schlichting wave transition.

The bypass transition is the transition induced by non-modal growth of small three-dimensional disturbances. This may happen in a high freestream turbulence environment. Small disturbances are amplified in streamwise direction in a form of characteristic

streaky structures and followed by secondary instability of streaks. The presence of an inflexion in the base flow profiles produces the breakdown of the streaks into turbulent spots [And99].

The present work is focused in the Tollmien-Schlichting wave transition scenario. The two-dimensional waves are the only flow disturbances and no freestream turbulence, surface roughness, or acoustic interference is assumed to be large enough for producing relevant influence to the whole transition process. The transition steps are illustrated in Figure 2.3.

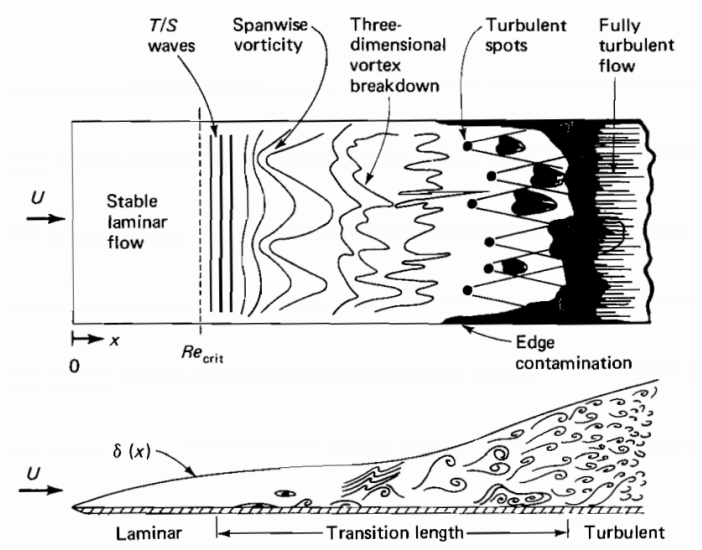

Figure 2.3: Transition to turbulence in a flat plate, [Whi74].

In this scenario, the linear growth phase of small disturbances can be observed and the transition is induced by the exponential growth of two-dimensional disturbances. The whole process is initiated at the receptivity stage. From the region near the leading edge until a certain x location, all disturbances are simply damped. This location is called point of neutral stability, and downstream of this point, some specific wave modes can be amplified, [Whi74]. The few waves which are propagated have exponentially growing amplitudes, in a two-dimensional process, until the start of a non-linear behavior. The amplified Tollmien-Schlichting waves modify the boundary-layer profile which becomes unstable giving rise to three-dimensional oblique wavelike disturbances. With higher frequencies, these oblique waves are also amplified and called Lambda-vortices. The presence of Lambda-vortices produces periodically inflectional boundary layer profiles, while small hair-pin vortices emerge at higher velocities. These vortices collapse

downstream and a periodic structure cannot be found in the flow anymore. At this point, a fully turbulent boundary-layer flow initiates.

2.3. Linear Stability Theory

The velocity component parallel to the wall of a flat plate boundary layer flow is assumed to be disturbed by a number of discrete two dimensional fluctuations of a wave which is propagated downstream. It is possible to represent one oscillation of the disturbance by the stream function:

$$\psi(x,y,t) = \varphi(y)e^{i(\alpha x-\beta t)} \tag{2.16}$$

where α represents a spatial frequency and $\lambda = 2\pi/\alpha$ is the wavelength of the disturbance. β is a complex number:

$$\beta = \beta_r + i\beta_i \tag{2.17}$$

where β_r is the circular frequency of the disturbance and β_i is the amplification factor. For $\beta_r < 0$ disturbances are damped and the mean flow remains stable, while for $\beta_r > 0$ the disturbance is amplified.

The ratio between α and β is also an important parameter:

$$c = \frac{\alpha}{\beta} = c_r + ic_i \tag{2.18}$$

Herein c_r is the wave propagation speed (or phase velocity) and c_i is another parameter to determine whether disturbances are damped or amplified.

If the mean flow is decomposed into a base flow velocity superimposed by a velocity fluctuation

$$u = U + u' \tag{2.19}$$

and

$$v = V + v' \tag{2.20}$$

using Eq. 2.16, the components of the velocity disturbances can be written as:

$$u' = \frac{\partial \psi}{\partial y} = \varphi'(y) e^{i(\alpha x - \beta t)} \tag{2.21}$$

and

$$v' = -\frac{\partial \psi}{\partial x} = -i\alpha(y)\varphi(y) e^{i(\alpha x - \beta t)} \tag{2.22}$$

The previous equations can be inserted into the Navier-Stokes equations leads to the following forth-order, differential equation for the amplitude of the disturbance:

$$(U - c)(\varphi'' - \alpha^2 \varphi) - U'\varphi = -\frac{i}{\alpha Re}(\varphi'''' - 2\alpha^2 \varphi'' + \alpha^4 \varphi) \tag{2.23}$$

also known as the *Orr-Sommerfeld equation* - the fundamental stability equation. The primes denote a differentiation with respect to the dimensionless coordinate y/δ_{99} All the other variables in the Eq. 2.32 are also set in dimensionless form.

The terms on the left side of the Orr-Sommerfeld equation are inertia terms, while the terms on the right side are the viscous terms derived from the motion equations. As boundary conditions for a boundary layer flow, the fluctuations should vanish at the wall and at the freestream:

$$y = 0: \; u' = v' = 0: \; \varphi = 0, \qquad \varphi' = 0; \tag{2.24}$$

$$y = \infty: \; u' = v' = 0: \; \varphi = 0, \qquad \varphi' = 0. \tag{2.25}$$

It was already proven by [Squ33] that a boundary layer with spanwise periodically disturbances keeps a two-dimensional pattern until higher Reynolds numbers. In this context, two-dimensional disturbances can also be used to obtain the most extended limits of flow stability.

The relation between a disturbance behavior in time and space represents a dispersion relation which can only be solved numerically. Further details can be found in [DRQKT10]. For two dimensional disturbances without spanwise modulation, the stability problem is limited to the analysis of the imaginary part of α, which is commonly called spatial growth rate. The integration of the growth rates along the x direction leads to the so called N-factor:

$$N = \ln \frac{A_{L1}}{A_{L0}} = \int_{x_{crit}}^{x} -\alpha_i dx \tag{2.26}$$

Where $A_{L1}$is the amplitude of the disturbance and A_{L0} is the initial amplitude of the disturbance at the neutral point (location where the amplification starts). For results here presented, the normalized TS wave amplitude, at the location where the plasma actuator is positioned, is also subtracted to the N factor values which are evaluated. The N factor is used in Chapters 7 and 8 to investigate the influence of a plasma actuator at diverse operational modes, according to the Tollmien-Schlichting wave amplitude.

For a boundary-layer flow with a certain periodic disturbance excited at a determinate location and frequency (such as $\beta_r > 0$), the amplitude of the disturbances increase up to a certain downstream location. Further downstream, this disturbance is damped. For a better analysis, if the disturbance frequency is systematically varied, the values found for the limit-grow rates can be illustrated in form of a diagram, or neutral stability curve [Duc12]. Such diagrams enclose the region of TS wave amplification and are used in the following chapters for investigating the influence of a plasma actuator at the stability properties of a flow. The neutral stability curve indicates the indifference of the spatial growth rate, or the situation where $\alpha_i = 0$. The inner region of the neutral stability curve is a region of amplification of flow disturbances, or unstable region, which reveals the frequency range that the boundary layer will be sensitive at a given Reynolds number.

3. Plasma Actuators

3.1. General description

Since proposed by Roth [Rot2003], the so called *One Atmosphere Uniform Glow Discharge Plasma* opened a new window of alternatives for aerodynamic flow control. In the following years, many different configurations were investigated for several applications. The present work refers to a common sort of actuator called Dielectric Barrier Discharger (DBD) Actuator, or simply Plasma Actuator. These actuators are basically composed by two electrodes which are separated by an insulating material and positioned on a plane surface. The lower electrode is covered and the upper electrode is exposed, Fig. 3.1. A high AC-voltage, from 1k V up to 50 kV, is then applied in the extremities of the electrodes with frequencies of 0.5 to 25 kHz (the AC signal is usually a sine wave). Because the voltage applied is high enough, the air barrier can be broken and plasma is then produced. The presence of a dielectric layer is important for providing the formation of a surface discharge, and not a current flow [FCG05].

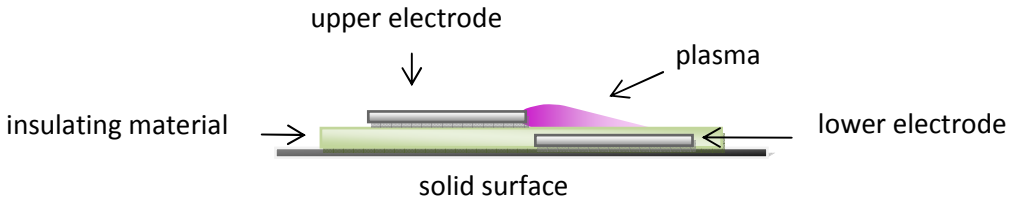

Figure 3.1: Plasma actuator schematic composition.

Plasma actuators are classified as glow dischargers, with the electron temperature about two orders higher than the ion or neutron temperatures, and a low degree of ionization, resulting in a thin volume of weakly ionized gas, [Kri11]. The accelerated molecules of ionized air collide with the neutral surrounding gas. The fundamental working principle of plasma actuators is the momentum transfer which occurs due to the

presence of plasma. This process is commonly called a plasma-actuator body force or simple actuator volume force.

However, there is no common agreement in the scientific community concerning the change of sign of the electrical field due to the operational AC voltage. Contradictory explanations suggest different directions for the momentum transfer, which would lead to opposite forces acting in the fluid field, see [Kri11]. Another critical point which promotes strong controversy is the difference of scales between the fluid flow and the gas-discharge problems. The air-flow scenario only require scales which are 4-8 orders lower than the scales which are necessary for solving the electromagnetic field equations. For this reason, some researches consider the effect of a body force produced by the plasma as a quasi-steady wall jet departing from the actuator in quiescent air conditions, [SLMOM10].

Notwithstanding the various complicated issues which belong to the scientific investigation, some advantages promoted by the use of plasma actuators are a cause for the great motivation to reach a full comprehension of the working principles of such devices. Once they are composed basically of two electrodes fixed on a flat surface, plasma actuators do not have any moving parts which could give rise to additional complications involving power consumption and response time. For that matter, the quick response time of plasma actuators allow that several operational modes can be used to counteract with different frequencies of Tollmien-Schlichting waves. Still regarding construction issues, plasma actuators have a very low weight, but the power supply used can represent a complex matter since a high range of operational parameters is required, like high voltage and different wave forms.

Some other problems can also be found when dealing with plasma actuators, like the noise production and ozone emission. Plasma actuators are also very sensitive to humidity and presence of dust, which can damaged the plasma region or even the electrodes.

3.2. Numerical representation

Since the use of plasma actuators aims at improvements of flow control, a robust quantification of its performance is necessary. A complex chain of processes is established from the input source until the final power saving energy is achieved. For quantifying the total energy loss, one should take into account the plasma generation, momentum

transfer and unusable power losses. Furthermore, the outright performance of a flow control system which uses plasma actuators must consider the type of energy source utilized, geometrical parameters of the electrodes, physical characteristics of the construction materials and environmental conditions. An accurate quantification of all previously mentioned parameters is essential for a satisfactory analysis of the plasma actuator efficiency. As a matter of fact, the magnitude of the body force created by the plasma actuator and its special distribution cannot be easily evaluated from traditional methods or even correctly estimated by the use of calibration models.

The recent work of Kriegseis [Kri11] presents a detailed investigation of the quantification of plasma actuators, light emission analysis and momentum transfer to the air flow. Among these topics, the last one is of great interest for the present work and the same approach is utilized in the numerical simulations here. Kriegseis used Particle Image Velocimetry (PIV) to investigate the momentum transfer and flow behavior in the region surrounding the plasma. The author applied a voltage from 8 up to 12 kV at a frequency of 11 kHz on the electrodes, and used two systems which operate simultaneously for measuring the electrical characteristics of the actuator and the velocity fields surrounding it.

The body force produced by a plasma actuator can be extracted from PIV measurements of the velocity field by a differential method. Considering the rearranged Navier-Stokes equation, Eq. 3.1, for steady two-dimensional flow, one can find the estimation for the plasma actuator's body force distribution, following Einstein's summation convention:

$$f_i - \frac{\partial p}{\partial x_i} = \rho u_j \frac{\partial u_i}{\partial x_j} - \mu \frac{\partial^2 u_i}{\partial x_j \partial x_j} \tag{3.1}$$

The changes of density which occur in the small plasma region are minimal and can be neglected.

The forcing terms are at least one order higher than the pressure gradient, therefore Wilke neglects in [Wil09] the small pressure changes, i.e.

$$\frac{\partial p}{\partial x_i} = 0 \tag{3.2}$$

The body force which departs from a plasma actuator can now be easily evaluated as a result of two components, in x and y direction, given by:

$$f_x = \rho\left(u\frac{\partial u}{\partial x} + v\frac{\partial u}{\partial y}\right) - \mu\left(\frac{\partial^2 u}{\partial x^2} + \frac{\partial^2 u}{\partial y^2}\right) \tag{3.3}$$

$$f_y = \rho\left(u\frac{\partial v}{\partial x} + v\frac{\partial v}{\partial y}\right) - \mu\left(\frac{\partial^2 v}{\partial x^2} + \frac{\partial^2 v}{\partial y^2}\right) \tag{3.4}$$

Another different approach for extracting the body force out of a velocity field was suggested in [AWGMS11]. The authors use the vorticity equation and consider only one resulting force in wall-parallel direction.

The present work uses the body force representation by Eq. 3.3 and 3.4, extracted out of PIV experimental data. Examples of forcing fields which were used in the simulations are shown in Figures 3.2 and 3.3.

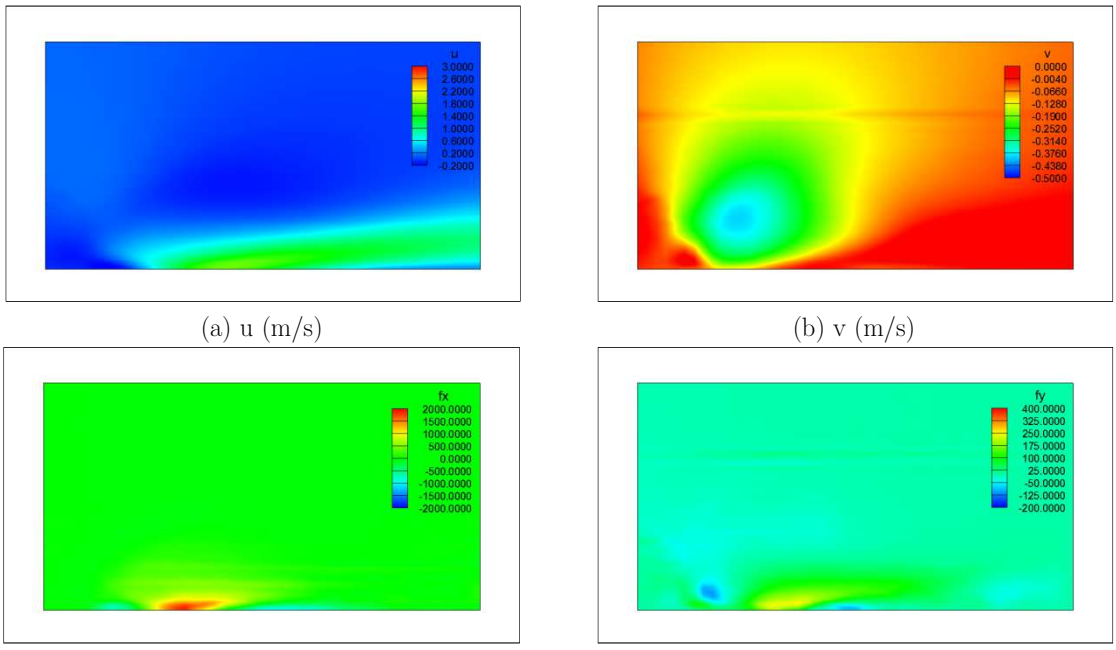

(a) u (m/s) (b) v (m/s)

(c) f_x (N/m^3) (d) f_y (N/m^3)

Figure 3.2: Velocity fields from experimental data and corresponding body force density for Power 1.

Figure 3.2 shows contour plots for velocity fields used to evaluate the body force distribution with a power supply called Power 1 applied to the actuator, equivalent to 8 kV in the original experimental configuration of the plasma actuator. However, due to the wide variety of actuators - many geometrical parameters and materials are possible to be used - a same voltage applied can produce different overall force values, according to the experimental configurations. Therefore, for scientific purposes it is more meaningful to refer to integral force values. For the investigated cases, the values for Power and integral force, which are applied to the actuator, are presented in Table 3.1

Integral force	X	y
Power 1	1.88E+03 N/m	1.58E+02 N/m
Power 2	6.64E+03 N/m	8.19E+02 N/m
Power 3	2.49E+04 N/m	1.32E+03 N/m

Table 3.1: Values of force distribution applied to the plasma actuators.

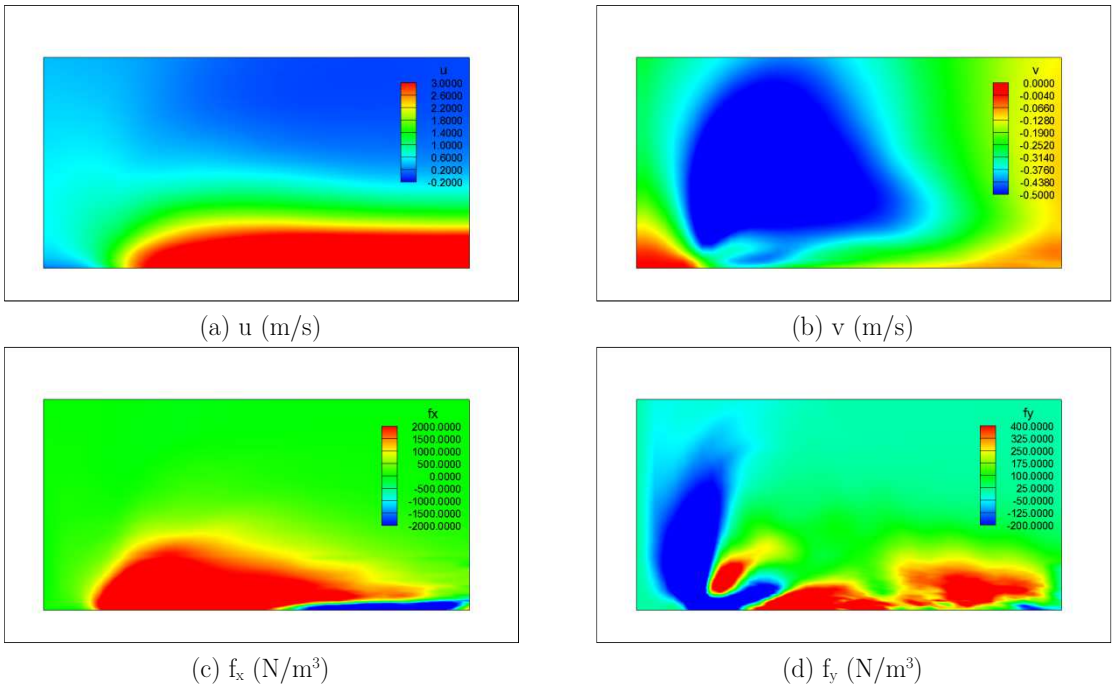

(a) u (m/s) (b) v (m/s)

(c) f_x (N/m^3) (d) f_y (N/m^3)

Figure 3.3: Velocity fields from experimental data and correspondent body force density for Power 3.

The wall jet effect can be observed in Figure 3.2a, where the wall-parallel component shows high values near the solid surface. The strong gradient found in this region will be further attenuated due to the presence of a boundary layer, resulting from a positive free-stream velocity. The suction region, right up the actuator, can be seen in Figure 3.2b, where the wall normal velocity component presents an area of negative values. As the values found for $\boldsymbol{v}$ are about one order of magnitude smaller than the values of $\boldsymbol{u}$, the force densities evaluated also reflect this proportion.

For comparison purposes, Figure 3.3 presents velocity and force density field obtained using Power 3. The contour levels were kept the same. Obviously, a higher power applied to the actuator produces a stronger wall jet and higher force values. This can clearly be seen comparing Figures 3.2 and 3.3.

The small area surrounding the actuator, where the velocity measurements are obtained, has a size of 9 mm×5 mm. The window is linearly interpolated to the grid used

for numerical computations, and the discretized source term is then added to the Navier-Stokes equations at the locations corresponding to the plasma region.

3.3. Plasma actuators and boundary layer flow control

Considering a flat-plate boundary layer flow with no pressure gradient, the fluid acceleration promoted by a plasma actuator can be used to influence the velocity profile and to modify disturbances which provoke turbulence transition. If the flow disturbances can be attenuated or even cancelled, the laminar-turbulent transition zone can be moved downstream to its natural point, promoting lower skin friction drag values. To delay transition is an important goal which can be achieved using plasma actuators with two basic strategies: modifying the boundary layer velocity profile or counteracting directly with the propagated velocity fluctuations.

For a flat plate boundary layer flow, a plasma actuator which is operated in continuous mode, Figure 3.4, provides additional momentum in the very near wall region, and an increase of the wall-parallel velocity component. This acceleration accentuates the negative curvature of the velocity profile at the wall (a similar effect can also be seen for Lorentz force actuators). Furthermore, the influence of a plasma actuator in a boundary layer flow also includes a small negative wall normal velocity component, the suction region, right up to the plasma region.

From the linear stability analysis, it is known that a certain combination of control parameters can promote boundary layer stabilization together with the attenuation of the disturbances propagated, due to velocity profile modifications.

The momentum equation, Eq. 2.4, in the wall-parallel direction can be written at the wall position $y = 0$, also considering dependency in y direction of the viscosity:

$$\mu \frac{\partial^2 u}{\partial y^2} = \frac{\partial p}{\partial x} - \rho f_x + \rho v_{wall} \frac{\partial u}{\partial y} + \frac{\partial \mu}{\partial T} \frac{\partial T}{\partial y} \frac{\partial u}{\partial y}. \tag{3.5}$$

The previous equation express the curvature of the boundary layer velocity profile (left side) and the terms which can influence it (right side) leading to modifications of the flow stability. An increased curvature provides higher flow stabilization, while a decreased curvature may cause the opposite effect.

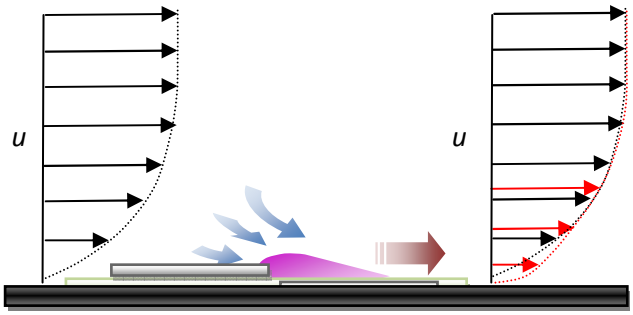

Figure 3.4: Plasma actuator in steady conditions modifying the boundary layer profile. More accentuate curvature is observed downstream the actuator.

Another method for boundary-layer flow-control using plasma actuators consists in acting directly on the propagated disturbances. The actuator is operated in pulsed mode at the same frequency of the dominant Tollmien-Schlichting wave which travels downstream. The amplitude and phase are adjusted to produce an opposite wave at the exact location of the actuator. With an accurate adjustment, the disturbances can be cancelled by superposition of velocities. However, this process does not cause strong modifications of the stability, because the mean flow is only slightly modified. For such an approach, sensors positioned near the actuator are necessary to collect information about the current flow disturbances. The use of an efficient control method is also important to provide a precise configuration for amplitude and phase shift values which are applied to the plasma actuator. Figure 3.5 illustrates the plasma actuator operating in unsteady mode. In the present work, the actuator which is operated in pulsed mode always produces a sinusoidal wave.

Here two different approaches can be distinguished:

- The use of a plasma actuator in steady operational mode to promote significant modification of the stability proprieties in a boundary layer flow is called *wave attenuation*. The wave amplitudes are decreased due to the changes of the growth rates.
- The method which aims to counteract with the disturbances already present in the flow operating a plasma actuator in pulsed mode is called *active wave cancellation*. The wave amplitudes are decreased due to a superposition of velocities.

Figure 3.6 summarizes the two different approaches and its respective effects.

Independently of the utilized operational mode of the plasma actuator, its direct effects on the velocity disturbances only last along a certain region downstream the actuator. Further downstream, the disturbances return grow, for unstable frequency modes.

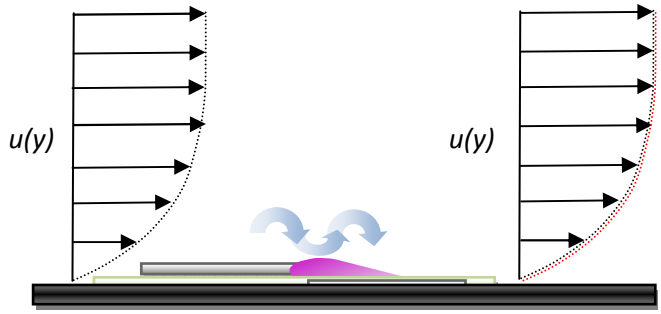

Figure 3.5: Plasma actuator in pulsed mode. Averaged velocity profiles are not strongly modified.

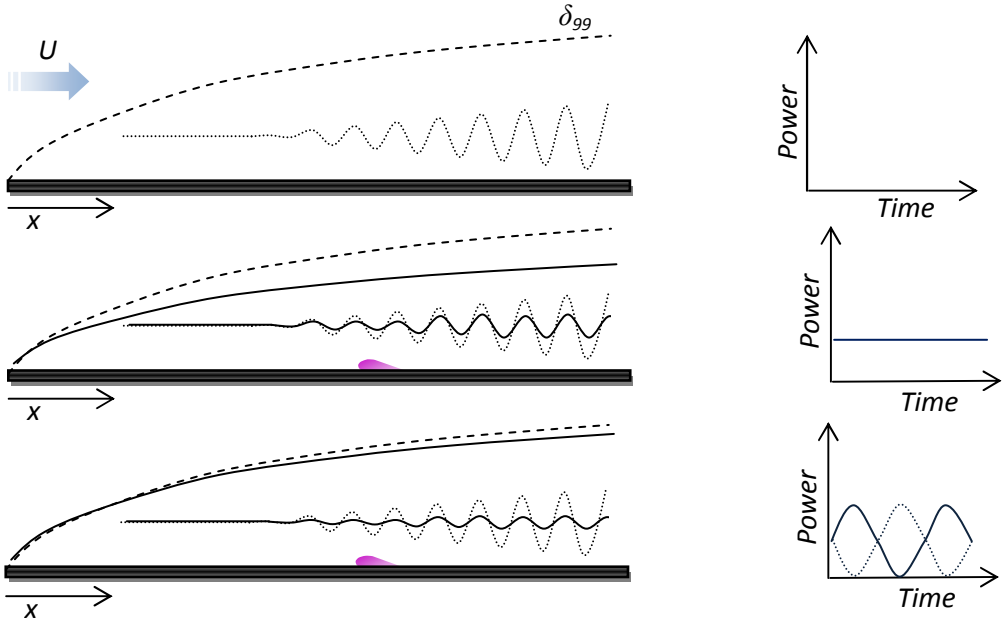

Figure 3.6: Different approaches for control of TS waves using plasma actuators. For continuous power, the additional momentum provides a thinner boundary layer and increases the stability. Cycle operation of the actuator provides the opposite velocity fluctuations which cancel the TS waves by superposition, without significant modifications in the flow stability.

4. Methodologies

4.1. Facilities

All the numerical results which are presented in this research work were evaluated using the Hessian High-Performance Computer (HHLR) located in Darmstadt, Germany and operated by the Technische Universität Darmstadt. The HHLR was designed for scientific applications with high communication need. The system is composed of 19 SMP nodes, 18 computer nodes and 1 login node, with a total of 580 processor cores.

For smaller test cases and lower communication needs the Center for Scientific Computing (CSC) in Frankfurt University, with multiple PC Linux cores, was utilized.

4.2. The numerical solver: FASTEST

FASTEST is the abbreviation of Flow Analysis Solving Transport Equations with Simulated Turbulence, the in-house code which has been constantly developed and improved at the Department of Numerical Methods Applied to Mechanical Engineering (FNB – Fachgebiet Numerische Berechnungsverfahren im Maschinenbau) at the Technische Universität Darmstadt [FAS05]. FASTEST is an efficient three-dimensional solver for the incompressible Navier-Stokes and heat transfer equations, profitable for multiple complex application fields, for steady or unsteady problems. It also supports laminar or turbulent flows (LES, k-ε Model) and uses a strongly implicit ILU method for solving the systems, [Sto68]. The code applies a fully conservative Finite Volume Method in non-orthogonal boundary fitted block structured numerical grids. Pressure-velocity coupling is done by using the SIMPLE method (Semi Implicit Method for Pressure Linked Equations). The options for time discretization which are available are: Euler (first and second order) and Crank-Nicolson. FASTEST is parallelized using Message

Passing Interface (MPI) and uses a non linear multigrid scheme for convergence acceleration. Formally, the numerical solution provided is of a second order of accuracy. The user has the option to choose between a Central Difference Scheme (CDS), first-order accurate upwind-differencing (UDS), or a hybrid combination of both methods with a specified ratio.

The present work uses Direct Numerical Simulations (DNS), Crank-Nicolson for time discretization and CDS.

4.3. Direct Numerical Simulations

DNS directly solve the fluid motion equations without any approximation or modeling. All relevant time and length scales are resolved in the fluid field, what causes DNS to be an extremely expensive tool, but also the most exact approach for turbulence simulations.

Nowadays, even with high-performance computers, DNS is only feasible for relatively simple geometries and relatively low Reynolds numbers. The CPU time for such simulations can be estimated by Re^3. The high costs of such simulations led to the development of alternative well-known methods like LES (Large Eddy Simulations) and Statistical turbulence models.

However, DNS is still the best tool for very detailed phenomenological investigations and, in the specific case studied by the present work, DNS allows a more realistic treatment of the disturbance amplification.

The complete solution of all turbulence scales provides important information for the comprehension of the flow structures and its development until laminar-turbulent transition. Additionally, DNS avoids the need of many restrictions with respect of the form or amplitude of the flow disturbances usually imposed in other models, because no linearization or other assumptions are made, [SRK02].

The first steps in the direction to the comprehension about turbulence scales started with the work of Kolmogorov, [Kol41], based on theoretical hypothesis and experimental observations. The smallest scales which are present in a turbulent flow are:

$$\kappa = \left(\frac{\nu^3}{\varepsilon}\right)^{1/4} , \tag{4.1}$$

$$t_\eta = \left(\frac{\nu^3}{\varepsilon}\right)^{1/2} \quad , \tag{4.2}$$

$$u_\eta = (\nu\varepsilon)^{1/4} \quad , \tag{4.3}$$

which are the Kolmogorov microscales for length, time and velocity, respectively. These relations were developed considering turbulence as a general phenomena depending only of ν and ε, where ε is the average rate of energy dissipation per unit mass:

$$\varepsilon \approx \frac{u_{rms}^3}{L} \tag{4.4}$$

where L is an integral scale, N the number of discretized points along a given direction, and h the increment size for the same direction.

All scales are considered as being associated with the motion and contain energy. Even the Kolmogorov microscales need to be resolved directly by the numerical grid. For a three dimensional geometry, the number of grid points which are necessary for a DNS can be estimated by:

$$N \approx \left(\frac{l_0}{l_\eta}\right) \approx Re_{turb}^{9/4} \tag{4.5}$$

where l_0 is the largest length scale and l_η is the smallest length scale. The turbulent Reynolds number is given by:

$$Re_{turb} = \frac{u_{rms} L}{\nu} \tag{4.6}$$

and u_{rms} is the root mean square of velocity.

The time step of the temporal integration has to be small enough and allow the convection of small turbulent structures along the smaller distance by the large scale velocity u_0:

$$\Delta t \approx \frac{l_\eta}{l_0} \approx \frac{l_0}{u_0} Re^{-\frac{3}{4}} \tag{4.7}$$

The total number of time steps M which is necessary can be estimated by:

$$M \approx \frac{l_0}{\Delta t . u_0} \approx Re^{3/4} \tag{4.8}$$

Thus, for a DNS study, relations between the flow parameters and the grid requirements are proportional, providing an immense increasing of the numerical efforts according to the Reynold number. Large numbers of grid points are needed together with a small time step, even for low Reynolds numbers and simple applications. Despite that, DNS is an important scientific tool, referred as a "numerical experiment" [JL09], [SÖ10]. DNS provides information which is hard or even impossible to be obtained in the laboratory. In practical cases, a highly accurate numerical scheme and correct boundary conditions are also necessary for the precise resolution of the time and space scales.

4.4. Tollmien-Schlichting wave excitation

A correct implementation of the disturbance excitation is important to avoid that additional momentum can produce certain interference on the boundary layer velocity profile. Additional momentum could lead to a wrong interpretation of the numerical results, due to stabilizing effects. A controlled environment is provided by artificial mono-frequency disturbances, which are excited according to [Alb11]. These disturbances develop downstream into TS waves. A time and space dependent body force is added to the Navier-Stokes equations according to:

$$FD(x,y,z,t) = \left(A2Dv_a(x) + A3Dv_s(x)cos\left(2\pi \frac{z}{L_z/n_z}\right)\right) v_r(y)\hat{\jmath}\, cos(2\pi f t) \tag{4.9}$$

It represents the type of oscillation also used in [RF95] to simulate blowing and suction. $A2D$ and $A3D$ are the two dimensional and three dimensional wave amplitudes, respectively. f is the TS wave frequency of excitation. L_z is a characteristic length (like the width of the flat plate) and n_z is the wave periodicity, both in spanwise direction. The ratio between these two quantities represents the spanwise wave length. The quantity v_a is given as follows:

$$v_a = \begin{cases} \frac{1}{48}\left(729{\xi_1}^5 - 1701{\xi_1}^4 + 972{\xi_1}^3\right), & \text{for } x_{d0} < x < 0 \\ & \text{where } \xi_1 = \frac{x - x_{d0}}{x_c - x_{d0}} \\ -\frac{1}{48}\left(729{\xi_2}^5 - 1701{\xi_2}^4 + 972{\xi_2}^3\right), & \text{for } 0 < x < x_{d1} \\ & \text{where } \xi_2 = \frac{x_{d1} - x}{x_{d1} - x_c} \end{cases} \tag{4.10}$$

and

$$x_c = 0.5(x_{d0} + x_{d1}). \tag{4.11}$$

The quantity v_s is defined as:

$$v_s = \frac{1}{2} + \frac{1}{2}cos\left(2\pi\frac{x - x_{d0}}{x_{d1} - x_{d0}} - \pi\right), \qquad \text{for } x_{d0} < x < x_{d1} \tag{4.12}$$

and v_r is given by:

$$v_r = \frac{1}{2} + \frac{1}{2}cos\left(\pi\frac{y - y_d}{r_{max}}\right), \quad \text{for } y_d - r_{max} < y < y_d + r_{max} \tag{4.13}$$

The quantities y_d, r_{max}, x_{d0} and x_{d1} are the reference points where the forcing term is applied, Figure 4.1.

For the two-dimensional case one has $A3D = 0$, and the forcing term in Equation 4.9 becomes:

$$FD(x, y, z, t) = \left(A2D v_a(x)\right) v_r(y)\, \hat{\jmath}\, cos(2\pi f t) \tag{4.14}$$

This force, plotted in Figure 4.2, acts in the wall-normal direction, but promote a sinusoidal oscillation of the velocity also in the wall-parallel direction.

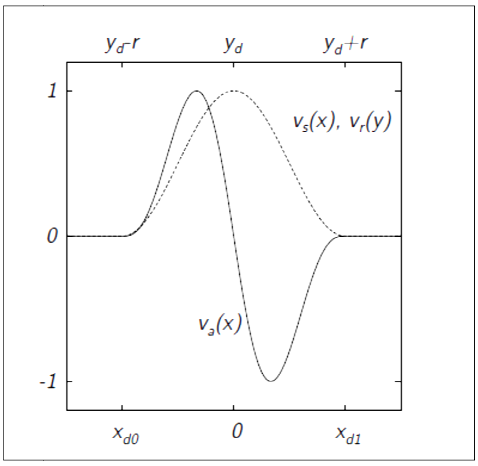

Figure 4.1: Variables for TS wave excitation, [Albr11].

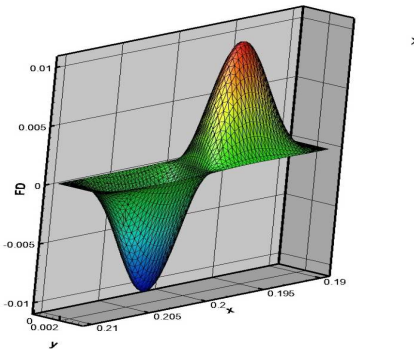

Figure 4.2: Two-dimensional body force illustration.

4.5. Plasma actuator body-force optimization

For investigations of active wave cancellation, the plasma actuator is operated in pulsed mode by means of a sinusoidal function.

$$F_s = A\sin(2\pi f + \theta) * F_{PIV} \tag{4.15}$$

where f is the frequency of actuation, F_{PIV} is the force evaluated based in experimental data, A is the forcing amplitude and θ is the phase angle necessary to produce a wave opposite to the TS wave at the actuator position.

The success of this approach strongly depends on the correct identification of the amplitude and the phase shift. In numerical simulations, these two parameters are possible to be adjusted “by hand”, but as a result of a long iterative procedure

("trial and error"). The use of an optimization algorithm which finds the best setup for the force input parameters is a better and more trustable alternative.

BOBYQA, the abbreviation of Bound Optimization BY Quadratic Approximation, is the chosen optimization algorithm in the present work. The short description presented here is based on [Pow09]. This optimization procedure is an improvement of the NEWUOA software [Pow06] for unconstrained optimization without derivatives. The use of quadratic models provides high accuracy in many cases using only a few function values.

BOBYQA is an iterative program composed of a package of Fortran subroutines, which searches for the minimum of a general function (frequently called objective function, F). In this case, the objective function is defined through the maximal TS wave amplitude at a certain location, given by $F = max(U_{rms})$ – evaluated from the DNS results using FASTEST. BOBYQA requires no derivatives of the objective function are required. The two parameters to be optimized are the amplitude A and the phase shift θ. They are stored as components of the input vector $\underline{x}$, subject to user defined bounds

$$a_i \leq x_i \leq b_i, \qquad i = 1,2 \tag{4.16}$$

Another input to the algorithm is m which represents the number of interpolations imposed to a quadratic approximation of $Q_k(\underline{x}),\ \underline{x} \in \mathcal{R}^2$, to $F(\underline{x}),\ \underline{x} \in \mathcal{R}^2$, where k is the number of iterations. m can be chosen in the interval $[n+2, 0.5(n+1)(n+2)]$, where n is the number of variables for optimization, in this case $n = 2$. At the beginning of the k-th iteration, the quadratic model needs to fulfill:

$$Q_k\left(\underline{y}_j\right) = F\left(\underline{y}_j\right), \qquad j = 1,2 \ \ldots m \tag{4.17}$$

We define $\underline{x}_k$ as the point in the set

$$\left\{\underline{y}_j : j = 1,2, \ldots m\right\} \tag{4.18}$$

with the property:

$$F(\underline{x}_k) = \min\left\{F\left(\underline{y}_j\right) : j = 1,2,\dots m\right\}. \tag{4.19}$$

The trust region radius is a positive number Δ_k defined at the start of BOBYQA and is adjusted during the runtime.

The iterative process follows with the construction of a step $\|\underline{d}_k\| \leq \Delta_k$ such that $\underline{x} = \underline{x}_k + \underline{d}_k$ and is inside the interval of Eq. 4.16. The new parameters are applied as input to the plasma actuator body force. Then, the numerical solver for the Navier-Stokes equations provides a new value for the objective function, $F(\underline{x}_k + \underline{d}_k)$. After that, one of the interpolation points may be replaced by $\underline{x}_k + \underline{d}_k$. The iterative values for $\underline{x}$ are defined as:

$$\underline{x}_{k+1} = \begin{cases} \underline{x}_k, & F(\underline{x}_k + \underline{d}_k) \geq F(\underline{x}_k), \\ \underline{x}_k + \underline{d}_k, & F(\underline{x}_k + \underline{d}_k) < F(\underline{x}_k). \end{cases} \tag{4.20}$$

A new trust region radius and a new approximation for the objective function are generated for the next iteration:

$$Q_{k+1}\left(\underline{\hat{y}}_j\right) = F\left(\underline{\hat{y}}_j\right), \qquad j = 1,2,\dots m, \tag{4.21}$$

and

$$\underline{\hat{y}}_j = \begin{cases} \underline{\hat{y}}_j, & j \neq t, \\ \underline{x}_k + \underline{d}_k & j = t, \end{cases} \qquad j = 1,2,\dots m. \tag{4.22}$$

where the index t represents the current interpolation point.

Let $\#F$ be the total number of evaluations of the objective function and $\underline{x}_*$ the optimal vector of control variables (amplitude and phase shift). It was shown in [Pow08] that if m is set to $2n + 1$ (n is the number of variables to be optimized), $\#F$ is at the same order of magnitude of n. If F is twice differentiable, $\nabla^2 Q_k$ is not a good approximation to $\nabla^2 F(\underline{x}_*)$ for small $\#F$. Indeed, when F is quadratic the final value of the Frobenius matrix form is

$$\|\nabla^2 F - \nabla^2 Q_k\|_F > 0.5\|\nabla^2 F\|_F, \tag{4.23}$$

but

$$\|\underline{x}_k - \underline{x}_*\| \leq 10^{-6}\|\underline{x}_1 - \underline{x}_*\|. \tag{4.24}$$

The Frobenius matrix norm is employed because Q_{k+1} is constructed from Q_k using a symmetric Broyden formula with the property

$$\|\nabla^2 F - \nabla^2 Q_{k+1}\|_F \leq \|\nabla^2 F - \nabla^2 Q_k\|_F, \qquad k = 1,2,\ldots. \tag{4.25}$$

Inside the trust region iterations, $\underline{d}_k$ is an estimative of $\underline{d}$ for solving the problem:

$$\left.\begin{array}{l} \text{minimize } Q_k(\underline{x}_k + d), \qquad \underline{d} \in \mathcal{R}^n, \\ \text{subject to } \underline{d} \leq \underline{x}_k + \underline{d} \leq \underline{b} \quad \text{and} \quad \|\underline{d}\| \leq \Delta_k \end{array}\right\}. \tag{4.26}$$

One updating procedure which is used in BOBYQA is the calculation of Q_k. $Q_{k+1} - Q_k$ is changed into a quadratic model defined by a system of linear equations of $(m+n+1)\times(m+n+1)$ dimension. This system is solved in $\mathcal{O}(m^2)$ operations necessaries for building the inverse matrix of the same system by another updating procedure.

If Ω_k is the $m \times m$ submatrix of the inverse matrix, it is necessary for numerical stability that Ω_k can be expressed as:

$$\Omega_k = Z_k Z_k^T \tag{4.27}$$

where Z_k is the real $m \times (m-n-1)$ matrix. In case of a negative eigenvalue is found in Ω_{k+1}, the program would express Ω_{k+1} as $Z_{k+1}S_{k+1}Z_{k+1}^T$ with S_{k+1} being a $(m-n-1)\times(m-n-1)$ diagonal matrix with elements set to $+1$ or -1. If necessary, BOBYQA moves a few interpolation points to restore the factorization $\Omega_k = Z_{k+1}Z_{k+1}^T$ in a subroutine called RESCUE.

A more complete explanation, followed by practical examples using BOBYQA is given in [Pow09].

5. Validation and verification

5.1. Base flow

For the numerical simulations of a flat plate boundary-layer flow, the used computational domain is illustrated in Figure 5.1. The distances in x direction are fixed, but the height of the domain h is one of the parameters under investigation. A uniform velocity profile is used at the inlet, with two free-stream velocity magnitudes: 10 and 16 m/s. Once studies of free-stream turbulence are not considered in the present work, there is no need for a disturbed inlet flow. The development of the boundary layer along a flat plate can be observed and compared with the theoretical solution for this simple case as a mean of validation. However, the singularity present at the leading edge may give rise to undesired pressure disturbances, or even numerical divergence. Located before the inlet and the flat plate leading edge there is a short distance in the bottom of the domain where the symmetry condition is also applied. This procedure was also applied in [Qua09] as an approximation for the sloped profile present in the real configuration. The inlet velocity is also applied as initial condition for the complete computational domain.

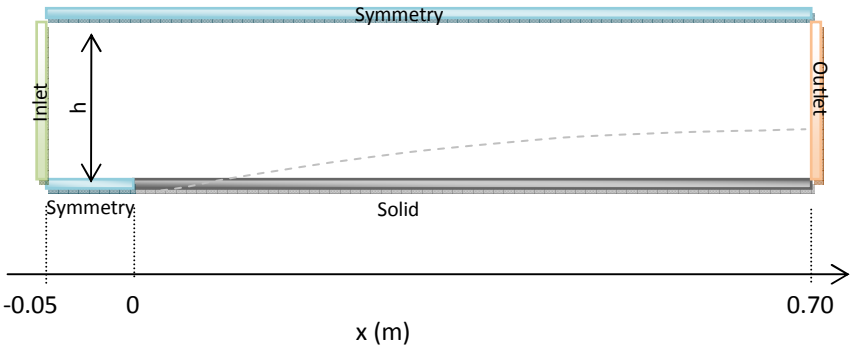

Figure 5.1: Illustration of the computational domain.

The symmetry condition, often used in RANS simulations to reduce the domain size, can also be employed at the top of the domain for DNS investigations. But, for such cases, it becomes necessary to investigate the influence of the domain height and confinement effects. On the solid wall, a no-slip condition is applied by simply considering zero velocities at the wall.

At the outlet, a convective condition is employed. This condition shall allow possible recirculation present in the flow to leave the computational domain by the outlet without producing significant undesired velocity reflections. The use of a prescribed velocity profile or even a single derivative condition could impair the solution in the complete domain. The convective outlet condition is used:

$$\frac{\partial \phi}{\partial t} + U_{conv} \frac{\partial \phi}{\partial n} = 0 \tag{5.1}$$

where U_{conv} is a velocity chosen under the consideration that conservation is maintained over the complete domain, i.e. U_{conv} is the velocity required to produce an outflow equivalent to the given inflow. Thereby, problems caused by pressure fluctuations reflected backwards and again inside of the domain can be avoided [FP02].

The computational meshes used in the present work are composed of hexahedral cells, grouped in a multi-block structure. Grids are refined in x and y direction. Cells are refined near and inside the boundary layer region using a spline function, in y direction. In x direction, elements are refined in the downstream direction. The coarsest grid, here called grid A, has 4.2E05 control volumes. grid B has 1.6E06 control volumes and the finest grid, grid C has 2.2E06 control volumes.

The numerical solutions for a flat-plate boundary-layer flow with zero-incidence are compared with the theoretical solution of Blasius, presented in Section 2.1. Figure 5.2 shows the comparison of the non-dimensional velocity profiles for inflow velocity of 10 m/s, at x = 0.30 m. No significant differences can be observed between the profiles. Small diffusive effects can be found in the results for Grid A. A similar behavior can be observed for the higher inflow velocity of 16 m/s, Figures 5.3. Even very small, the error between the computed velocity profiles and the theoretical solution can represent non-negligible changes in the stability proprieties of a boundary layer flow. Such differences need to be correctly

quantified such that they do not lead to wrong conclusions about the actuator effects.

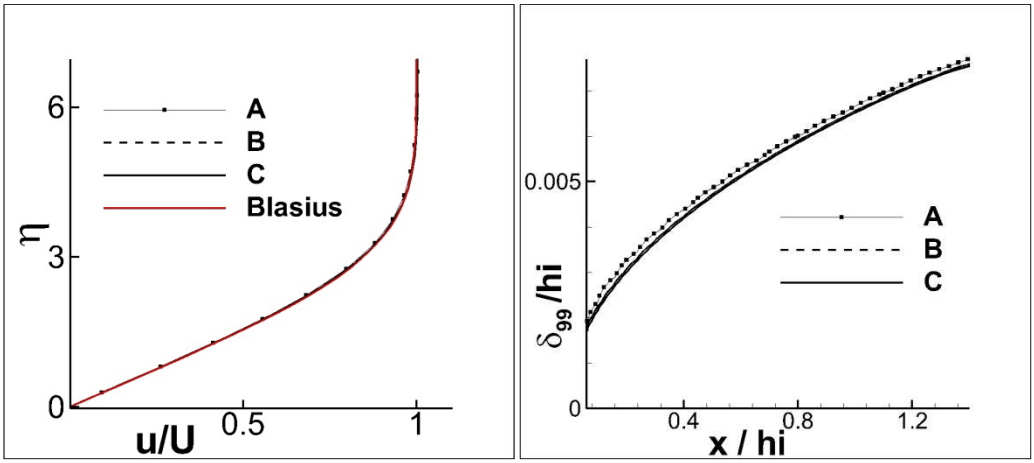

Figure 5.2: Boundary layer comparison and solution for different grids at inflow velocity of 16 m/s. At left, non-dimensional velocity profile at x = 0.3 m. At right, iso-velocity lines for u = 0.99 U. hi = 0.5 m.

Together with grid convergence tests, the influence of confinement effects was also verified. Diverse values for the domain height hi were tested. The reason for these verifications is the symmetry condition at the top of the domain. The use of such a condition may result in a small acceleration of the flow immediately after the boundary layer region, due to the portion of fluid which is retained by viscous effects and the mass conservation criteria.

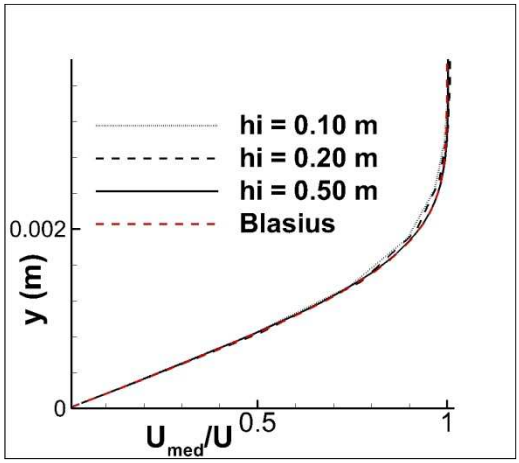

Figure 5.3: Confinement tests for boundary layer flat plate flow.

The effect of fluid acceleration can be erroneously associated with the presence of an additional pressure gradient in x direction. However, in both cases, with an additional pressure gradient, or a small flow acceleration due to the symmetry

condition, the consequent flow field may result in a boundary layer profile which is more stable than the standard Blasius profile. Even a very weak modification in the boundary layer velocity profile may eliminate the upper branch of the neutral stability curve and produce significantly amplitude reduction [GH89]. To avoid any misinterpretation of the numerical results, the top boundary should be set far enough from the flat plate.

Figure 5.3 shows comparisons for three confinement tests with different heights. The higher value tested, h = 0.50 m, provides a profile which is closer to the theoretical boundary layer solution. The other two lower values tested for *hi* produce confinement effects observed in the upper part of the boundary layer profile.

Grid convergence tests are presented in Figure 5.4, where the boundary layer velocity profile is compared to the theoretical Blasius solution for a different inflow velocity. From these tests, it is assumed that the use of grid C and the top boundary at $h = 0.5\,m$ provide the best base flow configuration for a good quantitative analysis of flow control.

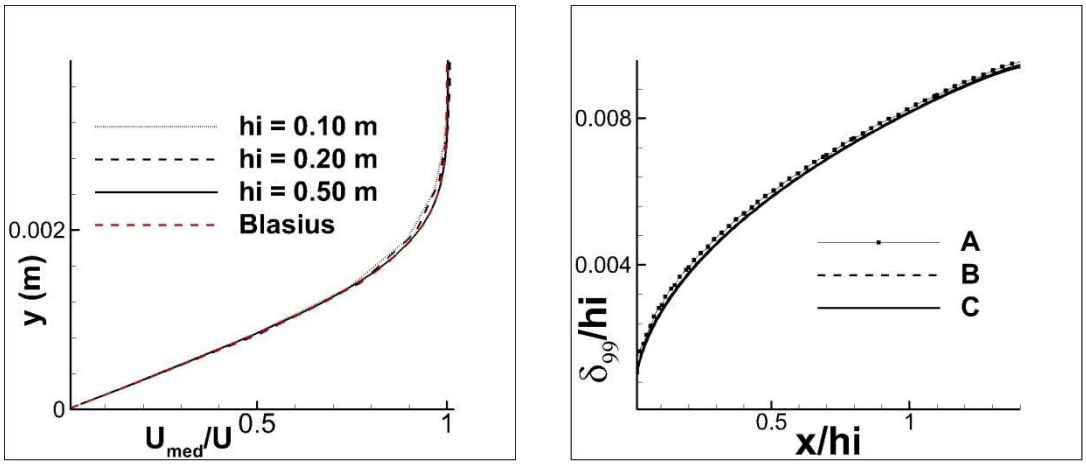

Figure 5.4: Boundary layer comparison and solution for different grids at inflow velocity of 10 m/s. At left, non-dimensional velocity profile at x = 0.3 m. At right, iso-velocity lines for u = 0.99 U. hi = 0.5 m.

5.2. Tollmien-Schlichting wave simulations

Periodical disturbances are added to the flow at x = 0.225 m and inside the boundary layer region, see Figure 5.5. These small flow perturbations grow exponentially and develop downstream the excitation point as two-dimensional

Tollmien-Schlchting waves. However, the correct amplification of such disturbances is not only dependent of the excitation method. The grid ratio and the numerical discretization method chosen may also produce additional energy dissipative effects, which lead to non-physical damping of the excited disturbances.

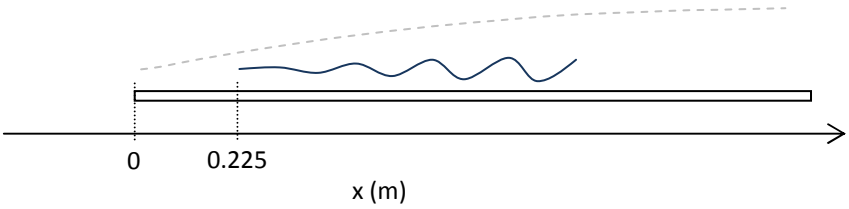

Figure 5.5: Wave excitation scheme.

Solutions using Upwind Differencing Scheme (UDS) and Central Differencing Scheme (CDS) were compared. The diffusive effects of UDS resulted in excessive and non-physical damping of the flow disturbances. But CDS provided the correct amplification of the TS waves. Figure 5.6 shows a comparison of both mentioned schemes, using grid C, 16 m/s as freestream velocity and $hi = 0.5\,m$. The frequency of excitation is 220 Hz. For the range delimited by the computational domain, this frequency mode should be amplified right downstream the excitation point, according to the stability theory for a flat plate flow, with zero incidence angle. As expected, the diffusive effects of UDS suppress the wave amplification, while CDS does not. Therefore only CDS is used in the following.

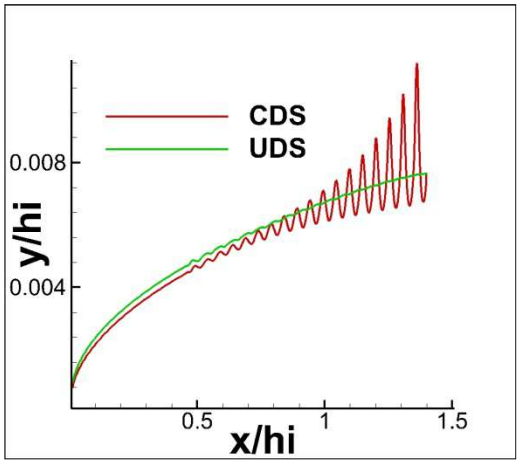

Figure 5.6: Iso-line of velocity $u = 0.99U$ for both schemes: Up-wind and CDS.

The influence of the grid refinement is also investigated. Numerical simulations of the flow over a flat plate are done using the three grids previously described, with TS waves excited at 220 Hz and 16 m/s. As illustrated in Figure 5.7, the coarse resolution of grid A provided TS waves of smaller amplitude in comparison with the other two tested grids. A low amount of grid points in the near wall region does not provide enough resolution for the natural amplification of disturbances inside the boundary layer.

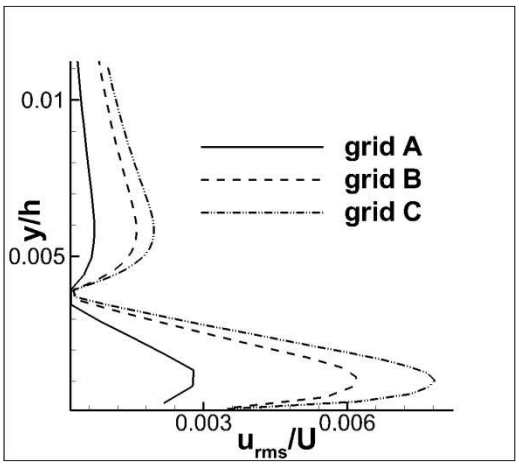

Figure 5.7: Grid tests for TS wave amplification. Averaged profiles of U_{rms} velocity in the wall parallel direction at x = 0.325 m.

As shown before in previous tests, for a simple base flow, the three different grids do not produce significantly different solutions, and the evaluated results presented values which are close to the theoretical Blasius solution. But the wave amplification phenomena require a more precise numerical resolution to provide results with a consistent physical meaning. Figure 5.8 shows the maximum values for the TS wave amplitudes plotted along x direction for the three tested grids.

The coarser grid promoted the immediate damping of the excited disturbances. Grid B, with an intermediate mesh resolution, promoted the wave amplification until a certain distance downstream the excitation point, followed by a further wave damping. Only the finest grid, grid C, was able to reproduce the full amplification of the excited mode along the investigated range. Due to this fact, for all the following results grid C is employed.

Numerical results obtained with DNS for the flat plate flow with artificially excited disturbances are analyzed according to the laminar stability theory. Time averaged profiles of the wall parallel velocity component are applied as an input for the Orr-Sommerfeld equation. The N factors obtained were compared with the

maximal amplitude of the TS waves resulting from numerical simulations. Figure 5.9 show results of these comparisons at several frequencies.

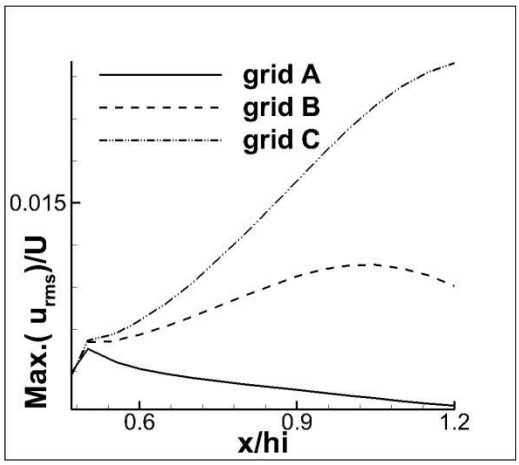

Figure 5.8: Maximum amplitudes of the disturbances plotted along x direction, for different grid resolutions. TS waves excited at 220 Hz and freestream velocity of 16 m/s.

A good agreement between the numerical results for the TS wave amplification and the theory given by Laminar Stability could be reached. In Figure 5.9-a, one can see the values for the maximal disturbance evaluated very close to the theoretical values for the N factor given by the Orr-Sommerfeld equation. The waves are excited at x = 0.225 m, at 220 Hz, and with a 16 m/s free-stream flow. For this configuration, disturbances are expected to be amplified downstream until the end of the flat plate, because this range is located inside an unstable region for a disturbance of 220 Hz. A higher frequency, 250 Hz, excited at the same point, Figure 5.9-b, is found to be immediately amplified, but also damped further downstream. The domain of interest is not completely inside of the unstable region for this frequency mode. These two last tests serve as validation for the present configuration. The computed growth of the waves in regions of amplification or damping, are in good agreement with the values of the N factors when evaluated at the same locations.

One additional test is made considering a lower free-stream velocity of 10 m/s, see Figure 5.9-c. The disturbances were excited at a frequency of 110 Hz at $x = 0.225$ m. This configuration corresponds to the flow situation found to be outside of the unstable region (corresponding to the frequency of 110 Hz), which is located a few centimeters downstream to the wave excitation point. The growth of the waves is well observed after $x = 0.400$ m, where the flow conditions are already

found to be inside the unstable region, which is in a good agreement with the theoretical LSA values.

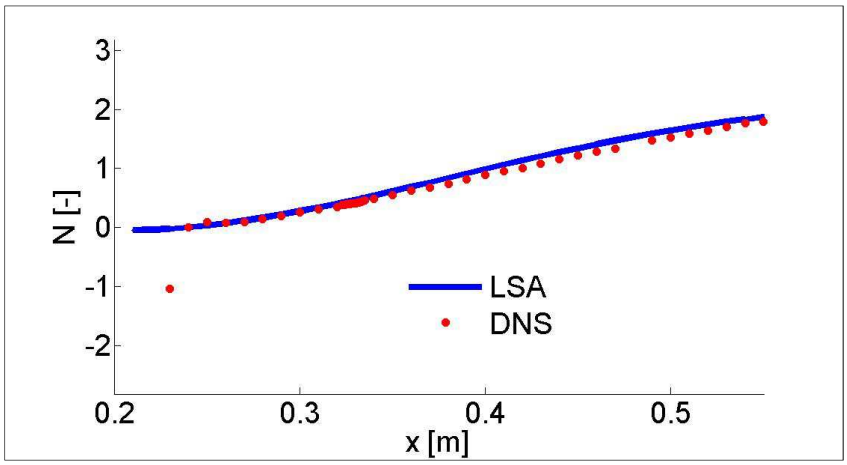

(a) Freestream velocity 16 m/s and TS waves at 220 Hz.

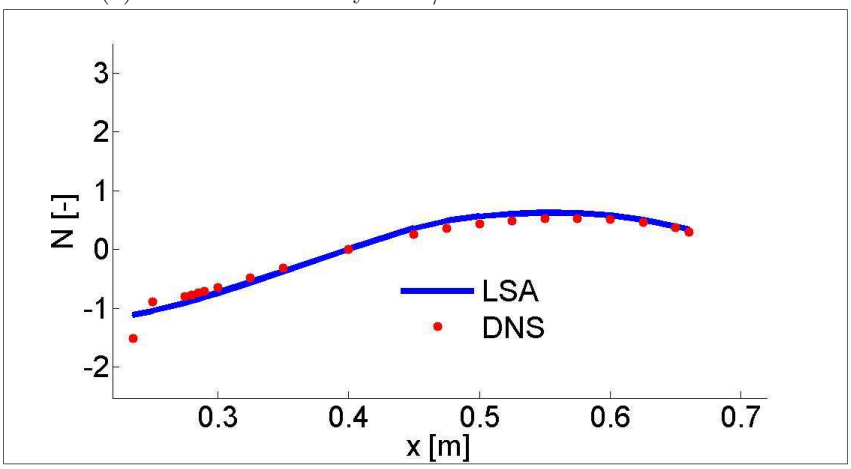

(b) Freestream velocity 16 m/s and TS waves at 250 Hz.

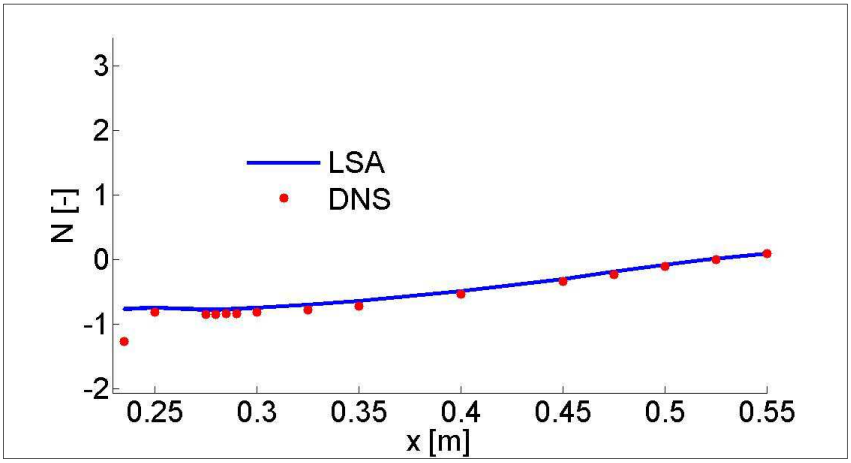

(c) Freestream velocity 10 m/s and TS waves at 110 Hz.

Figure 5.9: Laminar stability comparison of the wave growth rates (N factors) with the maximum amplitudes of the disturbances obtained with DNS simulations, evaluated with free-stream velocity of 16 m/s and several frequencies of the disturbance excitation.

Tollmien-Schlichting waves grow downstream the excitation point in a laminar regime while the maximal amplitude reached a value up to 1-2 percent of the free-stream velocity. For higher amplitude waves, three dimensional disturbances arise, and the development of hair-pin vortex starts. The threshold amplitude for the Tollmien Schlichting waves indicates the value above which continuing growth of flow disturbances occurs. TS waves with amplitudes superior to 1.8 % of the free-stream velocity cannot be cancelled by phase-shift correction (active wave cancellation) [LD06]. For this reason, the artificially excited TS waves should develop in a low-amplitude range. Figure 5.10 shows a few comparisons for different excitation magnitudes and their development downstream.

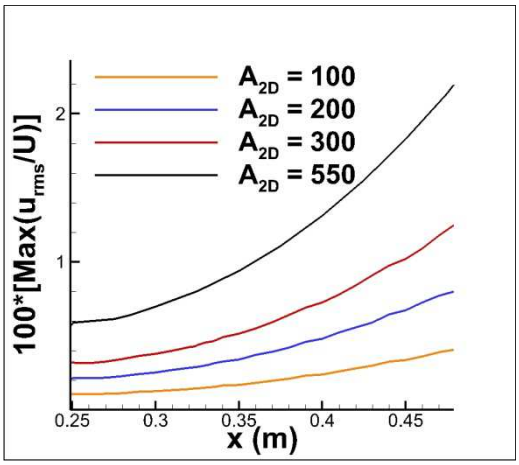

Figure 5.10: Development of Tollmien-Schlichting waves of different excitation amplitudes.

Tollmien-Schliting waves are velocity oscillations which move downstream. For the wall-parallel velocity component, there are two peaks of fluctuations in opposite directions, separated by a neutral point. The first of these peaks is located near the solid surface and has a higher magnitude than the second one, located right above it. Strong gradients in the region very near the flat plate are responsible for a phase angle of the oscillations related to the upper region. Another phase angle is found between the two peaks of fluctuations. Figure 5.11 illustrates the wall parallel velocity oscillations of a typical TS wave. The wall normal velocity component presents only one peak of oscillation about one order lower than the oscillations found in the wall parallel direction.

The neutral point of the Tollmien-Schlichting wave corresponds to the position where the direction of the velocity fluctuations changes. Curiously, in a dimensional analysis, this point is moved up according to the TS wave amplification

downstream the excitation point. But, considering non-dimensional parameters, the neutral point is actually displaced closer the boundary layer downstream the excitation point, as illustrated in Figure 5.12.

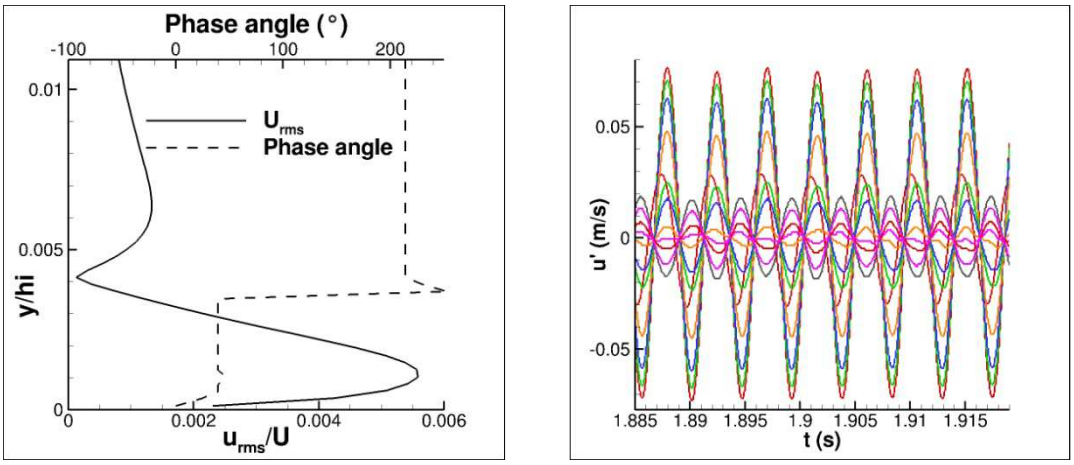

Figure 5.11: Tollmien-Schlichting wave in details, phase angle (left) and fluctuations (right) of the wall parallel velocity component.

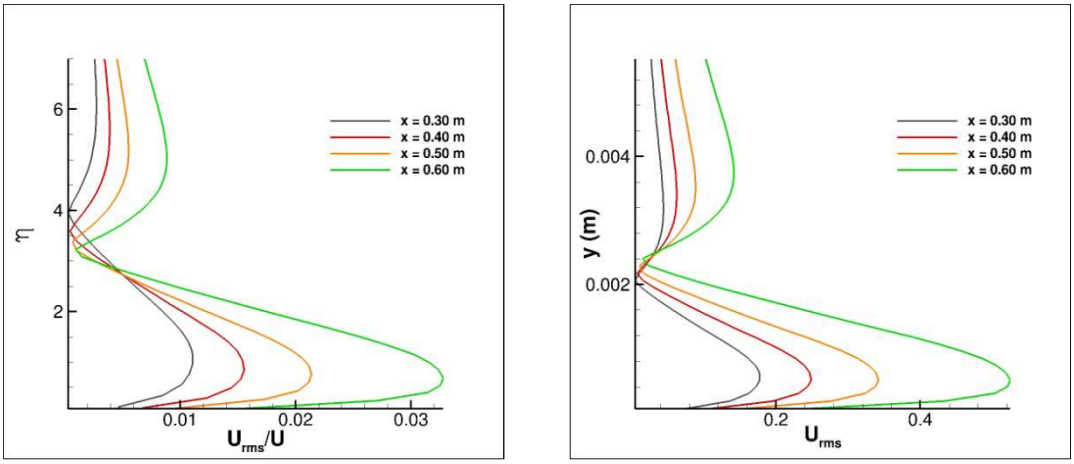

Figure 5.12: Tollmien-Schlichting wave and the position of the neutral point for dimensional (left) and non-dimensional (right) velocity profiles.

5.3. Plasma actuator simulations

The plasma actuator effects were first investigated in a quiescent air domain. For these tests cases, all fluid motion is uniquely promoted by a body force. From the instant when the actuator is turned on, the fluid surrounding the plasma is accelerated. In quiescent air, this phenomenon has some similarities with a wall jet. The actuator was positioned at $x = 0.325$ m from the flat plate leading edge and it is turned on when $t = 0$

Figure 5.13 shows profiles for the wall parallel velocity component inside the boundary layer region.

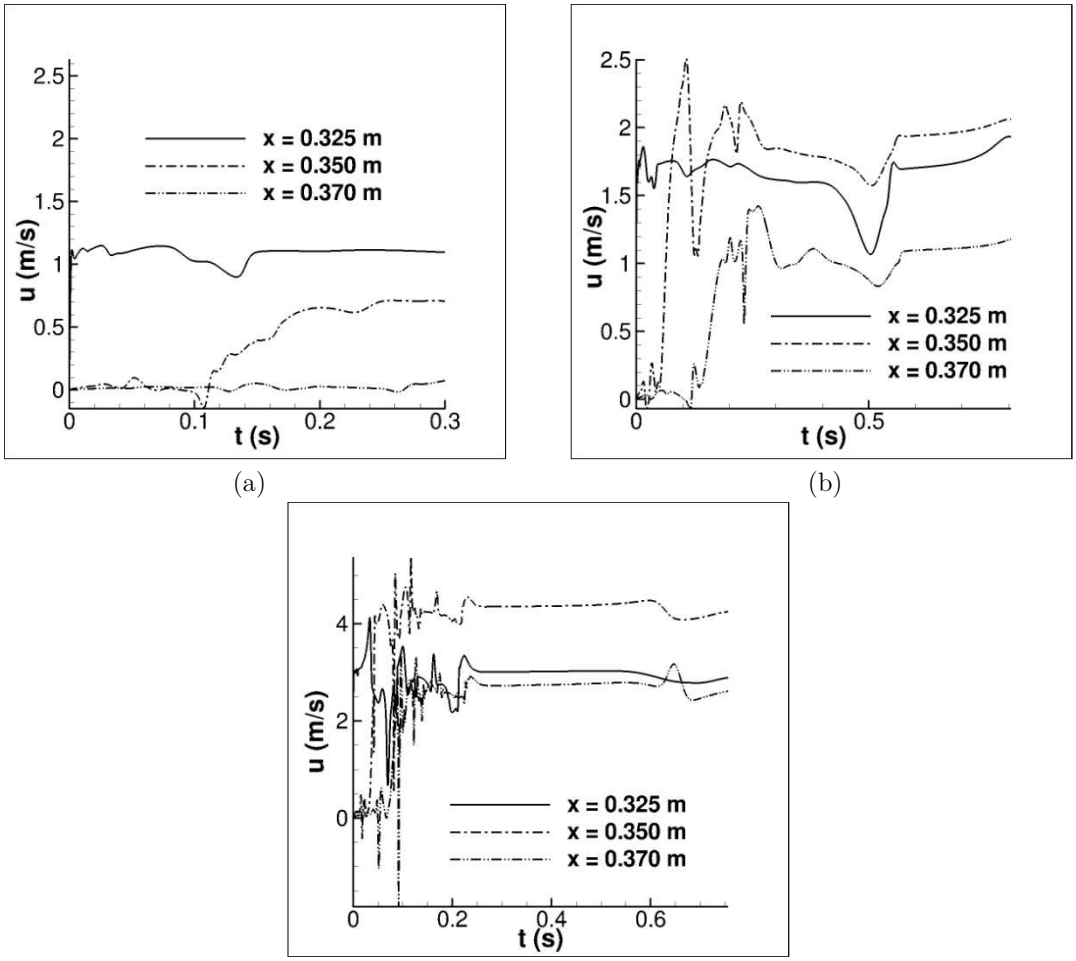

Figure 5.13: Unsteady velocity calculations for a plasma actuator in quiescent air and different body force magnitudes. (a) Power 1, (b) Power 2, (c) Power 3.

For the lowest power applied, Power 1, Figure 5.13-a, at the actuator location, the fluid response is immediate, with an acceleration about 1 m/s, well established after a short time. A few millimeters downstream and still inside of the region with strong influence of the plasma, the fluid surrounding the actuator position is accelerated after a few instants and a weaker wall jet is established. Further downstream, at $x = 0.370$ m, the influence of the plasma actuator is still not so strong. A weaker wall jet would probably reach this region after a longer time.

Using Power 2, Figure 5.13-b, the flow situation is very different from the previous case with a lower power. The immediate flow acceleration at the plasma location promotes velocity oscillations which are transported downstream. A

velocity peak appears at $x = 0.350$ m, and it is followed by two other peaks of small magnitude before a wall jet of higher speed at that location is established. Further downstream, oscillations are still propagated with a few velocity peaks of small intensity and the values for the wall parallel velocity component remain around 1 m/s – a value which is similar to the one found at the plasma actuator location for the previous test case.

Some interesting results are found for Power 3 applied to the plasma actuator, Figure 5.13-c. Very fast acceleration is found immediately after the plasma actuator is turned on, together with many velocity oscillations. The wall jet is established at a higher velocity magnitude at $x = 0.350$ m than at the actuator location. Further downstream, at $x = 0.370$ m, the wall jet is almost as strong as it is at the plasma actuator location, $x = 0.325$ m. Higher values for the body force applied in this case promote several flow disturbances immediately after the plasma actuator is initiated. These disturbances are consequently transported downstream. The presence of the actuator with Power 3 may increase the turbulence levels, creating a turbulent wall jet.

Assuming two-dimensional flow, the vorticity is evaluated from the velocity fields as the difference between the partial derivatives of the velocity components:

$$\vec{w} = \frac{\partial v}{\partial x} - \frac{\partial u}{\partial y} \tag{5.3}$$

Temporal evolution of the vorticity fields is shown in Figure 5.14 for Power 1 force magnitude applied to the plasma actuator.

Two zones of opposite vorticity emerge from the plasma actuator due to the flat plate shear stress, at the moment the actuator is turned on. These zones develop and give rise to an initial vortex of small diameter. After some instants, the vortex is amplified and convected away from the actuator. The diameter increases but the vorticity quantities decrease. The use of an actuator with Power 1 force applied produces an initial vortex which is convected before the wall jet is well established.

Figure 5.15 shows the vorticity maps for the test case with Power 2 applied to the actuator. At the beginning, the region of higher vorticity has also a higher intensity than the ones found for Power 1. This region is then subdivided, giving rise to two vortices of opposite direction. These vortices are subsequently moved up

and divided once more. The rotational disturbances are convected and have lower vorticity values before the wall jet is established.

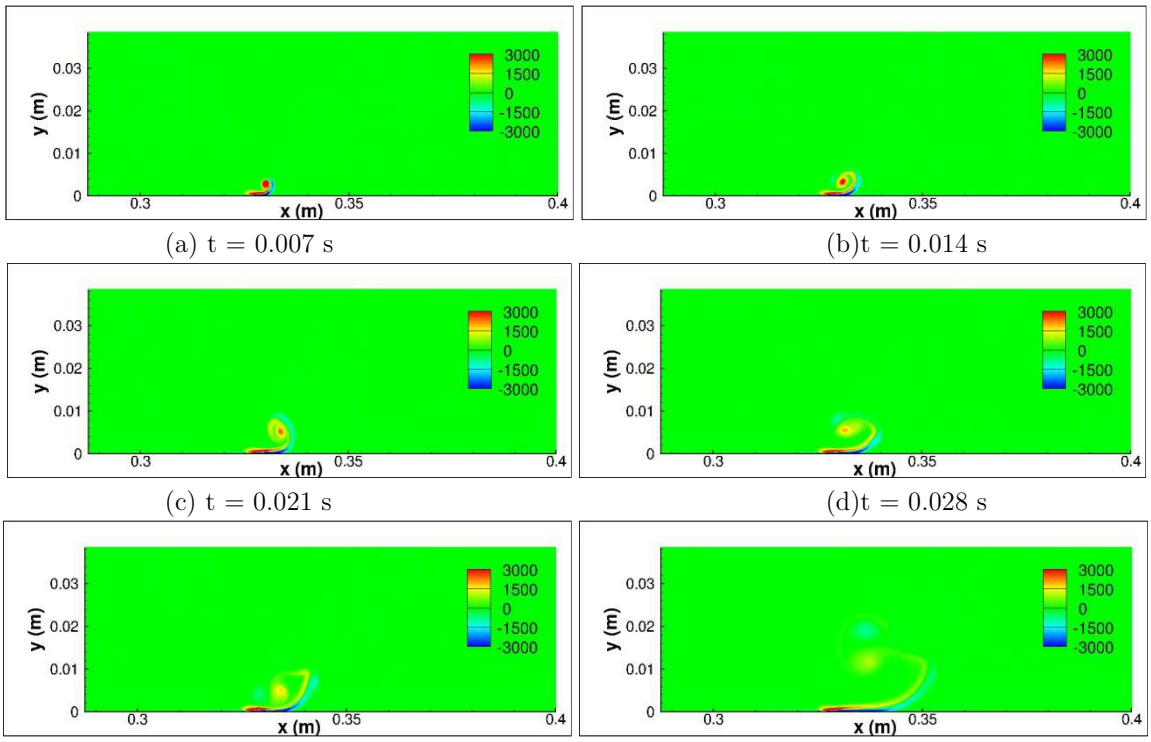

(a) t = 0.007 s (b)t = 0.014 s

(c) t = 0.021 s (d)t = 0.028 s

(e) t = 0.035 s (f)t = 0.060 s

Figure 5.14: Vorticity maps for temporal evolution of the plasma actuator wall jet in quiescent air for Power 1.

Finally, for Power 3 vorticity cores of different sizes appear at the very beginning, Figure 5.16. This fact indicates that the body force applied is strong enough to produce small vortices in the region surrounding the plasma right after the actuator is turned on. The vortices move up, in a symmetric shear, until the moment the upper recirculation breaks down into several other smaller vortexes. At $t = 0.0014\ s$, diverse small regions of high vorticity agglomerate in normal direction to the flat plate. The upper part of the group of small vorticity cores separates from the long structures near the solid surface, departing back in direction of the plasma actuator location. The zones of high and low vorticity are transported up and downstream, what indicates the presence of many vortices not only in the region very near the actuator.

Because the contour plots are maintained at the same color scale, one can notice by Figures 5.14, 5.15 and 5.16 that the use of Power 3 produces obviously higher vorticity and more vortices than Power 1 and 2. Big cores tend to be divided into smaller ones when they reach higher vorticity values. In all cases, zones of opposite vorticity are found on the bottom due to the high velocity gradients.

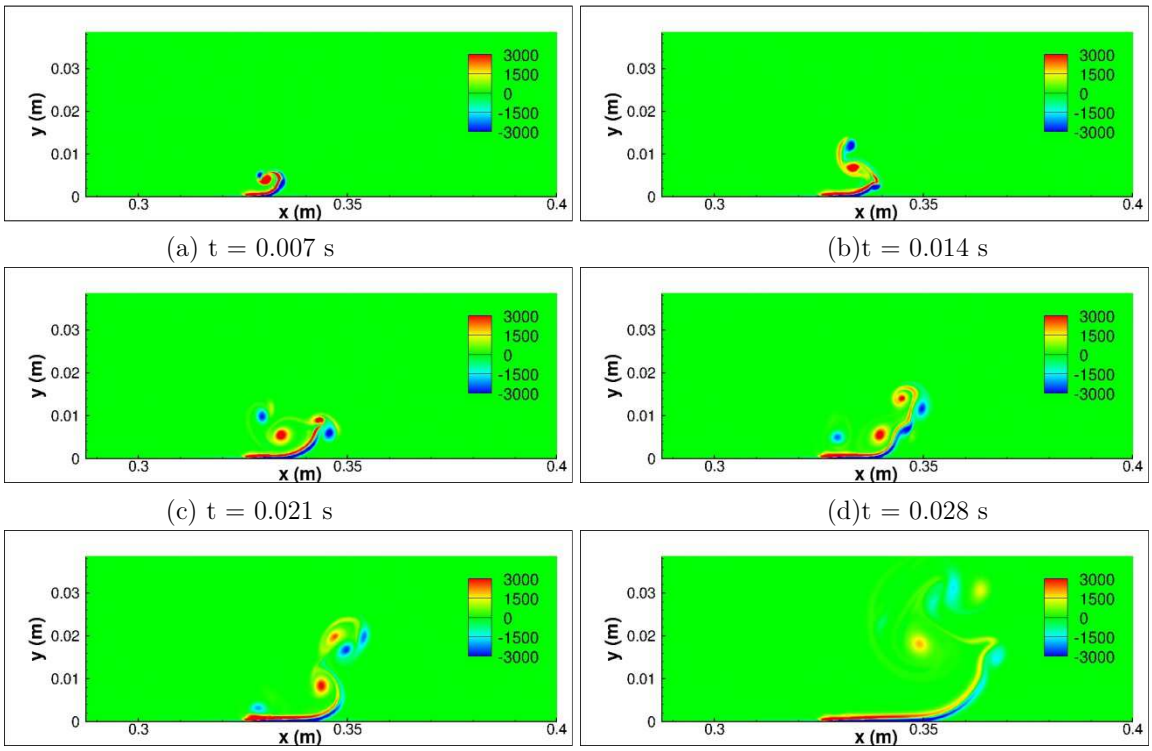

(a) t = 0.007 s (b)t = 0.014 s

(c) t = 0.021 s (d)t = 0.028 s

(e) t = 0.035 s (f)t = 0.060 s

Figure 5.15: Vorticity maps for temporal evolution of the plasma actuator wall jet in quiescent air for Power 2.

Quiescent air tests show the appearing of vortices caused by the plasma actuator wall jet. However, in a flow field the dynamic effects are dominant when there is a freestream velocity of significant magnitude, and the fluid dynamic effect of a plasma actuator cannot be characterized as a simple wall jet. It is well known from experimental investigations, that a very high power applied to the actuator may produce three-dimensional effects even at high free-stream velocities, due to the three-dimensional plasma structure which is formed. Nevertheless, no vortex or turbulent structures usually appear in a flow field due to the plasma actuator effects for the range of power which is used in the present work as an effective mean to promote boundary layer stabilization and wave cancellation. The velocity gradients found at the boundary layer are usually of a higher order when compared to the ones promoted by the presence of plasma for a relatively low power applied to the actuator. This fact would then suppress the possibility of the appearing of vortices which could disturb the turbulence control.

The effects of the plasma actuator body force in a flow field is investigated for several free stream velocities: 8, 10, 12, 14 and 16 m/s. The resulting wall jet can be evaluated by subtracting the base flow from the averaged velocity fields,

Figure 5.17. The actuator is once more positioned at $x = 0.325\,m$. For these tests, Power 1 force magnitude is applied to the actuator. The Reynolds numbers at the point where the actuator is positioned are 1.76E+05, 2.20E+05, 2.65E+05, 3.09E+05, and 3.53E+05, for 8, 10, 12, 14 and 16 m/s, respectively. As expected, for the same force magnitude applied, the wall jet is weaker for higher free stream velocities.

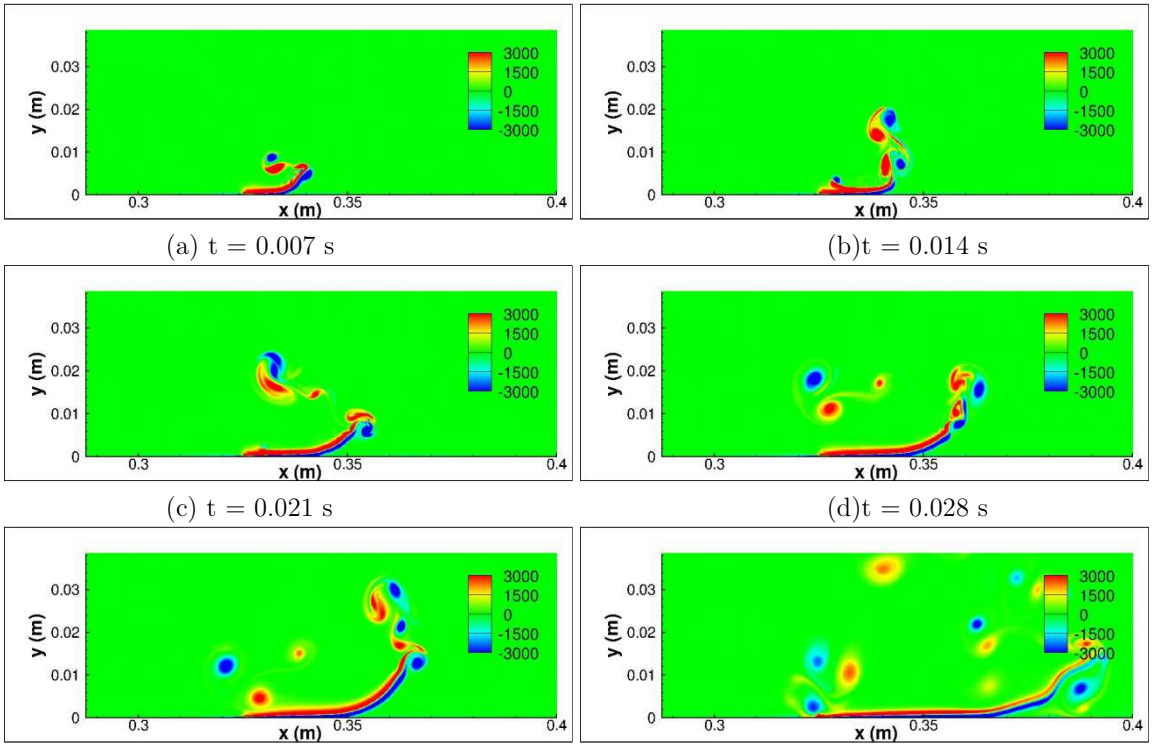

(a) t = 0.007 s (b)t = 0.014 s

(c) t = 0.021 s (d)t = 0.028 s

(e) t = 0.035 s (f)t = 0.060 s

Figure 5.16: Temporal evolution of the plasma actuator wall jet in quiescent air for Power 3.

The shape factor values are presented in Figure 5.18. A highest drop of the shape factor means that a higher influence in the boundary layer flow happens due to the presence of the actuator. For lower flow speeds, the shape factor modifications start a few centimeters upstream to the plasma actuator location. The highest drop is found for the lowest freestream velocity value, which corresponds to the strongest wall jet, in agreement with Figure 5.17. The relation between the freestream velocity and the drop of the shape factor is almost linear for the investigated cases.

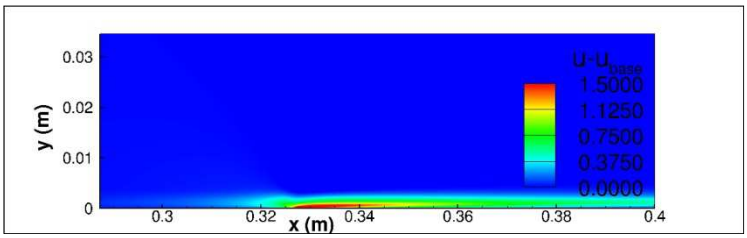

(a)8 m/s

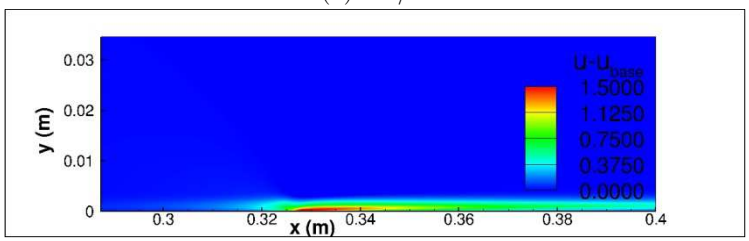

(b) 10 m/s

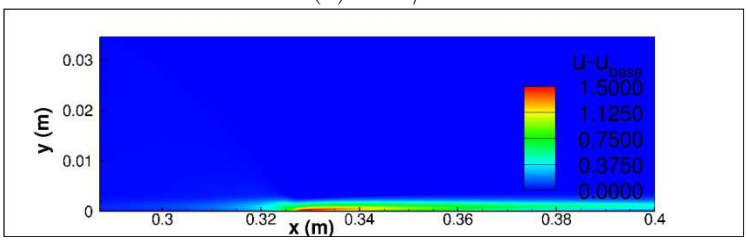

(c)12 m/s

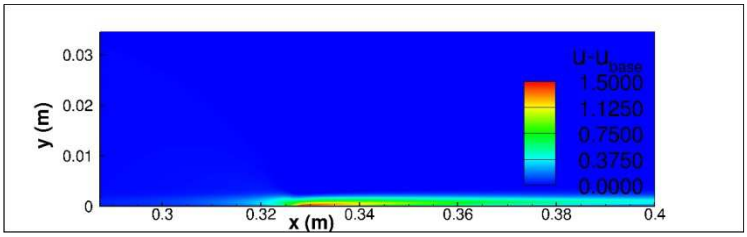

(d) 14 m/s

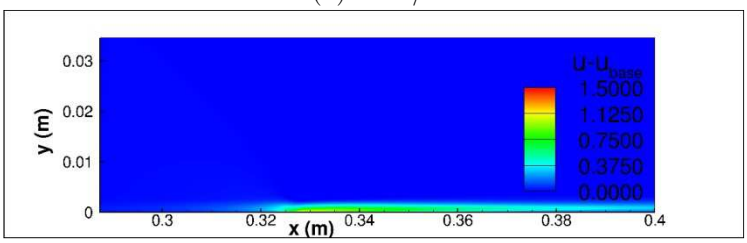

(e) 16 m/s

Figure 5.17: Contour plots for velocity fields of the wall parallel component. The pictures show the results for the time averaged field surrounding the actuator on, subtracted the base flow when the actuator is off.

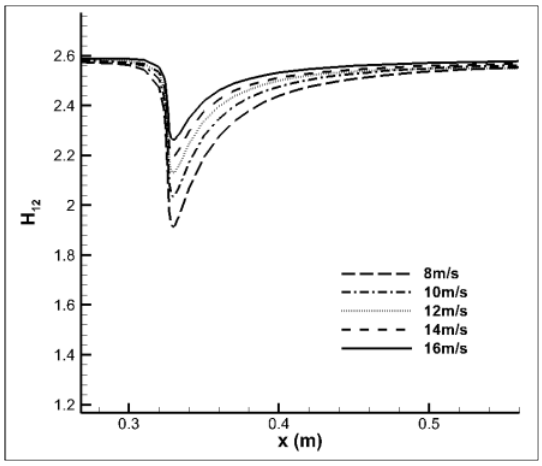

Figure 5.18: Results for the values of the shape factor along the x direction. The plasma actuator is located at x = 0.325 m.

5.4. Summary of the numerical procedures

The base flow solution evaluated with the numerical solver for the Navier-Stokes equations was compared to the theoretical Blasius solution. The results are in good agreement. Artificial disturbances were excited at the laminar boundary layer. These disturbances were amplified downstream, leading to Tollmien-Schlichting waves. The wave patterns were verified and the growth rates for the waves were compared to the Laminar Stability theory. A good agreement between the solutions evaluated from the theory and simulations was found for the finest numerical grid and the highest height of the computational domain. The natural wave amplification is a fluid dynamic phenomenon which requires high accuracy and minimal diffusive effects. The use of a diffusive scheme (such as Upwind) leads to unphysical damping of the flow disturbances, as well as a course grid. The range of amplification of the dominant frequencies was also compared to the theory and a good agreement was found. The final configuration, which was derived from all these initial steps, provided a suitable environment for reliable numerical simulations of the plasma actuator effects.

Experimental data were used to provide precise information about the body force intensity and location. The body force field was also interpolated and implemented in the numerical solver. Quiescent air test cases show the behavior of the wall jet departing from the plasma actuator and the appearing of small turbulent structures. The numerical simulations of the plasma actuator immersed in a boundary layer flow reveal the influence of the fluid acceleration according to

the free-stream velocity and power magnitude applied to the actuator. Shape factor modifications and fluid acceleration near the solid surface are higher for lower free-stream velocities.

6. Boundary-layer stabilization

The test cases presented in this chapter aim to investigate the stabilizing effect of a plasma actuator in a flat-plate boundary layer flow. The actuator is operated in continuous mode, promoting a modification of the velocity profile. In all cases, the disturbance excitation position is maintained at $x = 0.225$ m, and the wave damping caused by the actuator is quantified. The integral values of power supply which is applied to the actuator are previously described in Chapter 4. The influence of control parameters is verified for several actuator positions, with the respective Reynolds number at the two free stream velocities investigated:

- PA1: $x = 0.325$ m, $Re_x = 3.53E+05$ (16 m/s), $Re_x = 2.20E+05$ (10 m/s)
- PA2: $x = 0.375$ m, $Re_x = 4.07E+05$ (16 m/s), $Re_x = 2.54E+05$ (10 m/s).
- PA3: $x = 0.425$ m, $Re_x = 4.61E+05$ (16 m/s), $Re_x = 2.88E+05$ (10 m/s)
- PA4: $x = 0.475$ m, $Re_x = 5.16E+05$ (16 m/s), $Re_x = 3.22E+05$ (10 m/s)
- PA5: $x = 0.525$ m, $Re_x = 5.70E+05$ (16 m/s), $Re_x = 3.56E+05$ (10 m/s)

6.1 Influence of power supply

Test cases used to study the influence of the force magnitude applied to the actuator over the boundary layer flow are performed at two different flow speeds 10 m/s and 16 m/s, using one single actuator positioned at PA1.

Figure 6.1 shows results for the maximum amplitude of the disturbances using different forcing applied to the actuator with 10 m/s of free stream velocity. The use of low power (Power 1) promotes good wave attenuation until a distance about 0.1 m from the actuator position, the waves are damped until about $x = 0.425$ m. Ensuing this point and further downstream, the disturbances grow once more. Such a behavior is not observed for the other power supplies Power 2 and Power 3. The amplitude of the disturbances keeps decaying downstream the actuator position. For these two last cases, the disturbances attenuation is strong enough to avoid that any Tollmien-Schlichting

wave can develop downstream again. It can also be noticed, that the wave attenuation starts early upstream for the cases of higher power consumption.

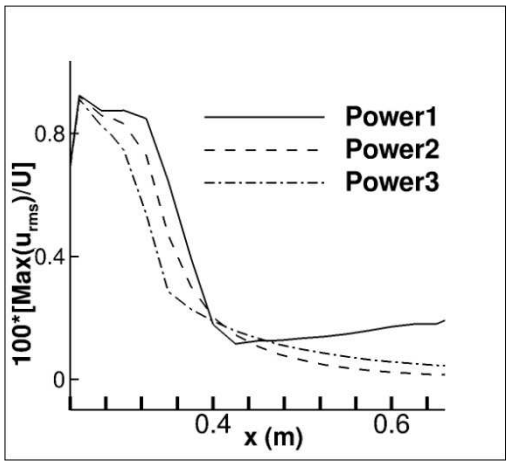

Figure 6.1: Maximum amplitude of the TS waves. Three different power supplies applied to one single actuator at position PA1, 10 m/s of free stream velocity. TS wave frequency of 110 Hz.

One interesting fact is found with the results for the highest power applied to the actuator: values for the amplitude of the maximal disturbances far downstream of the plasma actuator, at $x = 0.60$ m, with Power 3, are slightly higher than those values at the same location evaluated with Power 2. Before these investigations, it was expected that as higher the power is applied to the actuator, the lower should be the amplitude of the flow disturbances. One possible explanation for this phenomenon is the arising of additional disturbances, due to the strong forcing applied to the flow, together with the presence of TS waves.

For a better comprehension of this case, Figure 6.2 shows the averaged fluctuation profiles (U_{rms}) inside the boundary layer region at several locations. Results evaluated with Power 1 show the usual shape for a TS wave even for the region far downstream of the actuator position. For an actuator which is operated at Power 2 or Power 3, the U_{rms} profiles reveal the presence of a disturbance which has a maximum at the same position in y as the neutral point found for Power 1, Figure 6.2-d. From Figure 6.1, it is known that these disturbances also tend to progressively vanished downstream. The appearing of such waves occurs right downstream the actuator, after the TS wave attenuation process. The location in y where the TS wave has a maximum amplitude is moved up due to the influence of the plasma actuator. The magnitude of these disturbances is relatively small (about 10 %) when compared to the non-controlled TS waves. The velocity fluctuations in certain analyzed regions seem to be similar to the velocity fluctuation profiles found for a periodic disturbance after passing a wall jet, [De04]. Such

similarities may suggest that the boundary layer region under influence of the actuator presents a local combined effect which is able to promote the excitation of a secondary instability in a very limited region.

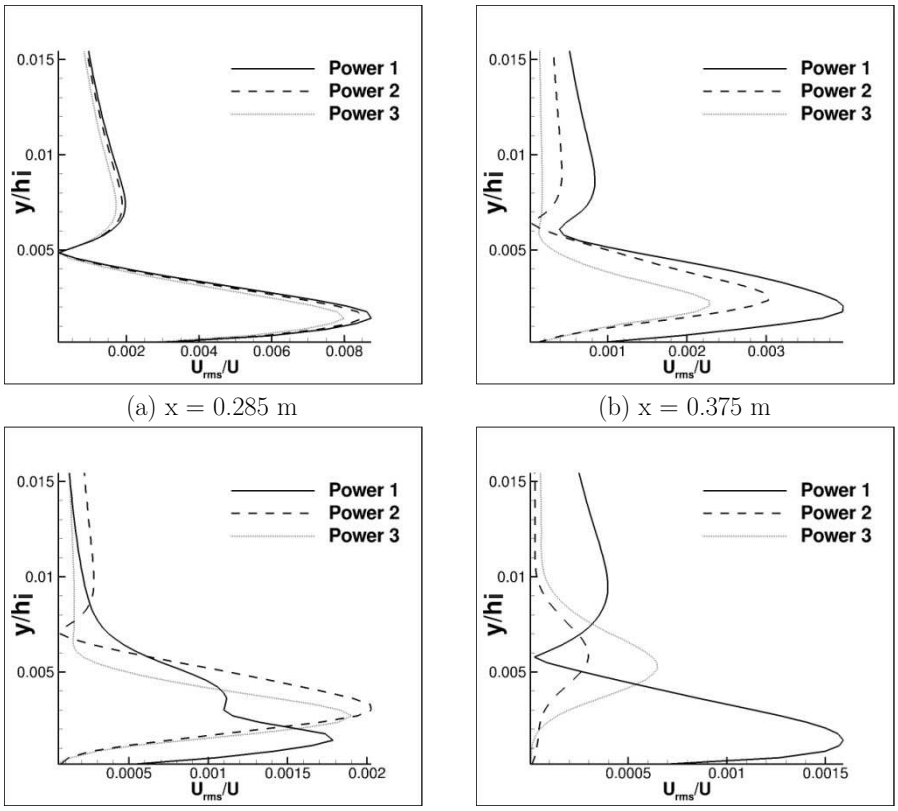

(a) x = 0.285 m (b) x = 0.375 m

(c) x = 0.400 m (d) x = 0.575 m

Figure 6.2: Profiles of the quadratic mean of the wall parallel velocity component inside the boundary-layer flow at several locations, 10 m/s.

Figure 6.3 show the contour maps for the fluctuations of the wall parallel velocity component with a free stream flow velocity of 10 m/s, actuator at position PA1 and different power supply. The use of Power 1, Figure 6.3-a, produces more accentuated wave damping at the upper part of the wave, which is deformed right downstream the actuator. Positive and negative velocity fluctuations take a different configuration, due to the wave distortion. For Power 3, Figure 6.3-b, after passing by the actuator region (marked with a small black line), the waves are strongly elongated. The spatial wave length of a TS wave downstream the actuator has about three times the wave length of the same wave upstream the actuator. Such modifications caused by the higher power applied to the actuator can strongly alter the velocity profile and stability proprieties of the boundary layer. The contour plots of Figure 6.3 show clearly the disturbances found in Figure 6.2.

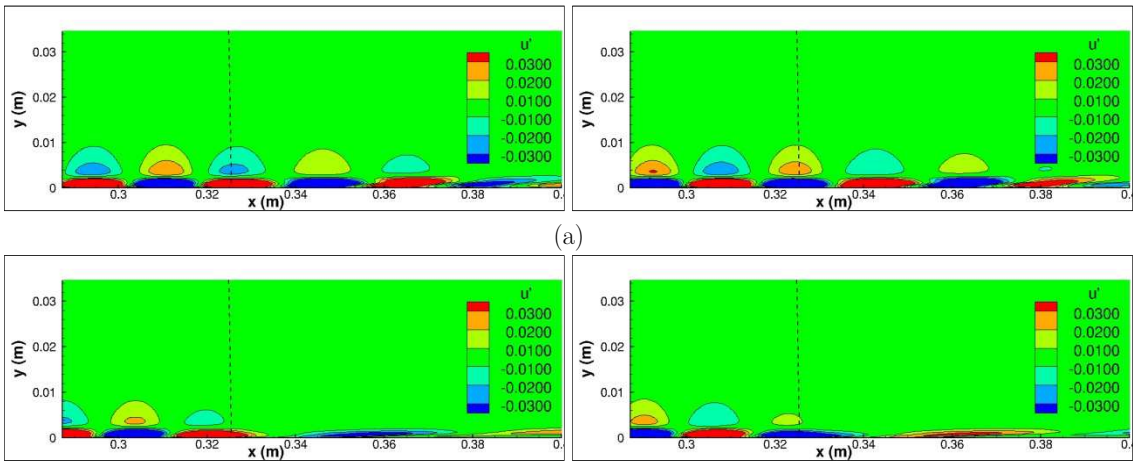

(a)

(b)

Figure 6.3: Contour maps for the wall parallel velocity component for 10 m/s free stream velocity. (a) Power 1 and (b) Power 3.

Figure 6.4 shows contour plots of the wall normal velocity profiles for the same test case with free stream velocity of 10 m/s and actuator operated at different power magnitudes. The wall normal velocity fluctuations are found to be about one order smaller than the velocity fluctuations in the wall parallel direction. The wall normal component of the velocity fluctuations nearly vanishes after passing the accelerated flow zone.

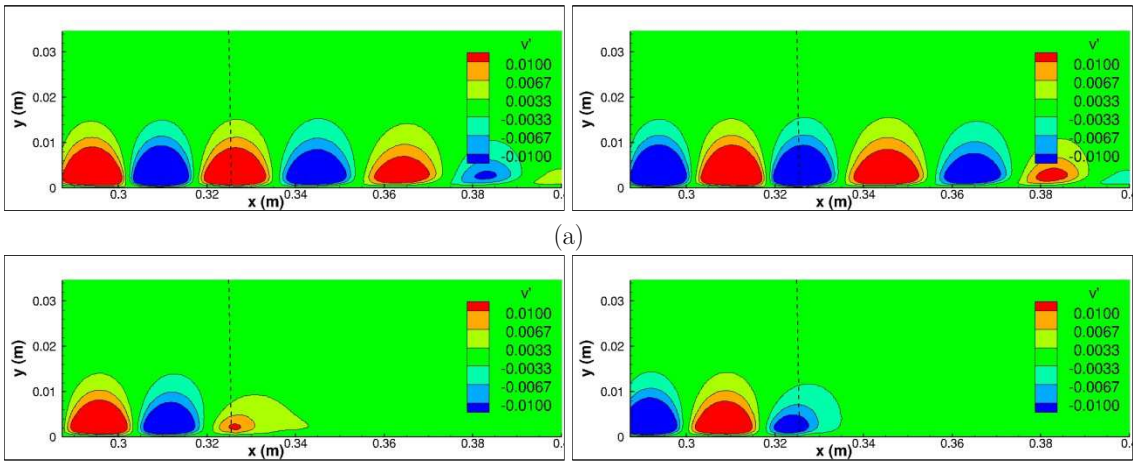

(a)

(b)

Figure 6.4: Contour maps for the wall normal velocity component for 10 m/s free stream velocity, (a) Power 1 and (b) Power 3.

The previous tests were repeated for a higher free stream velocity of 16 m/s. Results show that the higher flow velocity smoothes the effects of a too strong body force applied to the plasma actuator. In Figure 6.5 the maximum amplitudes of the disturbances are plotted along the x direction. The actuator is once more positioned at PA1 and is

operated at the three different power magnitudes. The disturbances are excited at $x = 0.235$ m at 220 Hz. Results show that for Power 1 and Power 2 the artificially excited waves growing downstream of the excitation point until the location of the actuator. These waves are then attenuated downstream of the actuator location for a distance of about 5-7 cm. For Power 3, the artificially excited waves are not re-amplified downstream the excitation point. The effect of the body force is strong enough to inhibit natural growth of disturbances, Figure 6.5. Amplitudes remain at almost a constant value until the proximity of the actuator, differently from the previous case, where the waves start being damped right before the excitation point for Power 3. For free stream velocity of 16 m/s, the attenuation process starts at a short distance upstream the actuator location. The strong attenuation effect obtained with Power 3 avoids the later growing of the Tolllmien-Schlichting waves, different from the cases with Power 1 and Power 2, where the waves restart to grow downstream. But differently from the case with lower flow speed, there is not strong modification of the wave length or distortion of the TS waves into a different disturbance.

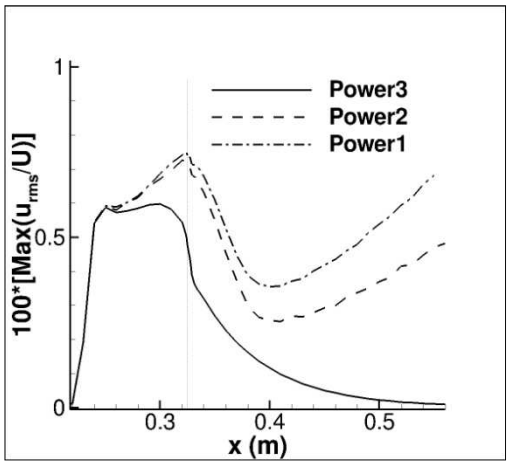

Figure 6.5: Maximum amplitude of the TS waves along x direction. Three different power supplies applied to one single actuator at position PA1, 16 m/s of free stream velocity.

Similarly to Figures 6.3 and 6.4, Figures 6.6 and 6.7 present the contour maps for velocity fluctuations in wall-normal and wall-parallel directions for a flow with 16 m/s. The effects of wave elongation are also found however, in smaller scale and for a higher speed.

The interesting behavior of a strong forcing applied to the flow by the plasma actuator operating with a higher power (Power 3) can also be explained by the change in the shape factor values, Figure 6.8-a. One can notice the elevation of the shape factor values upstream the actuator position for Power 3. The drop of the shape factor for such

strong power magnitude also occurs at a short distance upstream the point where it is expected to happened for a weaker forcing. Power 1 and Power 2 result in quite similar shape factor values, but the values obtained for Power 2 are somewhat lower. Further downstream the actuator position, at about $x = 0.50$ m the shape factor values are smaller than the values found for the region upstream the actuator using Power 1 and Power 2. This difference is more pronounced for Power 3. The considerable modification of the shape factor also changes the stability flow proprieties downstream the actuator, and consequently, the waves are not more amplified for high power cases.

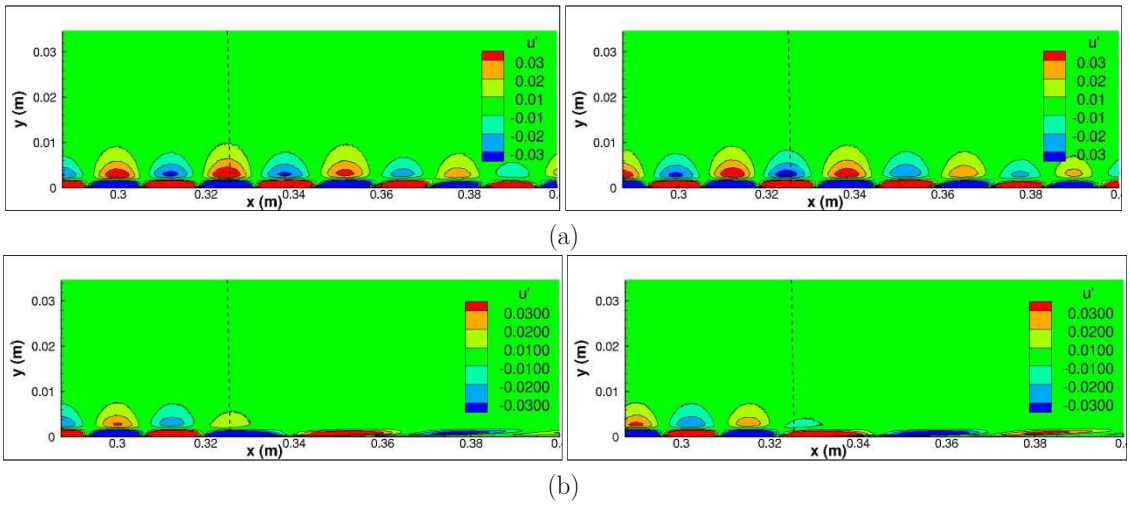

(a)

(b)

Figure 6.6: Contour maps for the wall parallel velocity component for 16 m/s free stream velocity, (a) Power 1 and (b) Power 3.

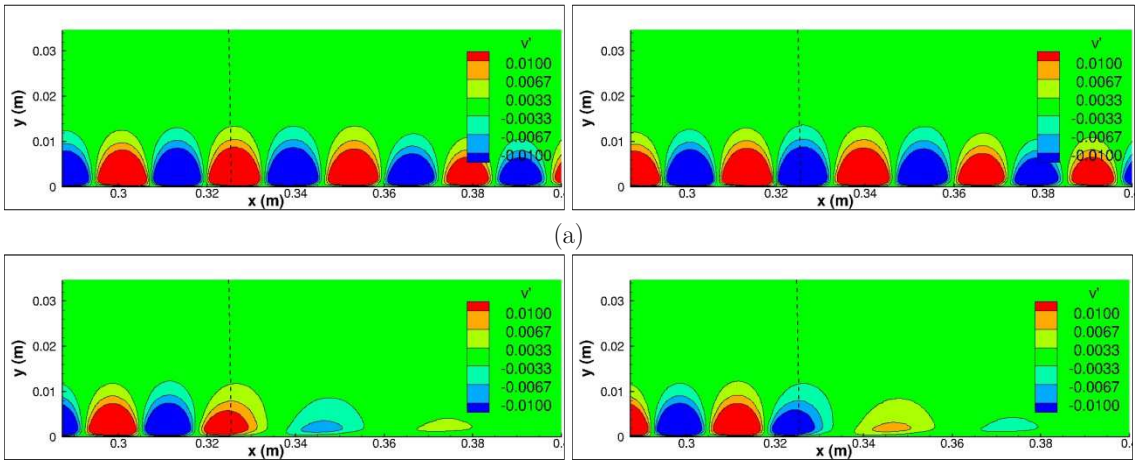

(a)

(b)

Figure 6.7: Contour maps for the wall parallel velocity component for 16 m/s free stream velocity, (a) Power 1 and (b) Power 3.

A comparison between the weakest and strongest power magnitude applied to the actuator is presented in Figures 6.8-b and c. The corresponding averaged velocity profiles

are plotted in the non-dimensional form. The velocity profiles obtained with Power 1 do not show significant differences, Figure 6.8-b.

Even though a significant wave attenuation can be obtained with this configuration, see Figure 6.5, and also significant drop of the shape factor values, only very small modifications occur in the boundary layer velocity profile, which are imperceptible in Figure 6.8-b. A different trend is seen for the use of Power 3 applied to the actuator, see Figure 6.8-c. The velocity profile at the plasma actuator location ($x = 0.325\,m$) shows an accentuated curvature near the flat plate. Downstream of the actuator position, the acceleration of the boundary layer profile is concentrated at the upper part, away from the solid surface.

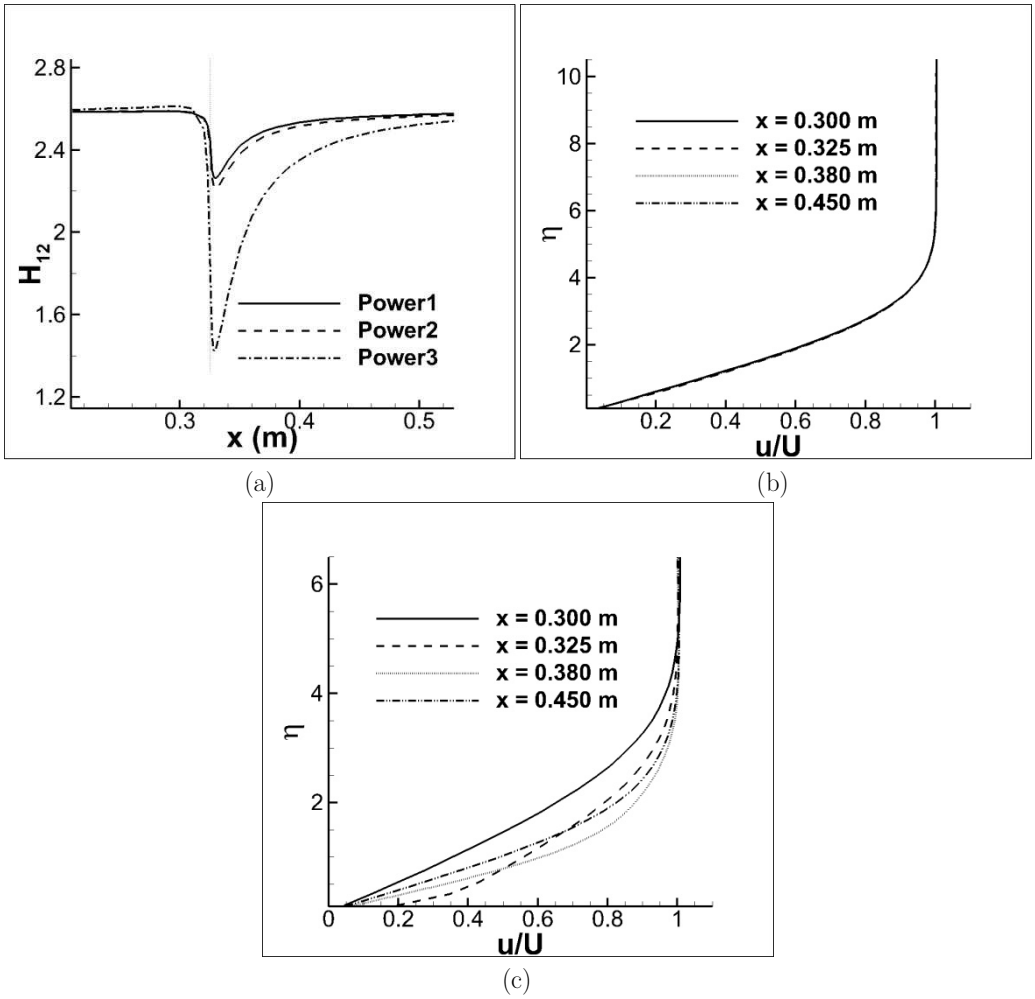

Figure 6.8: Analyzed results for 16 m/s free stream flow. (a) Shape factor for several power supplies. (b) Averaged velocity profiles for Power 1. (c) Averaged velocity profiles for Power 3.

The analysis of the first and second derivatives for the cases with Power 1 and Power 3 applied to the actuator in a free-stream flow of 16 m/s, Figure 6.9, show that higher peaks are produced by higher power applied to the actuator.

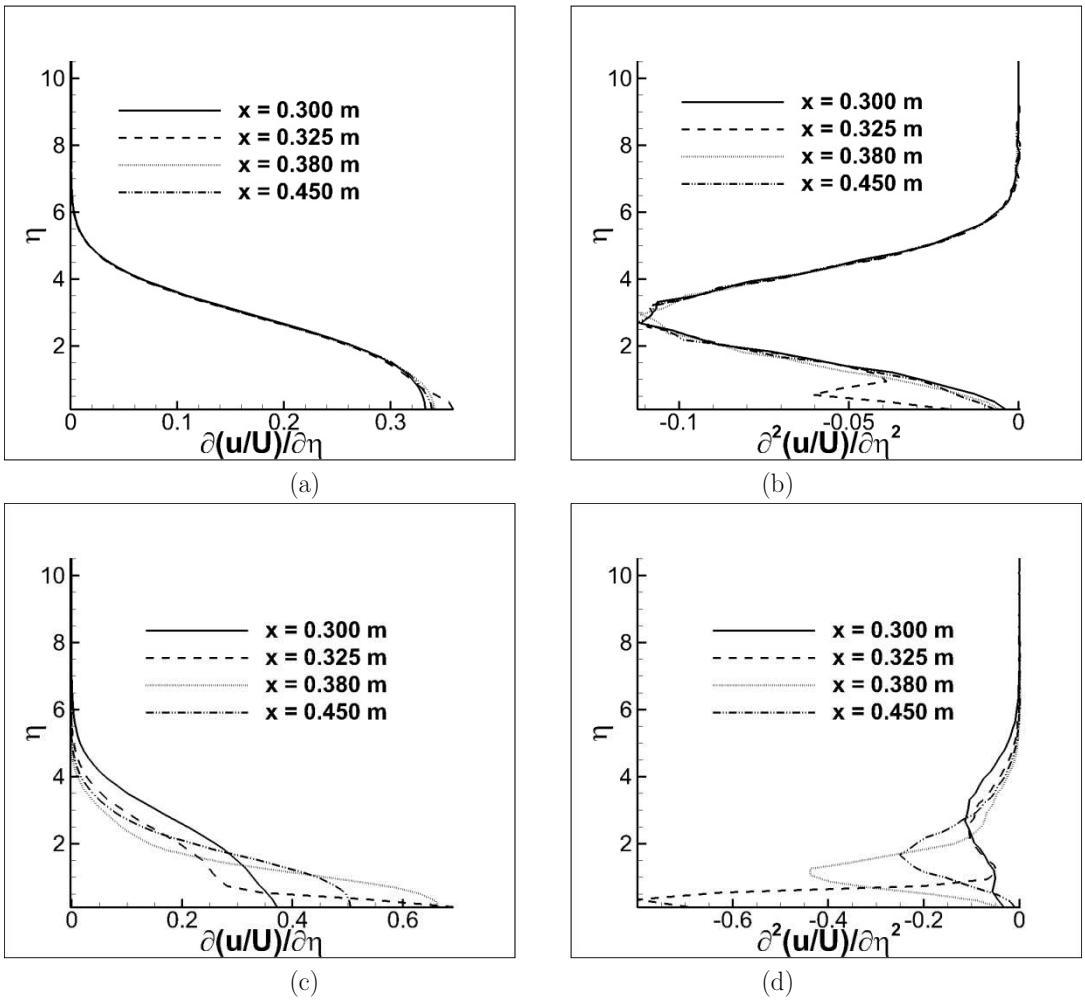

Figure 6.9: Derivatives profiles in several locations for the flow with 16 /s of free-stream velocity. (a) First derivative for Power 1 applied to the plasma actuator. (b) Second derivative for Power 1 applied to the actuator. (c) First derivative for Power 3 applied to the actuator. (d) Second derivative for Power 3 applied to the actuator.

The first derivative profiles for Power 1 applied to the actuator, Figure 6.9-a, are very similar, except for $x = 0.325$ m, which is the exact location where the plasma actuator is positioned. A very different scenario is found for the case Power 3, Figure 6.9-c. The first derivative profile at x =0.300 m has a maximum value similar to the previous case with lower power. But at the actuator location, x =0.325 m, the first derivative has a very different profile and its maximum value is about twicef the value found for the case with lower power supply. Such strong modification is also noticed further downstream at $x = 0.380$ m, and weakly at $x = 0.450$. For Power 1, Figure 6.9-b, the second derivatives also show similar profiles except for the location of the plasma actuator, where a small peak appears near the flat plate. For Power 3, Figure 6.9-d, the second derivative profile at the actuator location has a negative peak near the flat plate which is smoothed downstream. Higher peaks, which overcome the derivative values found for a

base flow without actuation, represent very strong modification in the boundary layer profiles and may inhibit the growing of velocity disturbances which travel downstream. The presence of negative curvature in the velocity profile corresponds to a stabilizing effect of the boundary layer flow.

For the boundary-layer flow promoted by a free-stream velocity of 16 m/s, such peaks of the derivative profiles are of lower magnitude, and they do not cause the destruction of the typical Tollmien-Schlichting velocity profile, as shown in Figure 6.10.

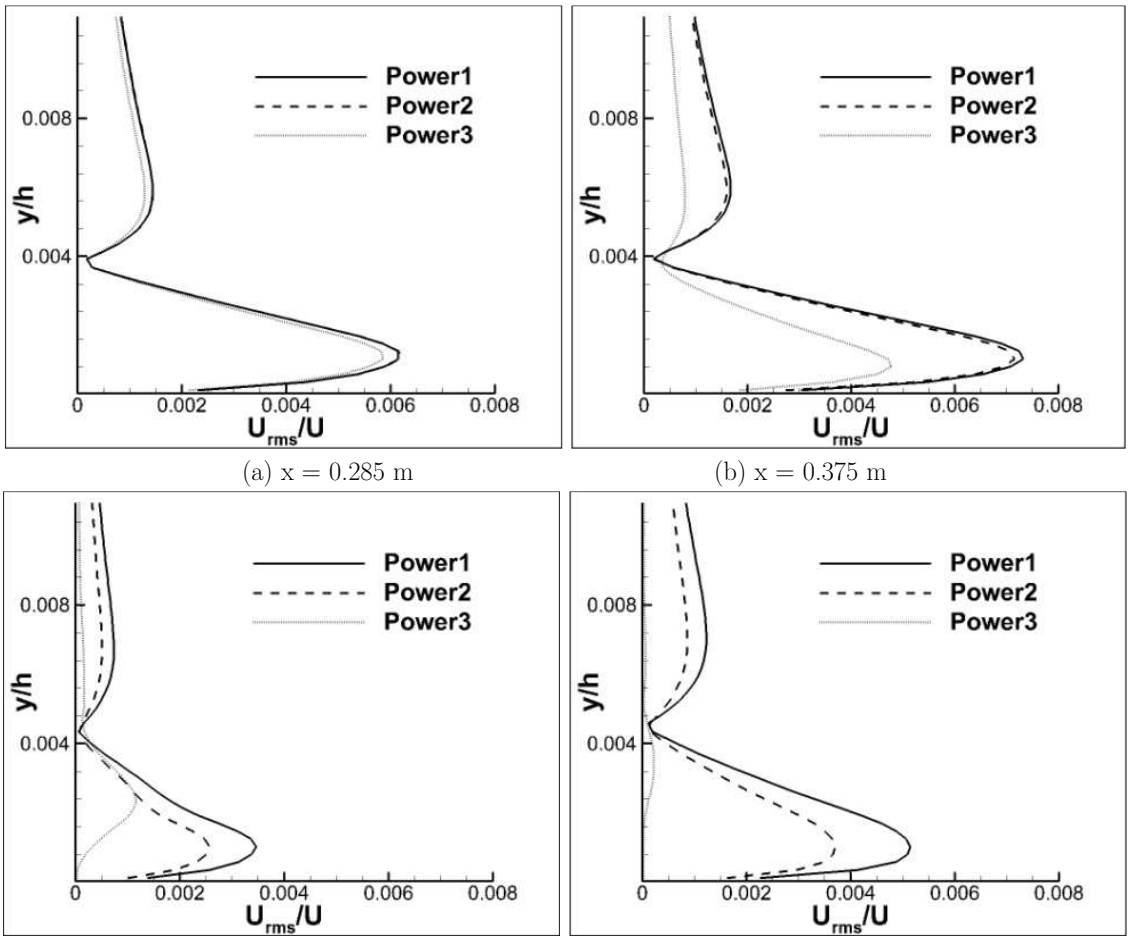

(a) x = 0.285 m (b) x = 0.375 m

(c) x = 0.400 m (d) x = 0.500 m

Figure 6.10: Profiles of the quadratic mean of the wall parallel velocity component inside the boundary-layer flow at several locations, 16 m/s.

Tollmien-Schlichting wave attenuation is stronger for Power 2 than for Power 1, because the maximum amplitudes reached downstream the actuator position are smaller, Figure 6.10-c and d. For Power 3, the wave attenuation is plenty stronger; the final amplitude of the Tollmien-Schlichting waves is almost one order of magnitude smaller. The maximum amplitude for higher power applied to the actuator is also elevated up from the flat plate in response to the strong wall jet. Between $x = 0.400$ m and

$x = 0.500$ m the waves return to grow for lower power, Power 1 and Power 2, but keep decreasing for Power 3.

The influence of the power magnitude applied to the actuator can also be verified in the spectral analysis of the frequencies found in the flow, Figures 6.11 and 6.12.

The Tollmien-Schlichting wave frequency for the previous tests is 220 Hz, excited in a 16 m/s flow. Results for the wall parallel velocity component at $y = 0.0004$ m from the flat plate show a small peak of the first harmonic frequency which is found in the region in front of the actuator location at $x = 0.300$ m for Power 1 and Power 3 applied to the actuator.

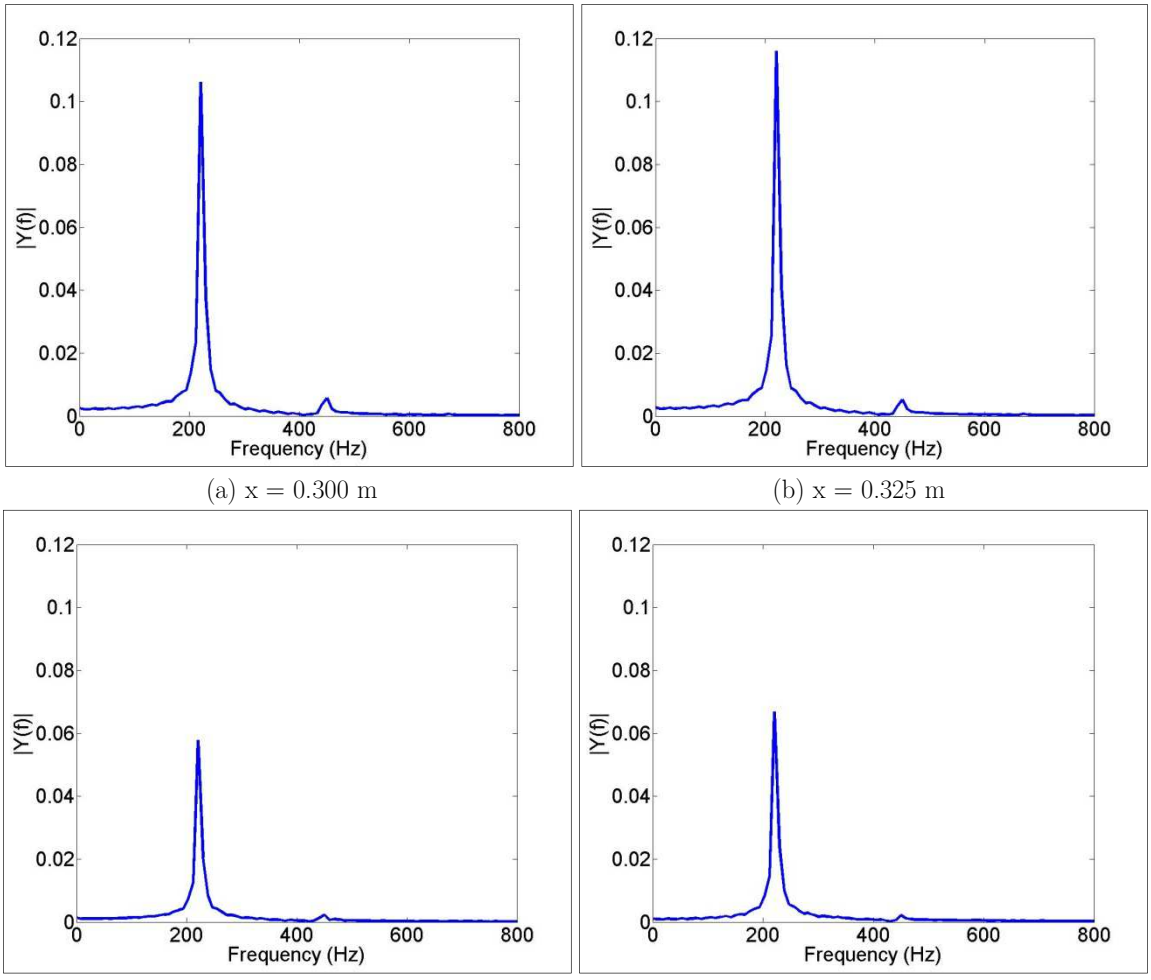

(a) x = 0.300 m (b) x = 0.325 m

(c) x = 0.380 m (d) x = 0.450 m

Figure 6.11: Fast Fourier Transformer of the wall parallel velocity component, Power 1 applied to the plasma actuator.

The dominant frequency 220 Hz has a higher peak which increases until the actuator position, $x = 0.325$ m, for Power 1. Downstream the actuator position, the frequency peak decreases, $x = 0.380$ m, but returns to be amplified at $x = 0.450$ m for Power 1,

while for Power 3 the values for the first harmonic peaks are negligible. For Power 3, the strong influence of the actuator suppresses nearly all frequency peaks, which have an insignificant magnitude downstream the actuator position, $x = 0.350$ m and $x = 0.450$ m. Even with a strong forcing, no other flow disturbance is promoted by the plasma actuator for this configuration.

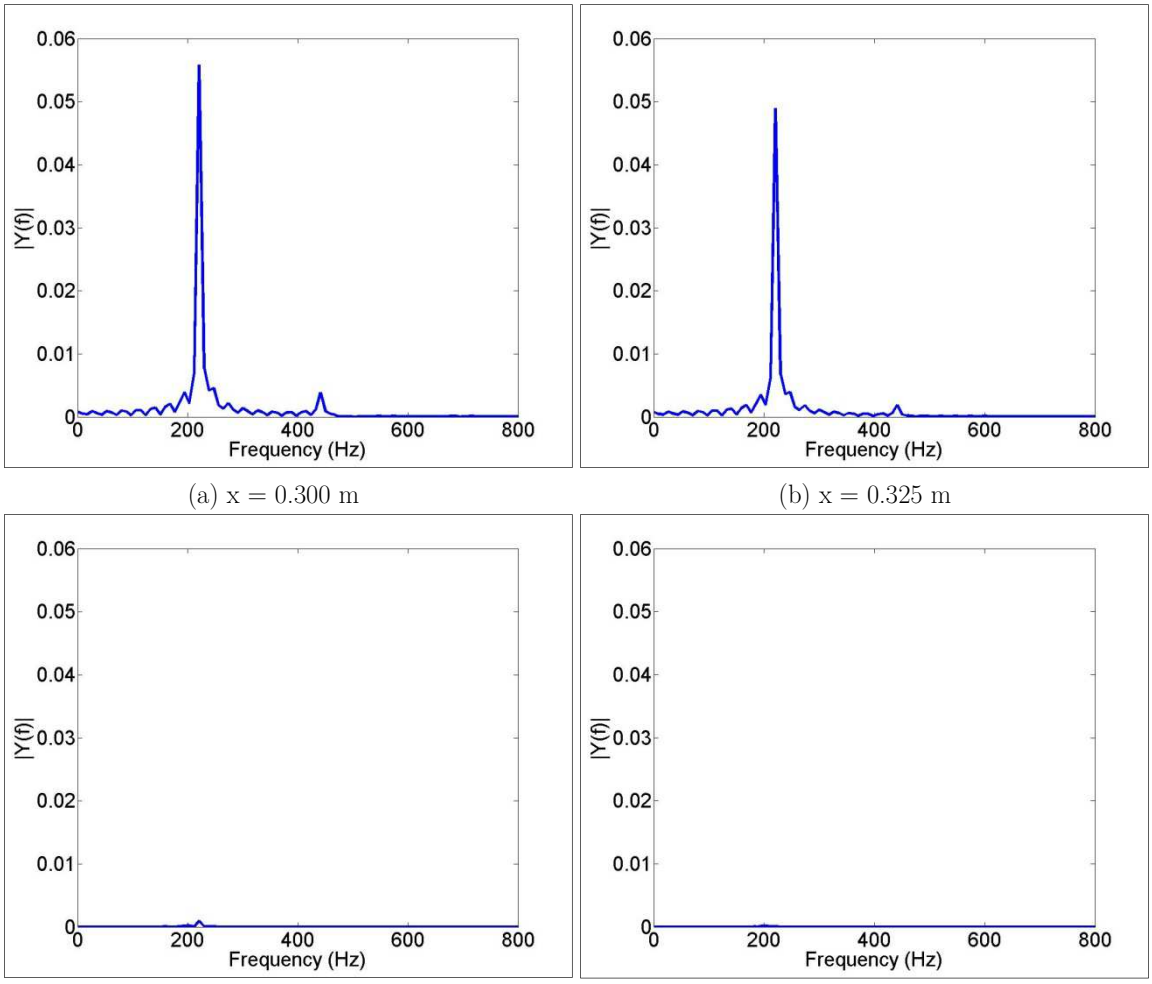

(a) x = 0.300 m

(b) x = 0.325 m

(c) x = 0.380 m

(d) x = 0.450 m

Figure 6.12: Fast Fourier Transformer of the wall parallel velocity component, Power 3 applied to the plasma actuator.

The influence of the power magnitude applied to the plasma actuator is also verified at the wave propagation speed. An estimation of the wave convective speed is evaluated using two probes which were separated by a short distance one from the other (0.01 m). The time necessary for a wave peak to pass by both probes was evaluated. For lower speed tests, Table 6.1, Power 1 caused an increasing of the wave speed of about 5 % of the free-stream velocity, while Power 3 promoted an increasing almost ten times bigger. In both cases, the wave speed is already accelerated even upstream the actuator position,

at $x = 0.280$ m, when compared with the base flow case. Higher power applied in low speed promotes, at most downstream positions, very small disturbances magnitudes which do not correspond to the correct shape of a TS wave. For that reason the results for wave convective speed at $x = 0.400$ m and $x = 0.500$ m are not presented in Table 6.1.

Table 6.2 presents similar results for a free-stream velocity of 16 m/s. The wave acceleration can be noticed in front of the actuator only for Power 3. At the actuator position $x = 0.325$ m, the influence of Power 1 promotes a small wave acceleration about 2.5 % of the free-stream velocity. Power 3, at the same position, causes an acceleration of about 20 % of the free-stream velocity which increases downstream up to values near the free-stream velocity. Accentuated deceleration occurs at $x = 0.400$ m for Power 1, at the coincident position where the waves return to grow and the zone of influence of the actuator becomes weaker.

The influence of the plasma actuator at the wave propagation speed is strongly dependent on the free-stream velocity and the force magnitude which is applied to the actuator. The changes found for the wave propagation speed in the previous cases indicate significant modifications of the stability of the flow promoted by the actuator, once the boundary layer velocity profile is also modified. The experimental work of Duchmann [Du12] showed an increased phase speed in order of 10% for pulsed operation of the plasma actuator, which is also in agreement with the Linear Stability Analysis.

Position	x = 0.280 m	x = 0.300 m	x = 0.325 m	x = 0.350 m	x = 0.400 m	x = 0.500 m
Base flow	3.40 m/s	3.40 m/s	3.71 m/s	3.70 m/s	3.70 m/s	3.71 m/s
Power 1	3.44 m/s	3.49 m/s	3.99 m/s	4.13 m/s	3.64 m/s	3.67 m/s
Power 3	3.54 m/s	3.51 m/s	9.07 m/s	6.75 m/s	-	-

Table 6.1: Results for wave convective speed in a boundary layer flow with a free-stream velocity of 10m/s.

Position	x = 0.280 m	x = 0.300 m	x = 0.325 m	x = 0.350 m	x = 0.400 m	x = 0.500 m
Base flow	5.43 m/s	5.44 m/s	5.58 m/s	5.58 m/s	5.55 m/s	5.54 m/s
Power 1	5.43 m/s	5.52 m/s	5.92 m/s	5.81 m/s	5.31 m/s	5.52 m/s
Power 3	5.53 m/s	5.58 m/s	8.90 m/s	6.93 m/s	8.60 m/s	13.91 m/s

Table 6.2: Results for wave convective speed in a boundary layer flow with a free-stream velocity of 16m/s.

6.2. Influence of the actuator's position

The aim of the following investigations is to verify if the position along x direction of a single actuator inside the boundary layer region has any influence on the Tollmien-Schlichting wave attenuation rate. First test cases are with 10 m/s free-stream velocity and Power 1 applied to the actuator. Results obtained for the maximum value of the disturbances along x direction are shown in Figure 6.13. The wave attenuation effect of one single actuator is investigated at several positions: PA1, PA2, PA3, PA4 and PA5 (defined in the beginning of this chapter). At $x = 0.325$ m, PA1, the wave amplitude has a U_{rms} value of about 0.8 % of the free-stream velocity. This value is found to be higher for tests with actuators at different positions, due to the natural exponential wave amplification.

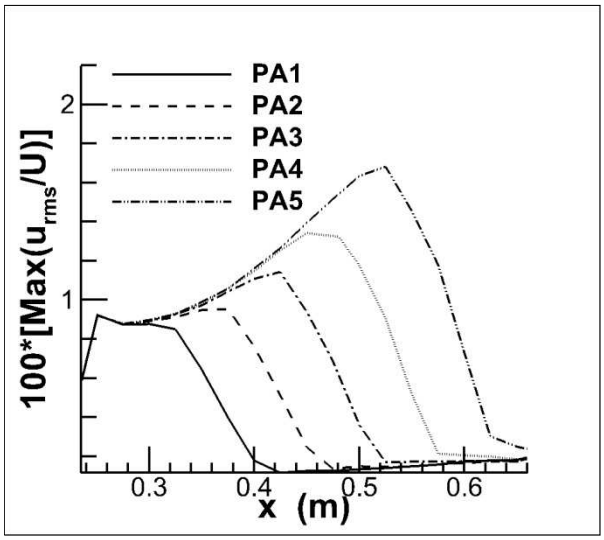

Figure 6.13: Maximum wave amplitudes for Power 1 applied to the actuator in several positions, 10 m/s of free-stream velocity.

The attenuation rate is evaluated as follows:

$$R = 100 * (1 - (A2/A1)) \tag{6.1}$$

Where R is the percentage of wave attenuation, $A2$ is the disturbance amplitude after actuation and $A1$ is the wave disturbance amplitude at the same location for the non-controlled case (natural wave amplification). Both, A1 and A2, are evaluated 0.1 m downstream of each actuator position. Table 6.3 presents results for the cancellation rates obtained.

Actuator Position	$\frac{A2}{A1}$	R
PA1	0.11	90.95
PA2	0.11	91.19
PA3	0.11	91.08
PA4	0.10	90.55

Table 6.3: Wave cancellation rates at 10m/s.

The maximum achievable attenuation-rate remains almost the same, about 90%, for all tested positions. A single plasma actuator performance in terms of wave attenuation is not strongly depending on its streamwise position inside the laminar region, due to the linear proprieties of the flow stability.

Similar tests were performed for a much weaker influence of the actuator, with only 40% of the Power 1 force magnitude, in a 16 m/s free-steam flow with TS waves at 220 Hz. The reason for this repetition in a different setup is to verify if the linearity found for the cancellation rate is due to the strong forcing, the existence of a limiting value for such effect, and the persistence of the same effects in a higher speed flow. Lower forcing applied to the actuator would also allow the observation of the further development after a first attenuation, despite the complete elimination. Results for the maximum disturbance amplitude are given in Figure 6.14 and the wave attenuation rates in Table 6.4.

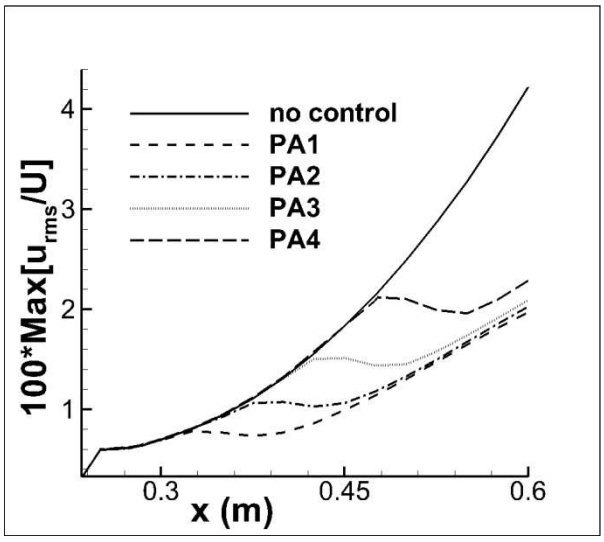

Figure 6.14: Maximum wave amplitudes with 40 % of Power 1 applied to the plasma actuator in several positions, 16 m/s of free-stream velocity.

One can notice, in Figure 6.14, that about 10 cm downstream the actuator position the attenuation effect is stronger, and downstream this point, the waves start to be

amplified once more. At the location where the waves restart to grow, for all actuator positions investigated, the inclination angle of the curves is apparently similar. The rate of the wave attenuation effect is slightly better at PA2, Table 6.4. However, this value is a ratio of the wave amplitude after actuation and the value for the wave amplitude at the same location for the uncontrolled case.

Actuator Position	$\frac{A2}{A1}$	R
PA1	0.55	44.43
PA2	0.55	44.65
PA3	0.56	44.05
PA4	0.57	43.04

Table 6.4: Wave cancellation rates at 16m/s.

Even there are only small differences among the wave attenuation rates at the four actuator locations the exponential growth of the TS wave promotes an absolute value of the wave amplitude which is higher at downstream positions. Higher amplitude of the TS wave is undesired, as for a certain value the appearance of second unstable modes is unavoidable. Thus, to keep the TS wave amplitude low is the aim for delaying transition to turbulence. Therefore, notwithstanding the wave attenuation rates have almost the same values for all actuator positions; the use of one single actuator at positions PA1, PA2 and PA3 may produce a longer transition delay than at PA4. This could not be observed in the previous case for a lower flow velocity due to the very strong forcing applied to the actuator which inhibits the further wave growth. For practical purposes, one can say that the effect of a single actuator is independent of its position in x direction when considering the related wave amplitude for the uncontrolled case, or that the additional stability promoted is the same. But for transition delay purposes, with low power applied to the actuator, it is of higher advantage to use the actuator at positions PA1 and PA2.

Figure 6.15 shows the values for the shape factor evaluated along the flat plate for the flow influenced by one single actuator at several positions.

The shape factor values remain about 2.59 in the region in front of the actuator position which is the theoretical value for a zero pressure gradient boundary layer flow (Blasius solution). A few millimetres upstream the actuator, the values for the shape factor start to decrease, reaching a minimum immediately downstream the actuator position, for all cases. After the drop, the values tend to return to the original value

further downstream. The drop of the shape factor values which is caused by the plasma actuator slightly decreases for actuators positioned more downstream. Such minimal differences also indicate that, for a same power applied to the plasma actuator at different positions, the wave attenuation effect is almost the same, but rather strong for an actuator which is positioned more upstream. This fact can be a consequence of the boundary layer growth. For more upstream positions of the actuator, the accelerated area represents a higher percentage of the boundary layer, when compared to more downstream positions which have a higher boundary layer thickness.

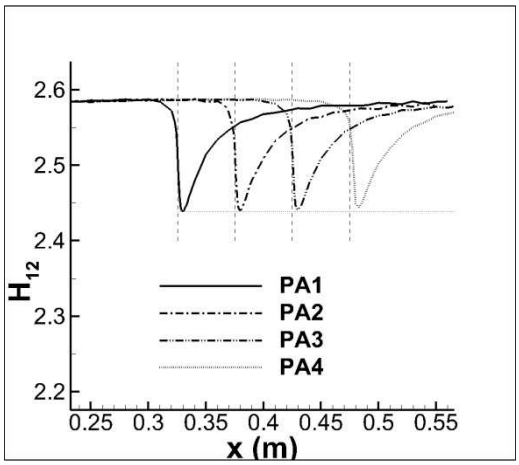

Figure 6.15: Shape factor values for the flow influenced by one single actuator at different positions, 16 m/s of freestream velocity.

The non-dimensionalized profiles of the wall-parallel velocity component at the point of maximum drop of the shape factor are compared with the base flow velocity profile (Blasius) in Figure 6.16-a and the respective derivatives in Figure 6.16-b and c. The differences found in the averaged non-dimensionalized profiles, Figure 6.16-a, in comparison with the Blasius profiles are concentrated in the bottom part of the boundary layer profile for all tested positions. For the first derivatives, Figure 6.16-b, a different shape can also be noticed at the bottom for all cases. Plots of the second derivative of the velocity profiles in Figure 6.16-c reveal an additional negative peak of the velocity profile in the bottom, where $\eta < 2$. The second derivative shows a certain sensibility to the actuator position. Results for the actuator positioned more downstream show a higher modification of the second derivative profile as the results for the plasma actuator positioned in more upstream positions.

From previous studies, it was found that a higher modification of the secondary derivative profile was provided by a higher forcing applied to the actuator. But in the present case, the same forcing was applied to the actuator in several positions. The small

differences of the values found for the secondary derivatives correspond to the boundary layer growth in that specific region.

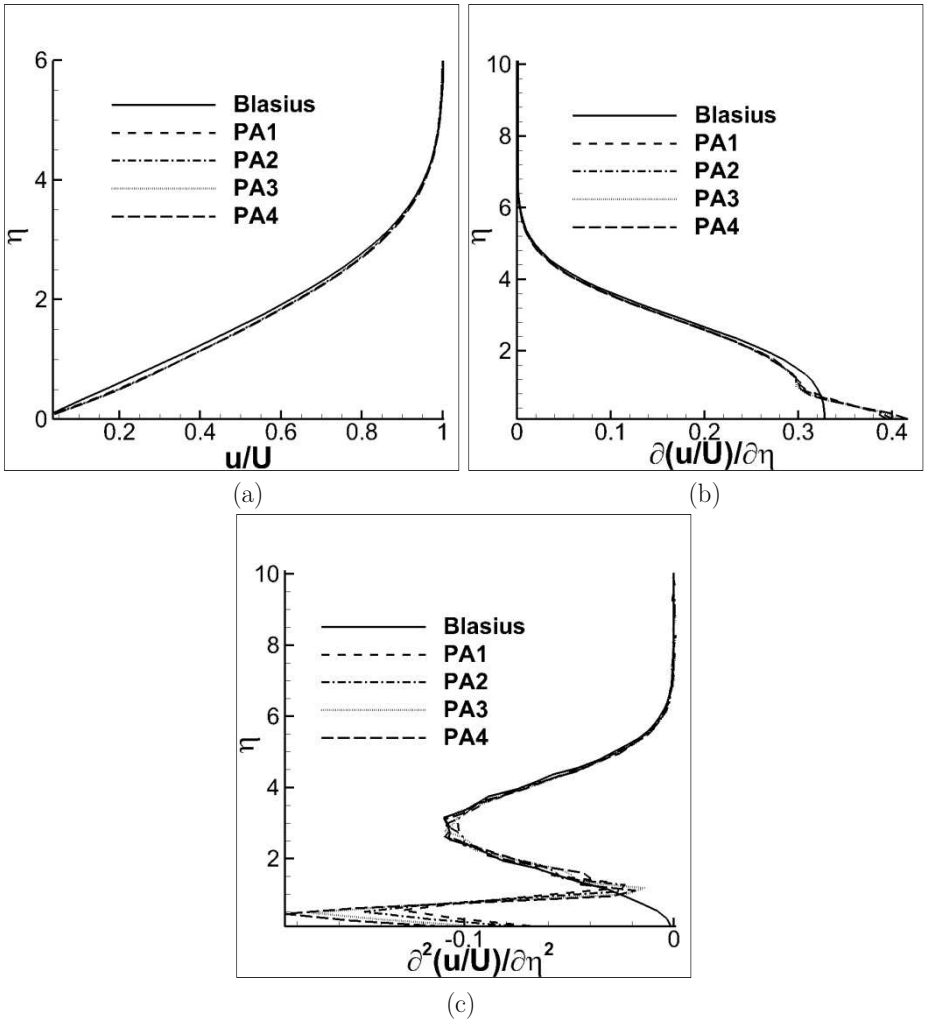

Figure 6.16: (a) Non-dimensional averaged velocity profile compared with the Blasius solution for several actuator locations. (b) First derivative. (c) Second derivative.

The influence of the actuator position over the TS wave attenuation rates is investigated using two different amplitudes of excitation, Figure 6.17.

Two-dimensional artificial disturbances are excited in two different amplitudes: A2D=550 and A2D=200. The values for A2D are described in Chapter 4, and they represent numerical amplitudes to be applied in a force density expression for TS wave excitation. These two values (200 and 550), excited at 220 Hz in a 16 m/s free-stream flow, lead to TS waves of amplitudes 0.8 and 0.25 percent of the free-stream velocity at PA1, respectively. The rates of wave attenuation, using one single actuator in continuous mode at two different positions PA1 and PA2, are presented in Table 6.5. The power applied to the actuator for these cases was 40 % of Power 1.

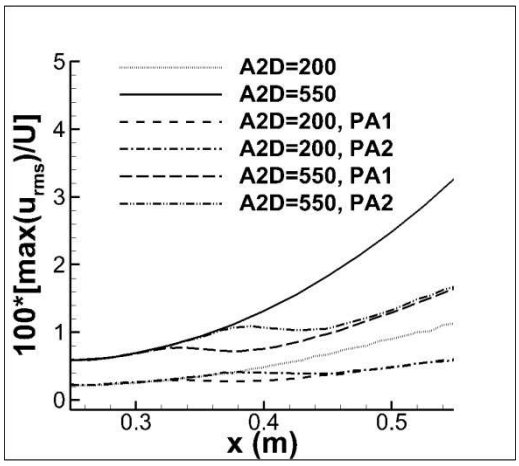

Figure 6.17: Maximum disturbances of the TS wave excited in different amplitudes and influenced by a single actuator in two different positions.

The maximum disturbance values show that downstream the region which is influenced by the actuator, the TS wave amplitudes have nearly the same values. For both cases, the wave amplitude is influenced by the actuator position only inside the restricted region between PA1 and PA2.

Results for the wave attenuation rates show very similar values for the two different wave amplitudes excited $\mathrm{A2D} = 550$ and $\mathrm{A2D} = 200$. In both cases, the actuator positioned in PA1 or PA2 provides an attenuation rate of about 44 %, related to the uncontrolled case. This fact leads to an important observation that the stabilizing effect of a plasma actuator is not dependent on the disturbance size, or its localization downstream. The wave attenuation characteristics are always related to the natural wave growth. When the boundary layer velocity profile is modified, the growth rates are also modified, and they act proportionally to the disturbances original size. In simple words, a plasma actuator which uses a power supply able to provide a certain rate of wave attenuation, will surely, inside the two-dimensional region, repeat such rates independent of the disturbance size.

A2D	Actuator Position	$\frac{A2}{A1}$	R
550	PA1	0.55	44.43
550	PA2	0.55	44.65
200	PA1	0.56	43.61
200	PA2	0.56	43.77

Table 6.5: Wave cancellation rates at 16m/s, for different wave amplitudes excited.

6.3. Arrays of actuators

Combinations of several actuators which operate simultaneously were investigated at different positions. The stabilizing effect of such arrays is compared with the performance of one single actuator.

6.3.1. Arrays of equally distributed power supply

The influence of several actuators which operate simultaneously using Power 1 in a boundary layer flow of 10 m/s free-stream velocity is investigated. The results for the maximum amplitude of the disturbances are plotted in Figure 6.18. The influence of a single actuator at position PA1 causes a strong attenuation of the disturbances amplitudes over a distance of about 0.1 m downstream of the actuator. From this point and further downstream, the waves return to grow once more. When using more than one actuator simultaneously, a similar effect can be found until about $x = 0.400$ m. Downstream this location, the effect of an additional actuator suppresses the wave amplification and there is no further growth of the waves. The value for the maximum disturbances amplitudes can be maintained very low, when using two actuators or more. From these studies, it was also found that the influence of the second actuator is dominant and the use of a third or a fourth actuator which operates at the same power does not produce relevant additional wave attenuation effects.

Figure 6.18 shows the curves of maximum wave amplitude of the flow influenced by one single actuator at position PA1, compared with the wave attenuation effects of several arrays of actuators.

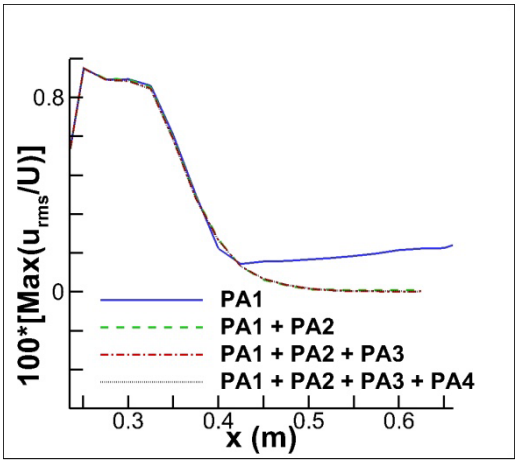

Figure 6.18 Maximum wave amplitudes for several arrangements of actuators, 10 m/s.

The curves which represent arrays of actuators in Figure 6.18 are superimposed and show the same values for TS wave amplitude downstream the first actuator position. Also, using arrays of actuators, the maximum amplitude of the disturbances remains at a very low value for a downstream position. Once for this configuration, arrays of two, three and four actuators present always the same values for the TS wave amplitudes, it is preferable, and more efficient, to use an arrays of only two actuators, for a lower energy consumption.

The velocity profiles for the last results of wave attenuation using several actuators were compared with the theoretical case of a constant suction-boundary layer profile, [Sch82] as shown in Figure 6.19. The lines correspond to the non-dimensionalized velocity profiles evaluated at 0.05 m downstream the position of the last actuator in the array.

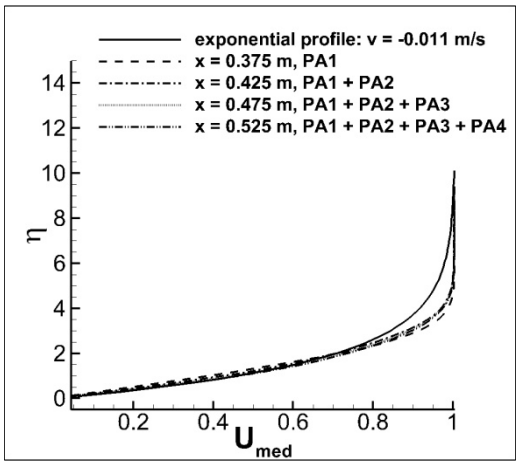

Figure 6.19: Comparison of the averaged velocity profiles with the exponential profile resulting of constant suction.

The cumulative effect of several actuators which operate simultaneously contributes to an approximation of the boundary layer modified profile into the velocity profile resulting from constant boundary-layer suction (exponential boundary-layer profile). However, the similarities are confined at the lower part of the boundary layer profile. At the upper part, the profiles are not in a good agreement even for the case with four actuators which are operated simultaneously.

A single plasma actuator produces a local effect of wave attenuation in a flat plate boundary layer. A suction boundary-layer profile could only be reached after a large region of suction, or the use of an array with large number of actuators. Thus, results of both techniques (constant suction and constant actuation) can be similar only in a certain extension, but a direct comparison is not the correct approach, [Vie11].

The influence of the second actuator position is also verified. Figure 6.20 shows values for the maximum disturbance amplitude using arrays of two actuators which operate simultaneously with Power 1 in a 10 m/s flow.

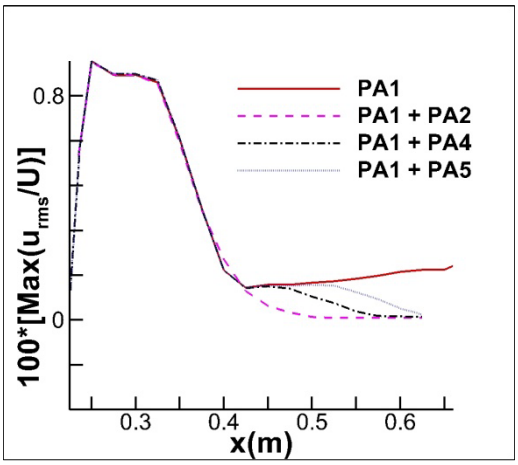

Figure 6.20: Maximum amplitudes for arrays of two actuators which are separated by different distances.

At downstream positions, away from the actuator array, the disturbances reach the same amplitudes, independently of the position of the second actuator. For two actuators which operate next each other (PA1 and PA2), the values for the maximum disturbances remain at low values in the region right after the array. An array with actuators which are separated by a longer distance, PA1 and PA4 for example, allows higher amplitudes in the region between the actuators, but the further downstream effect is the same as for the other configurations.

Similar tests are performed using actuators which operate simultaneously using only 40 % of Power 1, in a 16 m/s flow, with TS waves excited at 220 Hz. The values for the maximum amplitude for the disturbances along x direction are presented in Figure 6.21.

For such a configuration the use of additional actuators increases the stabilization of the boundary layer and reduces the wave amplitude downstream. This reveals a scenario which is different from the previous situation in a 10 m/s flow, where the use of three or four actuators does not provide any improvement in the wave attenuation. The use of low forcing in a higher free-stream velocity allows a quantitative analysis of the wave attenuation promoted by several actuators. The use of a single actuator at PA1 causes the waves to be hold at an amplitude value of 0.8 U for a distance of about 0.05 m from the actuator, followed by further growth after this point. Using two actuators at positions PA1 and PA2, the maximum wave amplitude decays until a distance about 0.10 m from the first actuator; remains constant for a short distance, and start to grow once again

downstream. For the use of three and four actuators the wave attenuation effect is obviously increased.

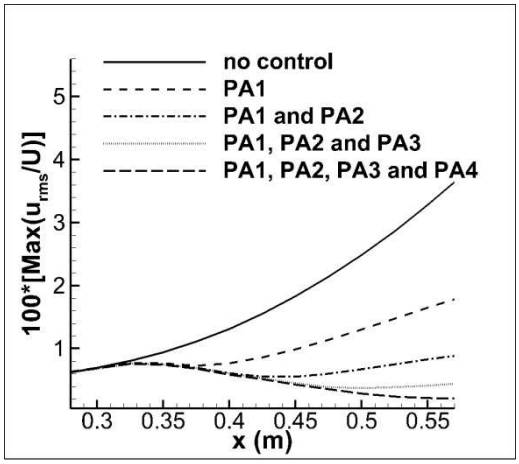

Figure 6.21: Maximum wave amplitudes for several arrangements of actuators, 16 m/s.

The values for the attenuation rates can be found in Table 6.6. A progressive decreasing of the waves according to the number of actuators used can be observed. For each actuator which is added to the array, the wave amplitude for a downstream position (away from the zone of influence of fluid acceleration provided by the plasma actuator) has a value of about half the value for the wave amplitude at the same position obtained with the influence of one actuator less.

Actuator Arrays	$\frac{A2}{A1}$	R
PA1	0.47	53.32
PA1 + PA2	0.23	77.30
PA1 + PA2 + PA3	0.11	88.09
PA1 + PA2 + PA3 + PA4	0.05	95.11

Table 6.6: Wave cancellation rates at 16m/s at x = 0.60 m, using arrays of several actuators.

The curves in Figure 6.21 have an inclination angle which differs according to the number of actuators used in the array. For a boundary-layer flow influenced by many actuators, this angle is very small and the waves seem not to grow after the fourth actuator until the end of the computational domain. As fewer actuators are used, the higher is the inclination angle of the curve indicating the wave amplitudes growing once more. This angle represents the stabilization proprieties of the actuated flow. Many actuators operating simultaneously accelerate the flow in the region close to the flat plate, modifying the boundary-layer velocity profile downstream of the actuator. This

modified profile has more stable characteristics and the waves do not return to grow with the same rates as before.

Figure 6.22 present the results for the shape factor values along x direction. The shape factor reaches lower values when several actuators work simultaneously. The major difference is found between actuators at positions PA1 and PA2. The difference of the minimum values for the shape factor which are reached with arrays of actuators decreases by about 50 % for each actuator which is turned on.

It was found for previous investigations (Section 6.2), that the position of one single plasma actuators along the x direction does not produce a significant influence in the drop of the shape factor. But the cumulative effect of wave attenuation promoted by modifications in the stability proprieties of a boundary layer flow influenced by arrays of actuators can be verified by the shape factor values

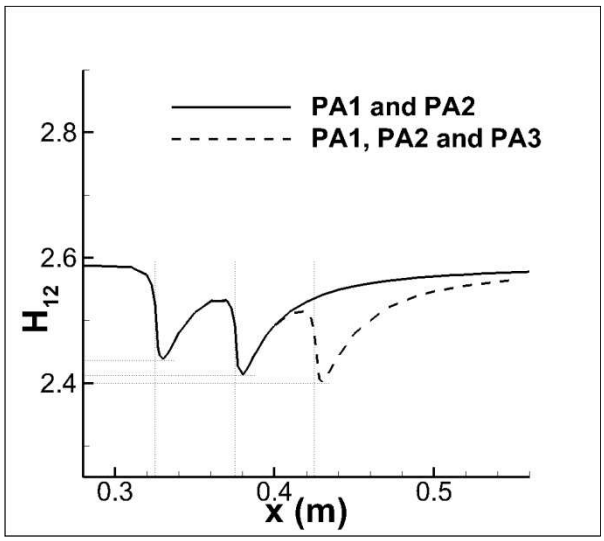

Figure 6.22: Values for the shape factor evaluated for the flow influenced by arrays of actuators which operate with same power.

6.3.2. Arrays of actuators with different power supply

The following tests aim to investigate the influence of the power distribution in arrays of two and three actuators which operate simultaneously. An increasing distribution means that the lower power is applied to the first actuator which is located at PA1. Similarly, a decreasing distribution means that the highest power is applied to the first actuator located at PA1.

The first studies include arrays of two actuators positioned at PA1 and PA2. In one configuration, the array of actuators has a decreasing power distribution with 40 % of Power 1 applied in PA1 and 20 % of Power 1 applied in PA2. An ensuing configuration uses an increasing power distribution applied to the same actuators, 20 % of Power 1 applied in PA1 and 40 % of Power 1 applied in PA2. A third array applies an equally distributed power in both actuators (40 % of Power 1 applied in PA1 and PA2). The resultant effect of such arrays over the maximal amplitude of the flow disturbances is presented in Figure 6.23.

The effect produced by an array of two actuators with an increasing power distribution keeps the TS wave amplitudes at an almost constant value along the region between both actuators. After the second actuator, the maximal wave amplitude decays to a value close to the values found for the use of an array of decreasing power. Further downstream the results for both cases are very similar. The effect promoted by the array of two actuators with decreasing power distribution keeps the wave amplitudes at a nearly constant, but lower, value along the region between the actuators. An array with equally distributed power promoted higher attenuation of the wave amplitudes due to the higher amount of overall power used. One more time, the effect of wave attenuation seems to be merely accumulative when observed further downstream, far from the region under direct influence of the array of actuators.

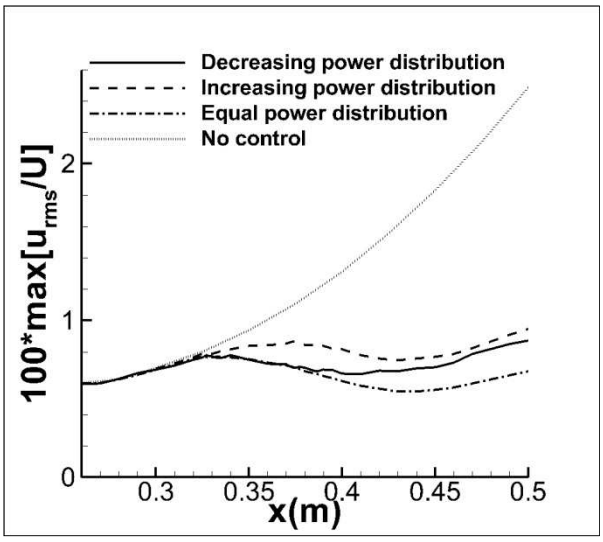

Figure 6.23: Maximal amplitudes of the disturbances influenced by arrays of two actuators with different power distributions.

A comparison of the shape factor values for an array of two actuators with increasing power compared with an array of two actuators with decreasing power is given in Figure 6.24.

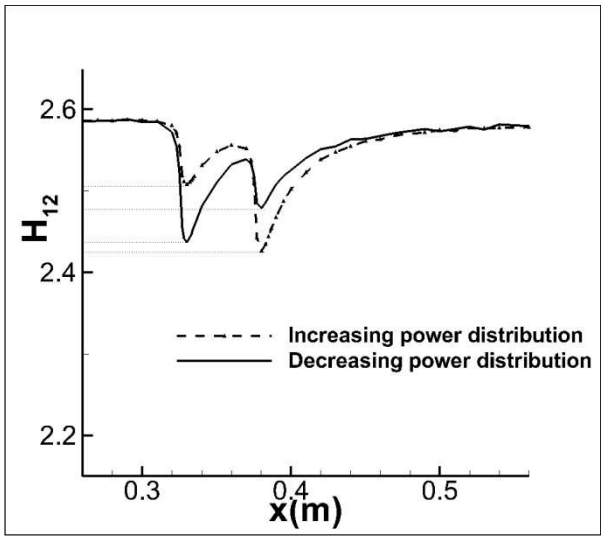

Figure 6.24: Shape values along x direction for arrays of two actuators operating with different power distribution.

The interesting point of this comparison is the difference in the minimum values which are reached for the same overall power applied to the actuators. As the first actuator provides the stronger modification in the boundary layer mean flow, it is of great benefit that a higher power is provided by this actuator. An integral above the curve which represents the shape factor values in Figure 6.24 would provide a higher value for an array of actuators with increasing power. In simple words, there is a small difference promoted by the power distribution of the actuators. A decreasing distribution promotes slightly stronger modifications of the shape factor values. This explains why the amplitudes of the maximal disturbances are maintained at a lower value between the actuators for this configuration. From these last investigations, a decreasing power distribution proved to be a best alternative for wave attenuation.

Results for wave attenuation using arrays of two actuators were compared with the results for wave attenuation using only one single actuator positioned at PA1. The power applied to the single actuator is 60 % of Power 1 which corresponds to the sum of the power applied to the array of actuators. Figure 6.25 shows that for one single actuator, the local attenuation effect is stronger in the region near the actuator. But the TS waves are only attenuated in a short region and then return to grow. For an array of actuators, the wave amplitudes are maintained low, due to the distributed effect which is extended

to a downstream region by the presence of a second actuator. The use of arrays of actuators presents the advantage to have prolonged the boundary layer extension with a modified velocity profile, which avoids the disturbances amplification.

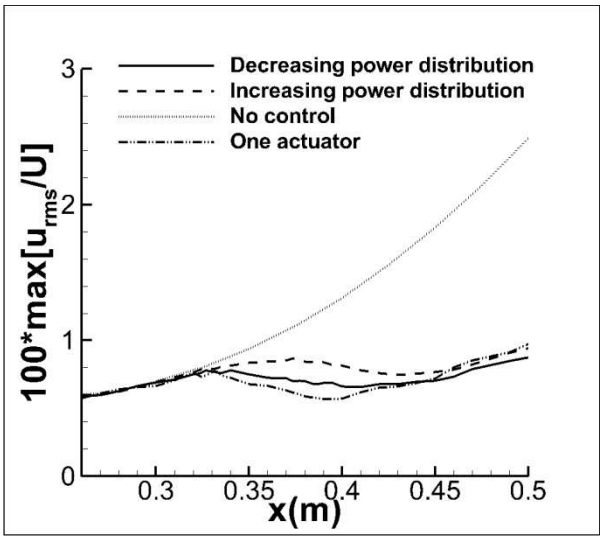

Figure 6.25: Results for wave attenuation using arrays of two actuators compared to the use of one single actuator.

Similar tests are performed using arrays of three actuators, with decreasing and increasing power distribution. For an array of three actuators with increasing power, 20 % of Power 1 was applied in PA1, 30 % of Power 1 was applied in PA2 and 40 % of Power 1 was applied in PA3. For an array of three actuators with decreasing power, 40 % of Power 1 was applied in PA1, 30 % of Power 1 was applied in PA2 and 20 % of Power 1 was applied in PA3. Results for the maximal wave amplitudes are given in Figure 6.26.

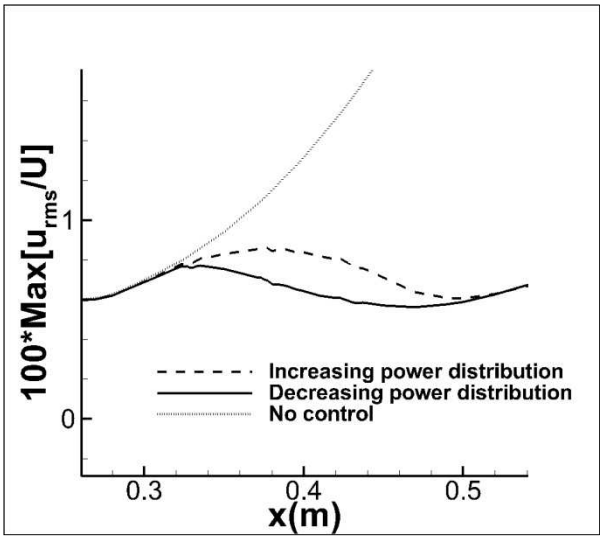

Figure 6.26: Maximal amplitudes of the disturbances influenced by arrays of three actuators with different power distributions.

Arrays of three actuators also show better results for a decreasing power distribution in the region between the actuators. Further downstream, away from the actuators, the wave amplitudes are similar for both kinds of power distributions.

Figure 6.27 presents the values for the shape factor evaluated for arrays of three actuators. The values obtained with a decreasing distribution are also slightly lower than the values obtained for an increasing power distribution due to the accumulative effects.

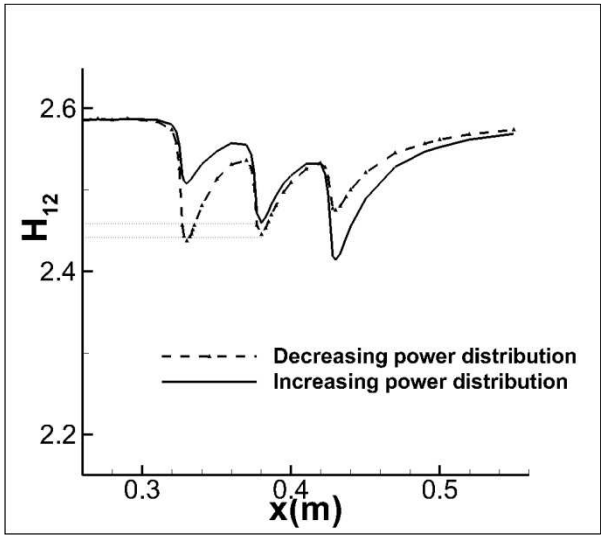

Figure 6.27: Shape values along x direction for arrays of three actuators operating with different power distribution.

In summary, for arrays of actuators, the power distribution does not exert significant influence in the wave attenuation for the very downstream region, away from the actuators. In the region near the actuators, a decreasing power distribution promotes lower disturbance amplitude values. Using a decreasing power distribution it is also possible to control the TS wave amplitude and keep it into a certain low value for a certain distance, with an extended array of actuators.

6.4. Multifrequency disturbances

For the following test cases, the artificial disturbances are excited at four frequencies simultaneously (110 Hz, 220 Hz, 235 Hz and 250 Hz) in a flat plate flow with 16 m/s of freestream velocity. Considering the present configuration, the four frequencies have different amplification zones downstream the excitation point. Frequencies 220 Hz and 235 Hz are normally frequencies that would be amplified until the end of the domain.

The frequency of excitation of 250 Hz is amplified but its unstable region ends before the end of the computational domain, resulting in wave amplification which is followed by natural damping. The frequency of 110 Hz is inside the range of frequencies that would not be amplified for the current test configuration. The multifrequency disturbance, which is a superposition of all four frequencies, illustrated in Figure 6.28-a, develops downstream the excitation point until the plasma actuator location, Figure 6.28-b, assuming an amplified shape. As the flow stability proprieties provide different amplification rates for each frequency, the interaction between them and their harmonics provides a dynamic scenario downstream the excitation point. This case is closer to a real situation, where not only one dominant frequency is present, but many other disturbances arise naturally inside the boundary layer region. The aim of this investigation is to analyze the attenuation of a multifrequency disturbance promoted by one single actuator which is operated in continuous mode at position PA1 with 40 % of Power 1.

Downstream the excitation point, at $x = 0.400$ m, the attenuation effects of the plasma actuator can be noticed together with a flow acceleration and reduction of all amplified modes, Figure 6.29.

The maximum amplitudes of the flow disturbances are plotted in Figure 6.30, where the wave attenuation effect of the plasma actuator over the multifrequency disturbances can be verified. The effect of the plasma actuator in continuous mode keeps the maximal amplitude of the disturbances at a nearly constant value in a distance about 0.05 m downstream the actuator position. Further downstream, the waves return to grow once more.

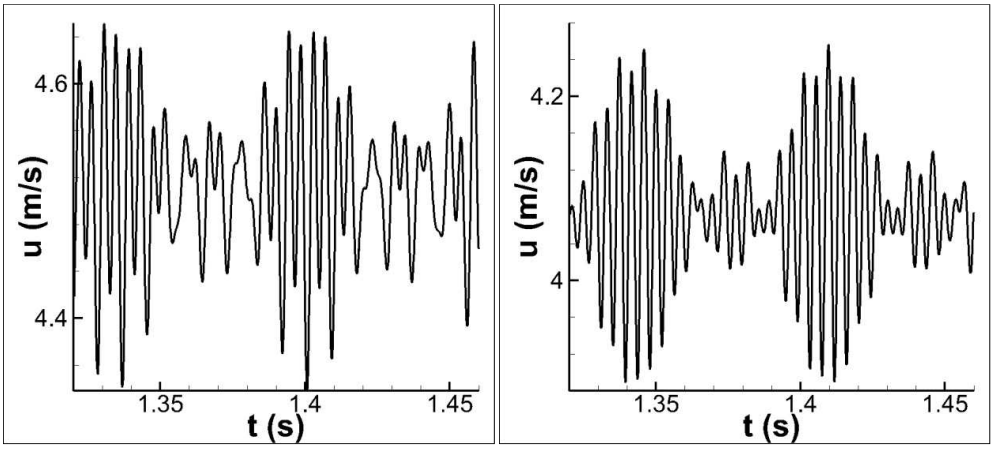

(a) (b)

Figure 6.28: Unsteady velocity for a multifrequency disturbance at y = 0.0004 m, (a) x = 0.240 m, (b) x = 0.300 .

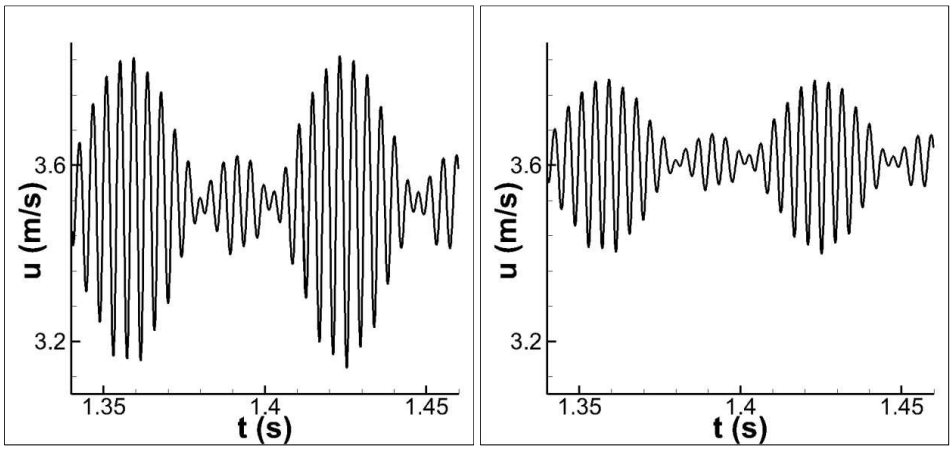

(a) (b)

Figure 6.29: Unsteady velocity for a multifrequency disturbance at x = 0.400 m and y = 0.0004 m with (a) plasma actuator off and (b) plasma actuator on.

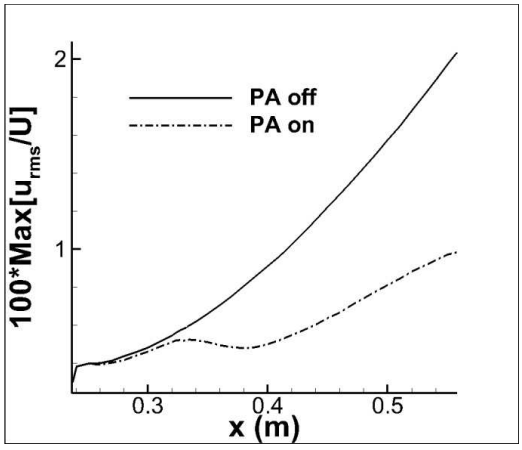

Figure 6.30: Maximal amplitude of a multifrequncy disturbance along x direction with and without plasma actuator effects.

The attenuation rates for the present case are compared with the previous tests for a simple TS wave attenuation. Results are shown in Table 6.7.

Disturbance	$\frac{A2}{A1}$	R
Multifrequency	0.53	46.86
Single frequency (220 Hz)	0.55	44.43

Table 6.7: Wave cancellation rates at 16m/s at x = 0.425 m, multifrequency and single frequency.

For multifrequency disturbances, the attenuation rate obtained is about 2 % higher than the rate obtained in previous investigations for a single frequency. In both cases, the plasma actuator is operated at 40 % of Power 1, at $x = 0.325$ m. This minimal difference between the evaluated rates indicates that the attenuation effect promoted by the plasma actuator remains almost the same even when more than one amplified modes are present

in the boundary layer. A spectrum analysis of the instantaneous velocities shows that all frequency modes are attenuated, Figure 6.31. The influence of the actuator over a multi-frequency disturbance did not cause a further amplification of any one of the frequency modes

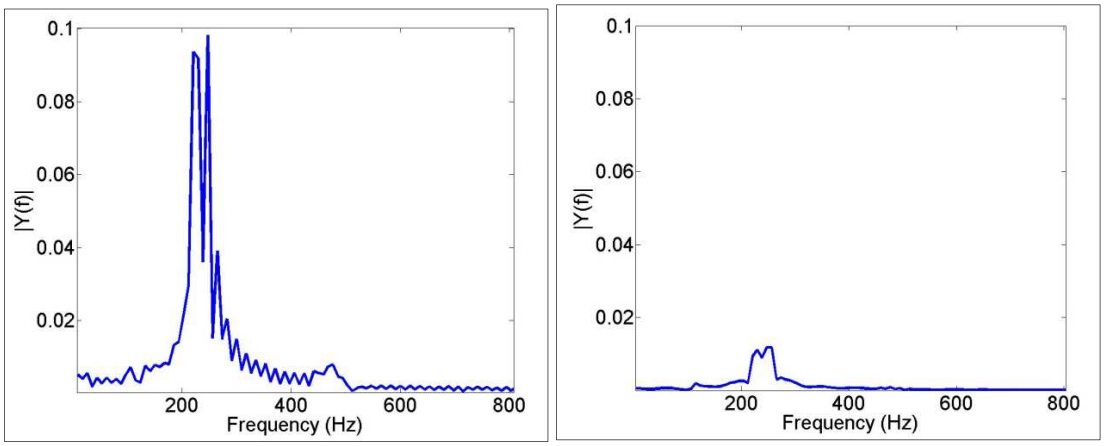

(a) (b)

Figure 6.31: FFT of the instantaneous velocities for a multifrequency disturbance. (a) Plasma actuator off. (b) Plasma actuator on.

6.5. Summary of the continuous actuation approach

Numerical simulations of a plasma actuator which is operated in continuous mode show the Tollmien-Schlichting wave attenuation by boundary layer stabilization. The influence of power supply related to the freestream velocity was investigated. For high power applied to the actuator there is a strong modification of the wave profile, wave convective speed and wave length.

Arrays of actuators which operate in low freestream velocity should be composed of a maximum of two actuators. In higher freestream velocity flow, the arrays of actuators with low power can hold the wave amplitudes at low values using low energy consumption. The effect of boundary layer stabilization is cumulative. The attenuation rates remain the same for different wave amplitudes in the laminar range. Arrays of actuators with decreasing power distribution present better results in the region near the actuators. Further downstream, arrays of actuators with decreasing or increasing power distribution present similar effects.

The stabilizing effect of a plasma actuator which is operated in continuous mode was shown also for multifrequency disturbances, where all the frequency modes were reduced downstream the actuator position.

7. Active Wave Cancellation

The investigations presented in this chapter use a plasma actuator which is operated in cycle mode.

The sinusoidal velocity modifications promoted by a plasma actuator, when correctly adjusted, counteract with the flow disturbances, which are cancelled by superposition. The plasma actuator is then represented by a forcing term defined as

$$F_s(x,y) = A + A\sin(2\pi f t + \theta) * F_{PIV}\,(x,y)\,, \tag{7.1}$$

where F_s is the body force density which is applied to the plasma actuator, A is the amplitude of the periodic actuation, f is the wave frequency (similar to the Tollmien-Schlichting wave frequency), t corresponds to the real time, θ is the phase-shift used to promote the superposition of the velocity fluctuations, and $\mathrm{F_{PIV}(x,y)}$ is the force density field evaluated from PIV data.

Tollmien-Schlichting waves are excited in a flat plate boundary-layer flow at x = 0.225 m, with a frequency of 220 Hz. The free-stream velocity for the test cases is 16 m/s. Waves are amplified right downstream the excitation point and the cancellation effect of the plasma actuator in cycle mode is investigated and compared with the boundary layer stabilization approach described in the previous chapter.

7.1. Periodic actuation

7.1.1 Influence of the control parameters

In a first instance, the influence of the control parameters for cycle mode operation of the plasma actuator can be determined by investigation of the local effects. For very low power amplitude applied to the actuator (less than 4 % of Power 1), the effects of wave

cancellation are weak (less than 10 %). The small influence in wave cancelation of low-power amplitude applied in cycle mode causes some difficulties to determine the correct phase shift. Figure 7.1-a shows a comparison between the results of different test cases where a low power amplitude is applied to the actuator. The maximum amplitude of the disturbances is evaluated along the flat plate. Using a fixed phase-shift value of 72.5°, and amplitude, A, values of 4 %, 7 % and 10 % of Power 1 are applied to the actuator, the wave cancellation results do not show strong differences. Actually, no significant effects in active wave cancellation are found for such configurations, as it can be seen in Figure 7.1-a: Downstream the plasma actuator location, indicated by a grey dashed line, the wave amplitude remains growing, what causes some difficulties for the evaluation of the correct value of the control parameters. The maximum amplitudes of the disturbances decrease as the power amplitude which is applied to the actuator increases. But in the region very near the actuator, there is a peak of the maximal amplitude which is more accentuated for 10 % of Power 1.

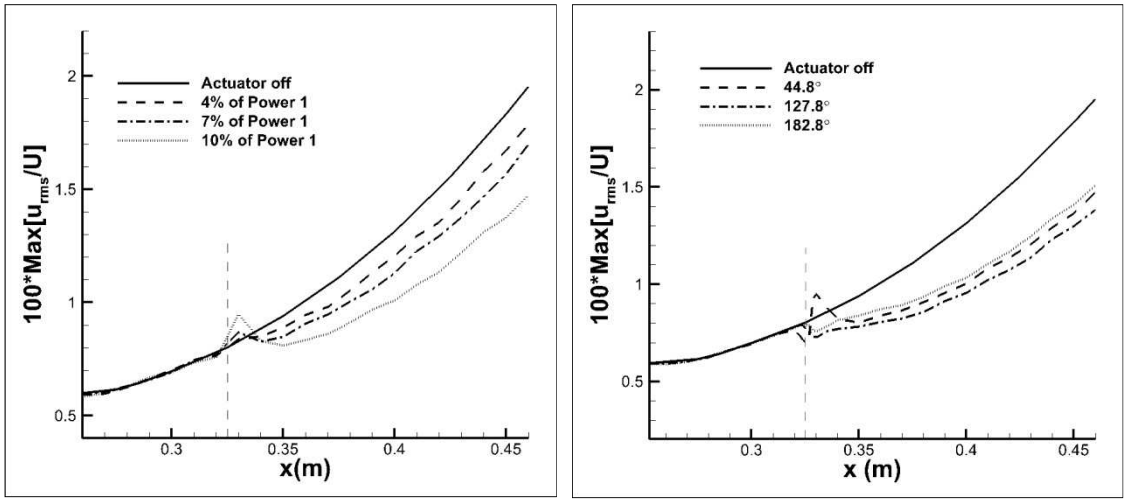

(a) (b)

Figure 7.1: Maximal amplitude of the flow disturbances along the flat plate. (a) Low power applied to the actuator with a wrong phase-shift value. (b) Different phase-shift values applied to the plasma actuator with power amplitude 10 % of Power 1.

The presence of the peak right above the actuator indicates that the chosen phase shift for these test cases has not an appropriate value. For low amplitudes of power applied to the actuator, even using a wrong phase shift value, a small reduction of the flow disturbances can be obtained. The reason why small wave reduction still happens in this case is not exactly the desired superposition effect, but a cumulative boundary layer

stabilization effect, which will be discussed in the following chapter. It is important to state that for low amplitudes applied to the actuator, the correct influence caused by the phase-shift change becomes hard to be determined in a position very downstream the actuator. Using low power, one needs to analyze the region right above the plasma actuator for a better evaluation of the phase-shift effects.

Figure 7.1-b shows results for the maximal flow disturbances evaluated with 10 % of Power 1 applied as amplitude, A, of the body force oscillation. Results for some variations of the phase shift values θ, are presented. Once more, due to the low power applied as amplitude, the phase-shift evaluation is not trivial. Values of the wave amplitudes obtained with a phase-shift of 44.8° are close to the values obtained with a phase-shift of 182.8°. Although both values for the phase-shift are not correct, a significant reduction of the wave amplitude can be already observed. The behavior of the maximal amplitude of the disturbances right downstream the actuator region can be a good indicator for the correctness of the phase-shift values. For real cases, the closer the sensor is to the actuator position; more precise is the information about the phase-shift effects. Wrong phase-shift values provide an accentuate peak of the amplitudes near the plasma region for significantly high amplitudes.

7.1.2. Optimization of the control parameters

To avoid a long trial-and-error process to determine the correct values for phase-shift and amplitude in Equation 7.1, an optimization method has been employed: the BOBYQA method introduced in Chapter 4. This method is applied to search for optimal values of A and θ in the cases with cycle operation of the plasma actuator.

One sensor for the wall parallel velocity component is positioned 0.015 m downstream of the actuator position. The sensor is positioned that close to the actuator for obtaining a quick perception of the modifications caused by the changes in the phase-shift values. A longer distance between the sensor and the plasma actuator would require more iterations of the optimization algorithm to find the appropriate combination of parameters. The sensor collects information of instantaneous velocity for the time related to one wave length – one cycle of the TS wave. From this data, the root-mean-squared (rms) velocity is evaluated for all grid points in y direction inside the boundary layer region. The maximum difference between these values, or the gradient of the TS wave in

y direction, is used as the objective function, F, for the optimization code.

The success of the optimization also depend on a good choice of the input parameters A and θ and the setting of reasonable bounds (trust region). A few preliminary tests are necessary to determine a good combination of the initial values.

An example of the optimization is shown in the following for active wave cancellation using one actuator in cycle mode operation. The initial values and bounds are given in Table 7.1.

After each iteration in BOBYQA, there is a waiting period equivalent to two wave cycles before the sensor starts to collect information for the next optimization. The values attributed by BOBYQA related to the objective function evaluated from the numerical simulations with the input values from Table 7.1 are shown in Figure 7.2. Good convergence of the objective function values is already reached after about 12 iterations.

	A	θ
Initial value	20 % of Power 1	128°
Lower Bound	10 % of Power 1	120°
Upper Bound	40 % of Power 1	150°

Table 7.1: Initial parameters used for the optimization.

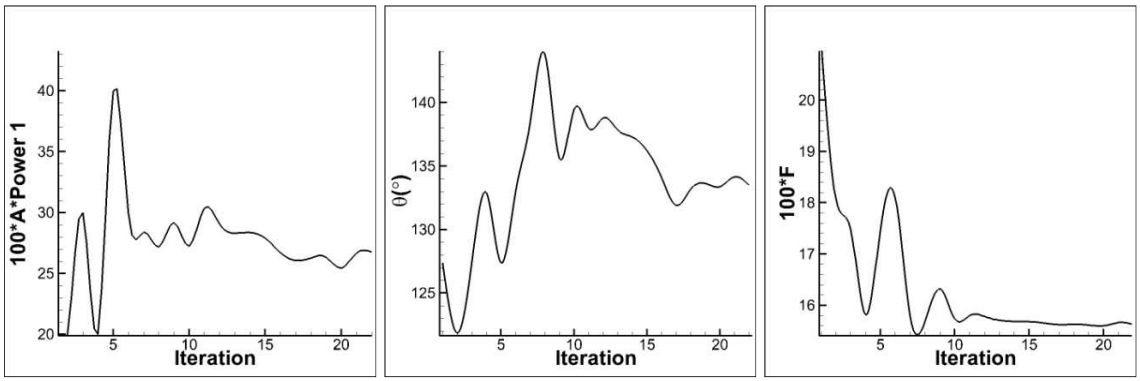

Figure 7.2: Example test case for the optimization with BOBYQA. From the left to the right, values for the amplitude, phase-shift and objective function.

The wall-parallel velocity component is used for the evaluation of the objective function. Numerical results in Figure 7.3 show the wall parallel velocity component at x = 0.340 m after a few iterations of the optimization algorithm. The reduction of the wave amplitudes at the sensor position after some optimization cycles can be clearly seen. The velocity oscillations seem to be combined in groups of three waves, due to the wait period of two cycles before the following collect of data for the next optimization.

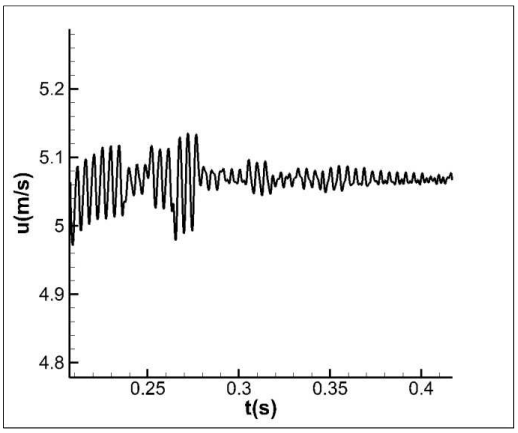

Figure 7.3: Time trace of the wall parallel velocity component at the wall-normal position of maximal wave amplitude at the sensor location.

Figure 7.4-a shows the maximal amplitude of the disturbances. For cycle operation of the plasma actuator and a correct parameter combination, the active wave cancellation reduces abruptly the disturbance amplitudes right at the plasma actuator location. At the sensor position, $x = 0.340$ m, the amplitudes remain constant for a short distance and downstream of this point start to decay once more, but at lower rates. This pattern found next to the actuator position corresponds to the typical local behavior of the wave amplitudes when active wave cancellation is correctly employed. A strong amplitude reduction at the actuator location, followed by further wave attenuation, is found for both cases: with and without optimization.

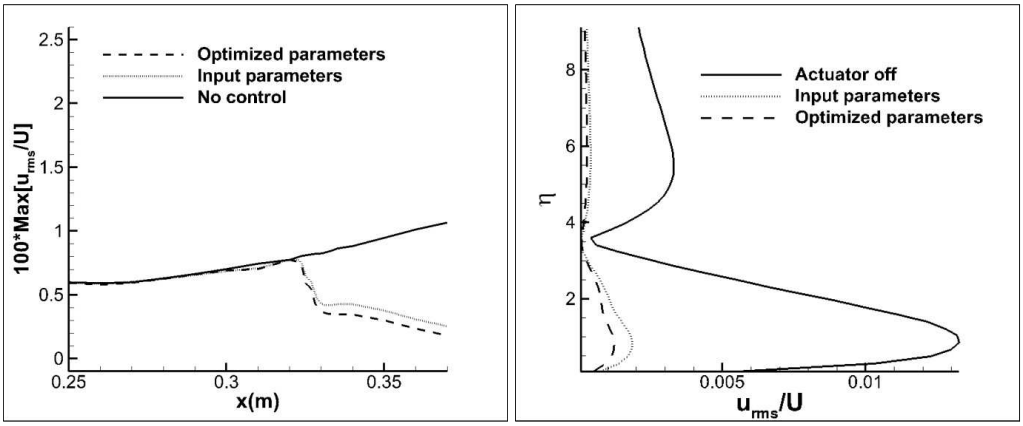

(a) (b)

Figure 7.4: Comparison of results for the use of an optimization algorithm. (a) Maximum amplitude of the disturbances. (b) TS wave profile.

Figure 7.4-b shows the root-mean-squared velocity at a downstream position x = 0.40 m, with a comparison of the TS wave profile9 evaluated for the non-controlled

case and the optimized case. Because the first choice of parameters is already able to provide a reasonable performance, the use of the BOBYQA optimization algorithm promoted about 10 % of improvement of the cancellation rates, in comparison with the non-controlled case.

7.2. Comparisons with Continuous actuation

A direct comparison of active wave cancellation technique and boundary layer stabilization (previously described in Chapter 6) is described in this section. The different effects of a plasma actuator which is operated in cycle and in continuous mode are detailed investigated.

7.2.1. Global power efficiency

In the following, the two operational modes for a plasma actuator, cycle and continuous, are considered having the same time averaged value for power supply, as illustrated in Figure 7.5-a. The case where the actuator is operated in cycle mode promotes active wave cancellation by superposition of velocity fluctuations, while the case in which the actuator is operated in continuous mode promotes attenuation of the flow disturbances by a modification of the boundary layer velocity profile and the flow stability properties.

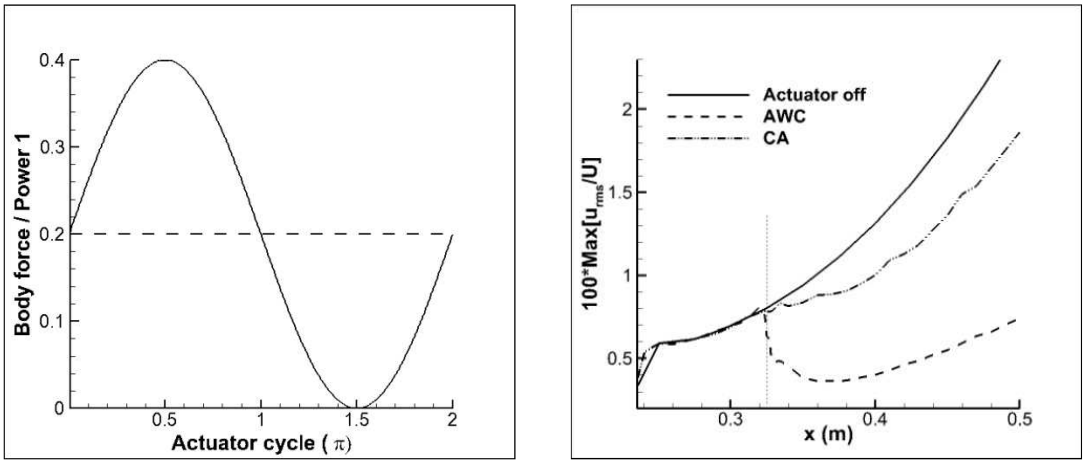

(a) (b)

Figure 7.5: Comparison between active wave cancellation and boundary layer stabilization for the same time averaged power supply. (a) Force distribution. (b) Maximal amplitudes of the TS waves.

Using the same time averaged value for power supply of 20 % of Power 1, very different effects can be obtained from both techniques. Results for the maximal amplitudes of the flow disturbances are shown in Figure 7.5-b. Cycle operation of the plasma actuator leads to much stronger reduction of the wave amplitudes. The amount of power applied in continuous mode operation is not enough to sufficiently modify the boundary layer velocity profile and promote the same amplitudes by wave attenuation. Mechanisms involved in the wave attenuation procedure include the change of the flow stability properties. To modify the complete boundary layer profile and the stability properties is a harder task than simply introduce disturbances in the flow, as it is done with the active wave cancellation method. For a same averaged value of power, continuous mode of operation only produces a small reduction of wave growth (about 20 %), but cycle operational mode is able to more significantly reduce the wave amplitude size.

The two approaches for reduction of the TS wave amplitudes using plasma actuators are once more compared, now using higher power applied in continuous operational mode. Values of 40 %, 60 % and 80 % of Power 1 are applied to the plasma actuator in continuous mode and compared to the previous cases presented in Figure 7.5. Maximal amplitudes of the disturbances more presented in Figure 7.6. The use of 40% of Power 1 in continuous mode was able to hold the wave amplitudes at an almost constant value for a distance of about 0.10 m downstream the actuator position. Using 60 % of Power 1, the wave amplitudes already show values which slightly decline downstream the actuator position until $x = 0.400$ m, point where the waves seems to return to grow once more. For 80 % of Power 1 applied to the plasma actuator, a strong reduction of the wave amplitude can be seen. The TS waves show decreasing values downstream the actuator position also until about $x = 0.400$ m, less than 0.1 m away from the actuator position. Similarly to the previous case with 60 % of Power 1 applied to the actuator, downstream the actuator, at $x = 0.400$ m, the waves return to grow once more. But, specially for 80 % of Power 1 applied in continuous mode, at a more downstream location, $x = 0.50$ m, TS waves amplitudes reach similar values for the case using the actuator in cycle operational mode with only 20 % of Power 1. Approximately four times the amount of power is necessary to be applied in continuous mode for reaching similar amplitudes of the TS waves about 0.20 m downstream the actuator position.

Figure 7.6-a shows the reductions of wave amplitude which occurs right at the actuator location for active wave cancellation. Using cycle operation of the actuator, the

flow disturbances are abruptly reduced at about 0.025 m downstream the actuator position and restart to grow right after this position. In contrast, for continuous operation of the plasma actuator, even higher power promotes smoother changes in the wave amplitudes 0.075 m downstream the actuator position. The values obtained for the TS waves amplitudes with active wave cancelation are lower than the values obtained with boundary layer stabilization until a distance about 0.1 m downstream the actuator, after this location, the maximal amplitude values are quite similar. This reveals that the boundary layer stabilization approach can be seen as a "slower" process for wave attenuation. The maximal effects obtained with this technique are revealed more downstream. On the other hand, using active wave cancellation, the wave reduction occurred immediately at the actuator location. But its effects remain at a shorter distance. The waves return to be amplified at a more upstream position using a cycle mode for the plasma actuator than using a continuous power distribution. With cycle operation of the plasma actuator the effect of wave amplitude reduction are merely localized and with a continuous approach, the modification of the boundary layer velocity profile and the stability characteristics are extended further downstream.

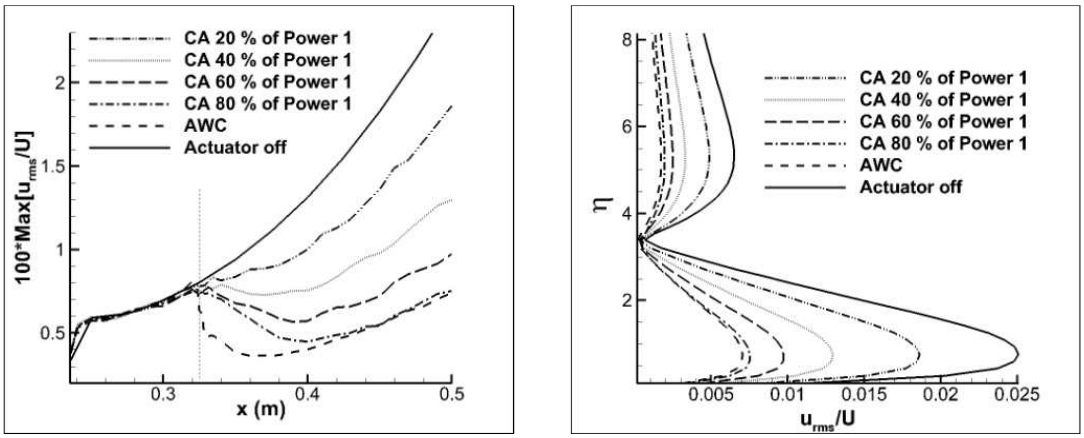

(a) (b)

Figure 7.6: Comparison between boundary layer stabilization: several power magnitudes applied to the plasma actuator and active wave cancellation (20 % of Power 1). (a) Maximal amplitude of the disturbances. (b) RMS of the wall parallel velocity component at x = 0.50 m.

Figure 7.6-b shows the averaged fluctuations of the wall parallel velocity component at $x = 0.500$ m using several power magnitudes applied to the plasma actuator in continuous mode compared to the cycle operation of the plasma actuator using low power. The maximum value of the wave amplitudes is decreased for a higher power applied in continuous mode. The use of 80 % of Power 1 in continuous mode and the use

of 20 % of Power 1 in cycle mode of operation promote similar results at this location.

The reduction of the wave amplitudes are quantified in Table 7.2. The wave cancellation rates are evaluated with reference to the non-controlled case, where the waves grow with natural amplification rates. Higher rates for wave cancellation, about 70 %, are reached for active wave cancellation and continuous actuation with 80 % of Power 1 at downstream locations.

Wave cancellation rates	x = 0.350 m	x = 0.400 m	x = 0.450 m	x = 0.500 m
AWC	59.15	69.40	69.99	70.19
CA with 20 % of Power 1	10.71	23.62	27.80	25.02
CA with 40 % of Power 1	20.02	42.438	45.94	47.80
CA with 60 % of Power 1	27.64	56.42	60.62	60.82
CA with 80 % of Power 1	31.72	65.929	70.18	69.67

Table 7.2: Wave cancellation rates evaluated for a comparison between active wave cancellation and continuous actuation.

The values for the shape factor are evaluated along the flat plate as a comparison of continuous and cycle actuation, see Figure 7.7-a. Using the same average value of 20 % of Power 1 applied to the plasma actuator, even the maximal wave amplitudes presented much lower values for cycle operational mode, the shape factor values are similar using the two different techniques. These two curves are superimposed in Figure 7.7-a because the values obtained are very similar. For reaching downstream the actuator position the same amplitudes for the TS waves, 80 % of Power 1 is necessary to be applied in continuous mode, while only 20 % of Power 1 is necessary for cycle operation. These quantities are also reflected in the minimum values reached for the shape factor drop which is caused by the plasma actuator influence in the flow. Using continuous actuation, a more pronounced change in the shape factor values is necessary to promote wave amplitude reduction at the same magnitude as using active wave cancellation. But, as the boundary layer modifications promoted by continuous actuation are stronger, they remain until a more downstream position. Shape factor values obtained with the use of only 20 % of Power 1 applied to the actuator in both techniques reveal a small drop near the actuator location. Downstream the actuator location, for lower power, the shape factor values return to values about 2.59 which are expected for a laminar boundary layer flow. Using higher power, the shape factor reduction is extended, what also indicates the change of the flow stability properties. The shape factor values are extremely dependent on the quantities of momentum which are added to the flow, no matter how they are

added. Higher power applied to the actuator promotes always higher drop of the shape factor until a more downstream position.

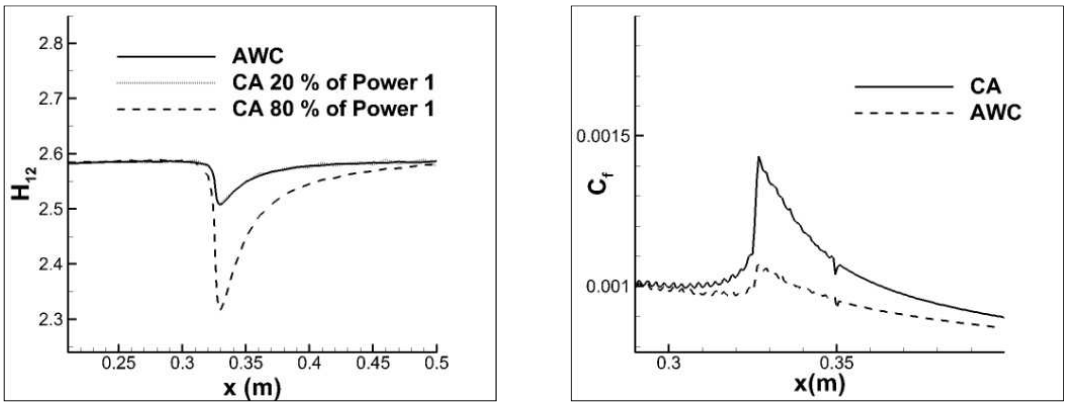

(a) (b)

Figure 7.7: Comparison of both techniques: active wave cancellation and boundary layer stabilization using Continuous Actuation. (a)Shape factor values. (b) Wall friction coefficient.

Figure 7.7-b shows a comparison of the wall friction coefficients for active wave cancellation with 20 % of Power 1 applied as amplitude and continuous actuation using 80 % of Power 1. The use of higher power in continuous mode promotes a peak of high values for the wall friction coefficients due to the presence of higher gradients caused by the higher quantities of momentum added to the flow.

7.2.2. Local effects

In this section, the behavior of the velocity fluctuations passing through the flow region which is accelerated by the influence of the plasma actuator observed in detail. Two operational modes for the plasma actuator are investigated: Continuous actuation (CA) using 80 % of Power 1, and cycle operation (AWC) using only 20 % of Power 1 as amplitude of the power oscillation. The time averaged results are subtracted from the instantaneous flow snapshots enabling the observation of the TS waves. Artificial disturbances are once more excited at $x = 0.225$ m and the plasma actuator is positioned at PA1, $x = 0.325$ m.

Figure 7.8 shows the contour maps for the fluctuations of the wall parallel velocity component. Due to the velocity superposition which occurs for the active wave

cancellation process, it is important to distinguish the right phase angle when a certain amount of power is applied to the actuator, for a better observation of the fluid dynamic effects. The graphics positioned at the left side of Figure 7.8, indicate the magnitude of power which is applied to the actuator in cycle mode at a specific instant. For the actuator which is operated in continuous mode, applied power remains constant.

The light grey vertical lines in Figure 7.8 indicate the phase angle in which the body force is evaluated. The respective contour plots positioned at the right side of Figure 7.8 show the results for the velocity fluctuations at the same instant as the indicated amount of power is applied to the actuator.

Results evaluated with the actuator in continuous operational mode do not present significant changes of the velocity fluctuations in the wall-parallel direction. The boundary layer stabilization process is smoother and the higher wave attenuation rates for this case are found about 0.1 m downstream the actuator position, as it was already shown in previous investigations. For this reason, nearby the actuator no remarkable effects can be noticed else than a slightly reduction of the wave amplitude.

For an actuator which operates in cycle mode, the fluctuations are distorted after passing the actuator region. The region of highest velocity fluctuations is lifted up from the flat plate. An immediate strong reduction of the wave amplitude can be noticed a few centimeters after the actuator location especially at the TS wave upper fluctuations. The instant when the maximum forcing is applied to the actuator is found to be the moment when the region of negative velocity fluctuations reaches the actuator position. Similarly, at the instant when the region of positive fluctuations reaches the actuator location, the power supply is approximately zero.

Distortions of TS waves for cycle mode operation of the plasma actuator happen on the bottom, near the solid surface. An elongated region of constant velocity is formed underneath the highest TS amplitudes. This also corresponds to the region where the highest gradients of velocity are found.

Even with these shape modifications of the TS waves a significant wave amplitude reduction right at the actuator location is produced. The waves return to their original form a short distance downstream the actuator.

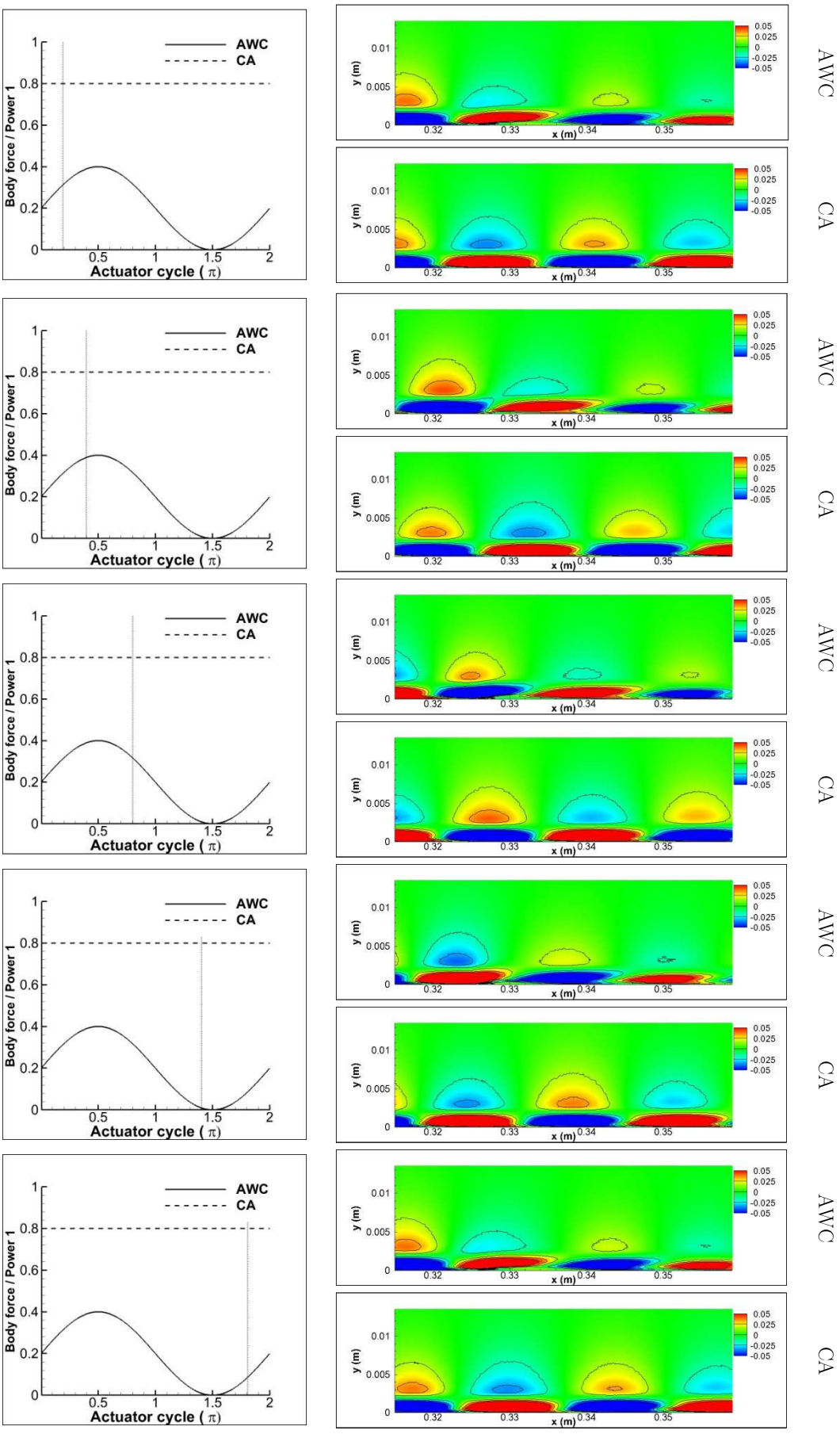

Figure 7.8: Comparison of velocity fluctuations in wall parallel direction for cycle and continuous actuation.

Figure 7.9 shows results for the wall normal velocity fluctuations. The graphics on the left side again indicate the force magnitude which is applied to the plasma actuator in cycle mode. At the right side, contour maps of the velocity fluctuations are compared for cycle and continuous operational modes. When using continuous actuation, such as the wall parallel velocity shown in Figure 7.8, for the wall normal component almost no difference can be noticed from the regions of fluctuations upstream and downstream of the actuator position.

The use of cycle operation for the plasma actuator produces strong modifications of the wall normal velocity fluctuations when passing through the actuator region. The flow disturbances are elongated and pulled to the actuator position. In these short instants when the distortions happen, a small region of velocity with the same direction appears right at the actuator location. The moment when such a shape modification occurs indicates that the actuator is pulsing in the direction of the velocity fluctuation for that specific instant. Since the aim of active wave cancellation is to superimpose velocity fluctuations and cancel the TS waves, the actuator in cycle operational mode should not produce an impulse in the same direction of the fluctuation, but against it. In practical terms, for cycle mode operation, the highest value of power applied to the actuator produce a strong suction, or negative values for the velocity fluctuations in wall normal direction. High suction should be produced at the right moment, when positive velocity fluctuations in wall normal direction pass the actuator position. Likewise, the lowest power at the actuator should be applied when fluctuations of negative velocity in wall normal direction pass the actuator position. Such suction cannot be seen in the fluctuation maps for continuous actuation because the averaged values are subtracted from the instantaneous flow field.

Even the phase shift of the cycle mode of the plasma actuator operation has not a perfect agreement with the velocity fluctuations in the wall-normal direction the wave cancellation results are very satisfactory. This contradiction is due to the phase shift which is already present in the natural TS wave propagation. The velocity fluctuations in wall-normal direction travel with a short delay (about $\pi/2$) related to the velocity fluctuations in wall-parallel direction. Additionally, the wall-parallel velocity fluctuations are almost one order of magnitude higher compared to the wall-normal fluctuations. For this reason, the best choice is to adjust the plasma actuator parameters in order to counteract with the wall-parallel velocity fluctuations.

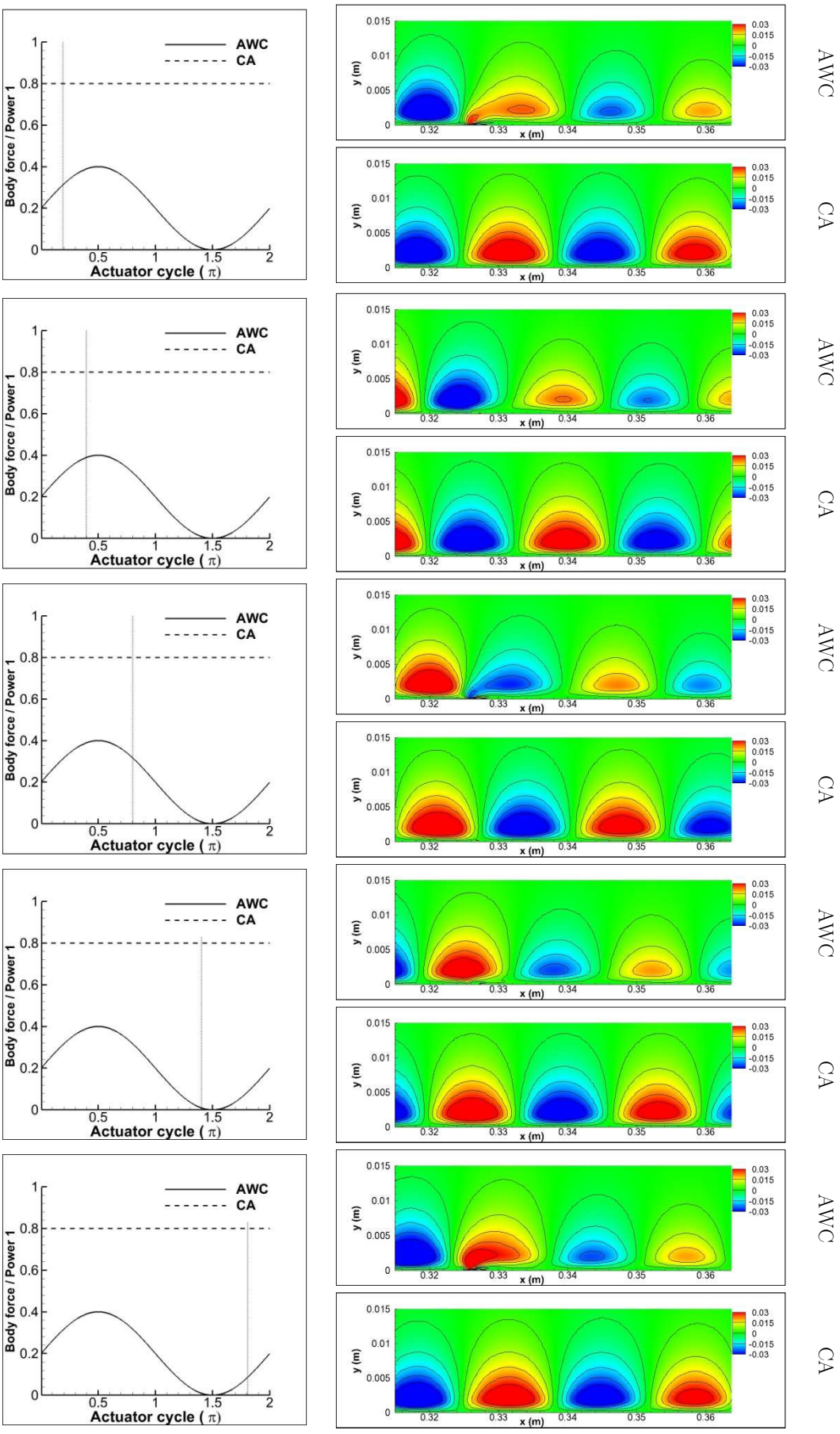

Figure 7.9: Comparison of velocity fluctuations in wall normal direction for cycle and continuous actuation.

The optimization algorithm provides a value for the phase shift to be applied at the actuator and provide the maximal wave cancellation result. This value is found to be the correct value for producing the opposite disturbances in wall-parallel direction. Once the fluctuations of u and v are coupled and travel together downstream, to operate the plasma actuator in a phase shift opposed to the highest fluctuations is more effective against the growth of the TS waves.

7.2.3. Downstream effects

In this section, the behavior of the TS wave is analyzed downstream of the fluid region which is directly influenced by the plasma actuator. Two test cases are considered: boundary layer stabilization using 80 % of Power 1 applied in continuous mode (CA); and active wave cancellation (AWC) using 20 % of Power 1 as amplitude for the cycle operation of the actuator. Like in the previous section, these two cases are chosen due to some similarities in the wave amplitude values which are found downstream. Even two different techniques are employed, with a different amount of power applied in each case, and the physical principles which are involved are also distinct, at positions far downstream of the actuator location, the TS wave amplitudes have similar values. The correct analysis of such cases, using a quantitative study of the flow characteristics downstream the actuator position, contributes for understanding the reduction of the wave amplitude.

From previous results, it was already concluded that after a certain distance downstream the actuator position, the TS wave return being amplified. This happens for both techniques continuous and cycle operation. For cycle operation, the position where the waves return to grow is located closer the actuator, while for continuous mode, this position is found further downstream. The aim of the present investigations is to determine the flow characteristics which are able to provide wave amplification or attenuation for both techniques. In other words, the reason why the waves grow again is sought.

Figure 7.10-a and b shows results in a region about 0.10 m around the actuator position for both techniques continuous and cycle operation. Contour plots are always kept the same to facilitate the comparison. In these figures, the wall parallel velocity component is analyzed: the averaged base flow field (boundary layer with excited TS waves) is subtracted from the averaged flow field influenced by a plasma actuator. The results are similar to a wall jet and represent the overall flow acceleration which is promoted by the actuator.

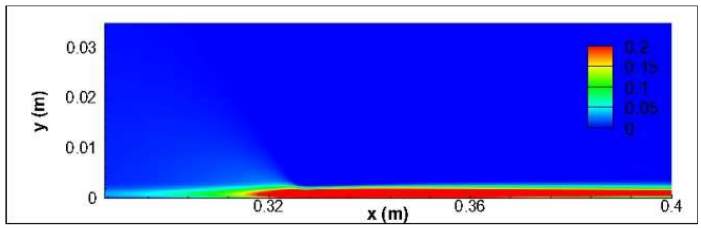

(a) CA. $u - u_{base}$

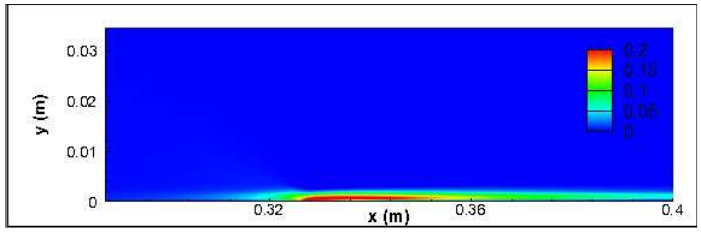

(b) AWC. $u - u_{base}$

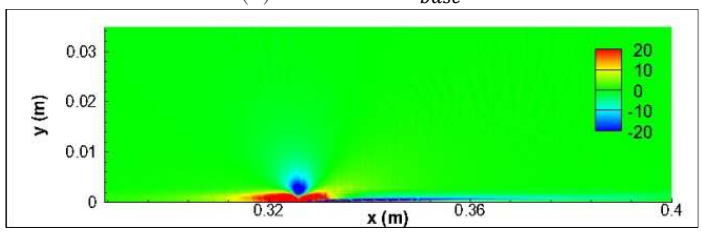

(c) CA. $\frac{\partial(u-u_{base})}{\partial x}$

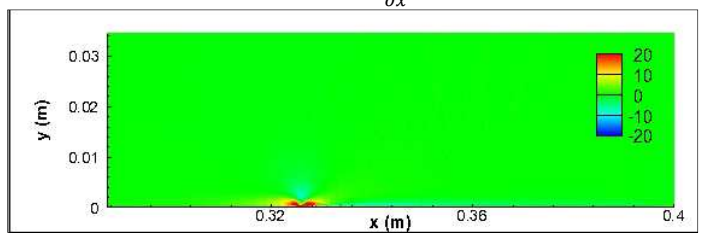

(d) AWC. $\frac{\partial(u-u_{base})}{\partial x}$

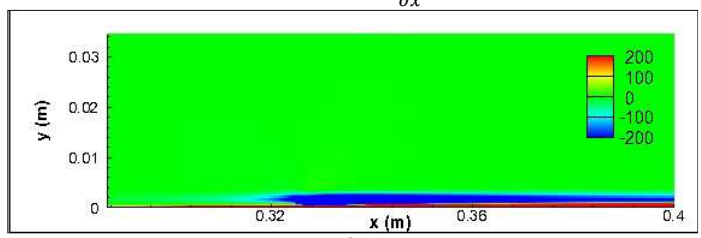

(e) CA. $\frac{\partial(u-u_{base})}{\partial y}$

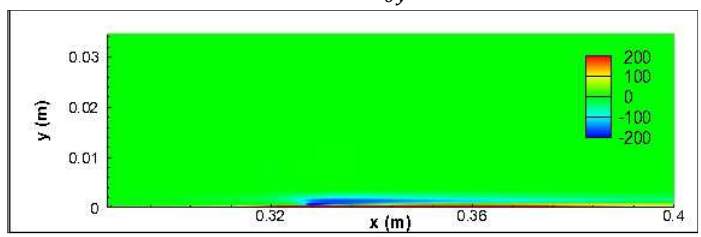

(f) AWC. $\frac{\partial(u-u_{base})}{\partial y}$

Figure 7.10: Downstream effect comparison between Continuous Actuation (CA) and Active wave cancellation (AWC). Contour maps show results of the time averaged wall jet, derivatives in x and y for the wall parallel velocity component.

For continuous actuation, Figure 7.10-a, it can be seen a much stronger flow acceleration next to the wall, obviously caused by the higher power applied to the actuator. The wall jet resultant of cycle operation, Figure 7.10-b, even much weaker, produces the same wave amplitudes downstream due to the superposition of velocity fluctuations. Figures 7.10 - c, d, e, f present the contour maps of first derivatives in x and y direction of the wall parallel velocity. These figures reveal similar patterns, but in different magnitudes, found for both cycle and continuous mode operation. Lower derivative values are found for cycle operation due to the lower power used.

The contour maps of the derivatives of the wall normal velocity component in x direction, Figures 7.10-c, d, show a zone of high values right upstream of the actuator position, followed by an elongated lower zone in x direction downstream of the actuator position. A small zone of negative values is also found right on the top of the actuator. These zones reflect the areas of flow acceleration and deceleration. Strong fluid acceleration happens in front of the actuator and deceleration follows downstream. The derivatives in y direction, Figures 7.10-e, f, have about one order higher magnitude compared to the derivatives in x direction. The actuator influence is stronger in y direction, especially for continuous mode, because the velocity profiles are then modified.

A closer view in the magnitude of the derivatives is shown in Figure 7.11, where the averaged velocity profiles of the wall-parallel component, and its derivatives in several locations, are plotted. At the actuator position, $x = 0.325$ m in Figure 7.11-a, only very small differences can be seen between the two techniques in the velocity profiles and first derivatives. The use of continuous actuation with 80 % of Power 1 produces a strong peak in the second derivative near the flat plate. For cycle operation of the plasma actuator, this peak has a much smaller magnitude and it is already completely vanished a few centimeters downstream the actuator. In Figure 7.11-c, one can see the second derivative profile for cycle operation of the plasma actuator at the location $x = 0.350$ m – which is only two centimeters downstream the actuator position. At this point, the second derivative takes the standard shape without the lower peak caused by the influence of the plasma actuator. From Figure 7.6-a it was previously found that for a similar configuration in cycle operation of the plasma actuator, the waves restart to grow after 0.025 m downstream the plasma actuator. For continuous operation of the plasma actuator, the second derivative profiles have the lowest values caused by the plasma acceleration close to the flat plate until position $x = 0.400$, which is 0.075 m

downstream the actuator position.

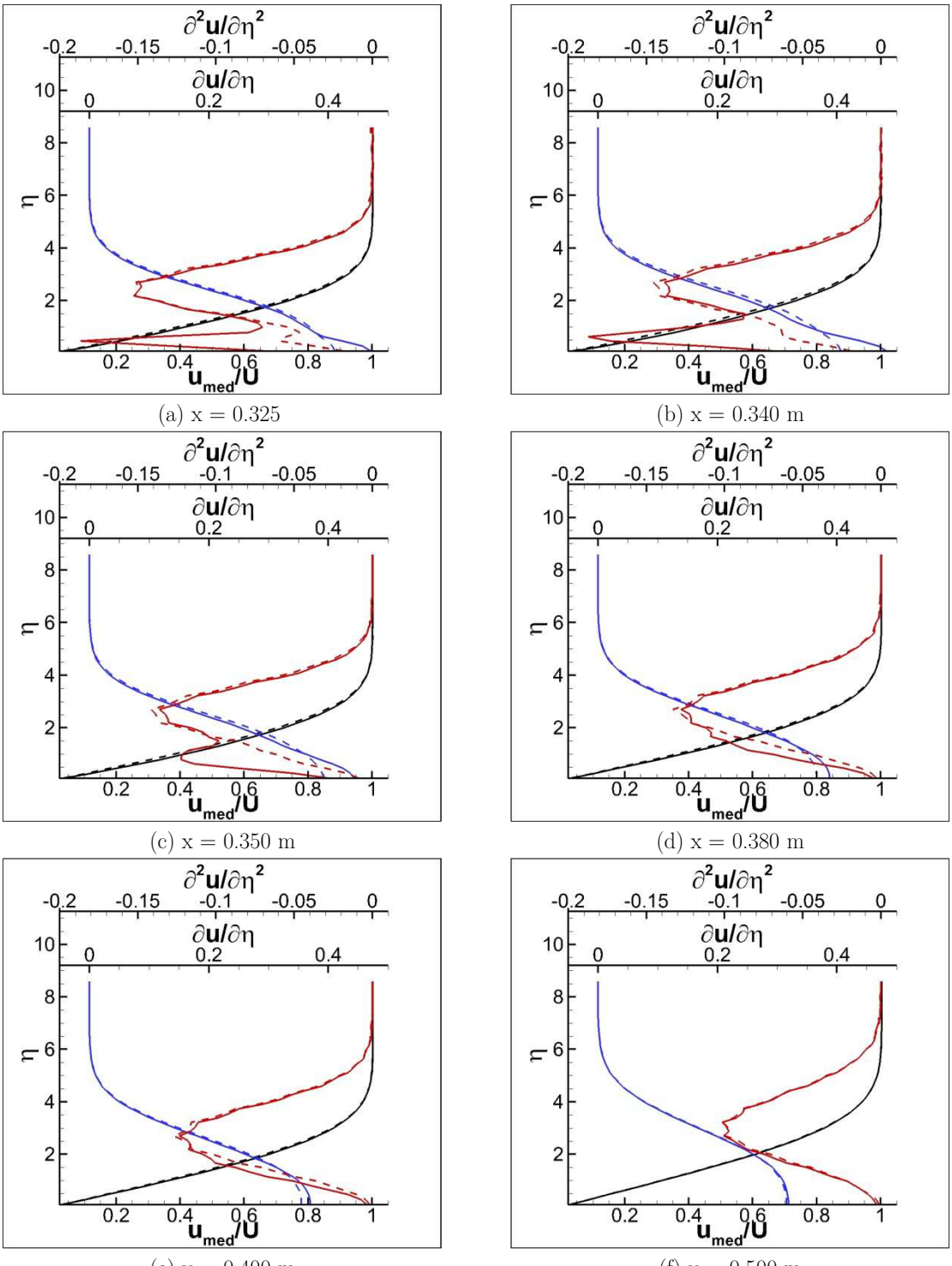

(a) x = 0.325

(b) x = 0.340 m

(c) x = 0.350 m

(d) x = 0.380 m

(e) x = 0.400 m

(f) x = 0.500 m

Figure 7.11: Comparisons between Active Wave Cancellation (AWC) and Continuous Actuation (CA) of the averaged velocity profile, first and second derivatives. Solid lines are used for Continuous Actuation and dashed lines for Active Wave Cancellation.

Also according to Figure 7.6-a, for 80 % of Power 1 applied to the plasma actuator in continuous mode, the TS waves restart to grow after 0.075 m downstream the actuator position. At a further downstream position, $x = 0.500$ in Figure 7.11-f, the averaged velocity profile and the first and second derivatives profiles show a good agreement for both approaches continuous and cycle mode. At this position, the waves present the same amplitude in both cases.

The presence of a lower peak in the second derivative profile is an indicator whether the flow disturbances are being attenuated or amplified. The absence of such a peak also shows that the influence of the plasma actuator is not present in a determined location. From that point and further downstream the standard initial properties of the flow should be considered, such as the growth of TS waves.

Figure 7.12 presents a comparison of the two techniques using the rms velocity fluctuations for several locations. The changes in the position of the neutral point indicate modifications in the flow stability properties. A normal TS wave grows downstream the excitation point and has a modification of the neutral point which is moved up, in non-dimensional scale (η). Thereby, as a disturbance is amplified in a boundary layer flow, the point of zero disturbances, or neutral point, is located at a higher position, as previously explained in Chapter 6.

At the actuator location, Figure 7.12-a, a first reduction of the wave amplitude is already found for cycle operation and it is intensified downstream, Figure 7.12-b. At $x = 0.350$ m, the location where the TS waves return to grow for cycle operation, the neutral point of the TS wave is located in a lower position for AWC. At $x = 0.400$ m, Figure 7.12-e, both methods provide the neutral point at a same location, with also similar wave amplitudes. The situation in Figure 7.12-e can be compared to Figure 7.12-a at the actuator position: the neutral point is located at the same position but the wave amplitudes are smaller due to the plasma actuator effects.

Figure 7.12-d shows results for $x = 0.380$ m, where the waves influenced by an actuator in continuous mode are still inside the attenuation zone, and the waves influenced by an actuator in cycle mode already started to grow once more. Even the magnitude of the amplitudes found at this location are smaller for AWC, the neutral point is positioned at a higher position as compared with the upstream profiles. This indicates that the disturbances are already inside of an amplification zone, and the influence of the actuator is not strong anymore for AWC.

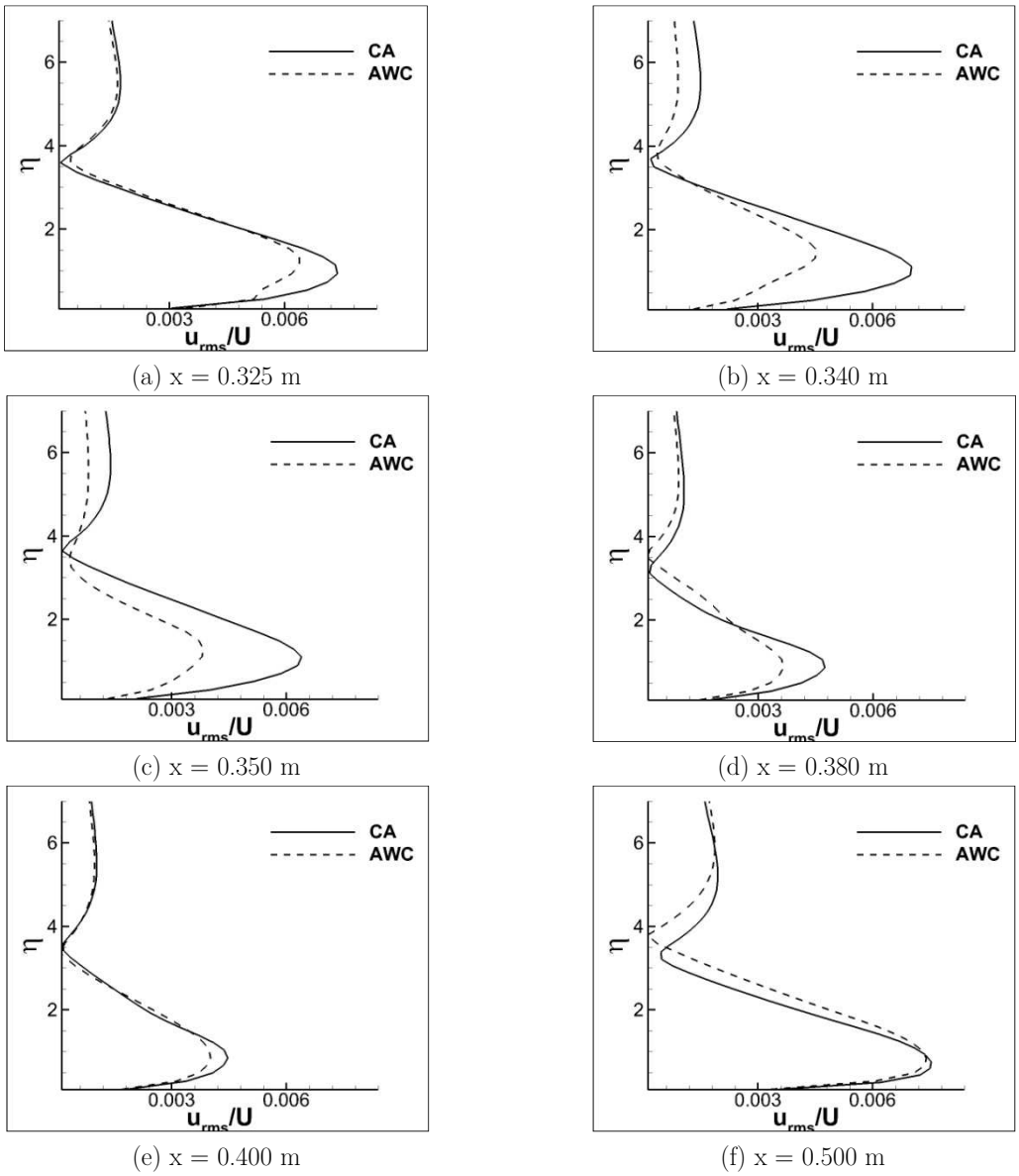

(a) x = 0.325 m (b) x = 0.340 m

(c) x = 0.350 m (d) x = 0.380 m

(e) x = 0.400 m (f) x = 0.500 m

Figure 7.12: Tollmien-Schlichting waves in several position for comparison of cycle mode operation (AWC) and continuous actuation (CA).

A plasma actuator operating in continuous mode is able to hold the neutral point height until a certain position downstream. Further downstream, beyond $x = 0.500$ m, for continuous actuation, the neutral point is located at a lower position, which is contrary to the development of the TS wave in a Blasius boundary layer flow. The use of a plasma actuator in cycle mode of operation does not produces significant modifications in the movement of the neutral point, which is found at a slightly higher position further downstream, Figure 7.12-f.

As another indicator of the flow stability, the neutral point, when it is moved to lower positions downstream, denotes that the flow disturbances can be amplified in lower rates.

The continuous actuation modifies the stability properties of the flow. In a different form, the cycle operation of the plasma actuator only reduces the amplitudes of the disturbances. The coincident amplitude values reached by these two techniques at $x = 0.500$ m are produced by two distinguished scenarios, and the TS waves are found in different stages of development, due to the different locations of the neutral point.

The wall-normal component of the velocity fluctuations is about one order of magnitude lower than the wall parallel velocity component. Results for the averaged flow using the wall-normal velocity component subtracted the averaged values for the base flow (boundary layer with excited TS waves) are presented in Figures 7.13-a and b for continuous and cycle operation of the plasma actuator.

The region right above the actuator concentrates negative values for the wall normal velocity component, due to the suction which is a response to the flow acceleration of the wall parallel velocity component. High power used in continuous actuation promotes the largest suction area. Similarly, stronger effects are found using continuous mode for the behavior of the first derivative in x and y direction, due to the higher quantities of momentum which are added to the flow by the plasma actuator, Figures 7.13-c, d, e, f

The wall-normal velocity component derivative in y direction has a similar shape as the wall-parallel velocity fluctuations derivative in x direction, but with different magnitudes, Figures 7.10-c, d.

The elongated regions where high values are found for derivative in y direction of the wall normal velocity component correspond to the areas where the lowest values are found for the derivatives in x direction of the wall-parallel velocity component. Regions where meaningful values for these derivatives are found are also extended along the distance where the amplitudes of the waves are reduced. This behavior is found to be the same for cycle and continuous operation, but it is extended until a more downstream distance according to the amount of power which the actuator is operated.

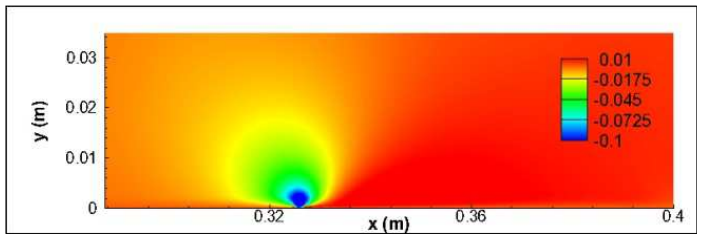

(a)CA. $v - v_{base}$

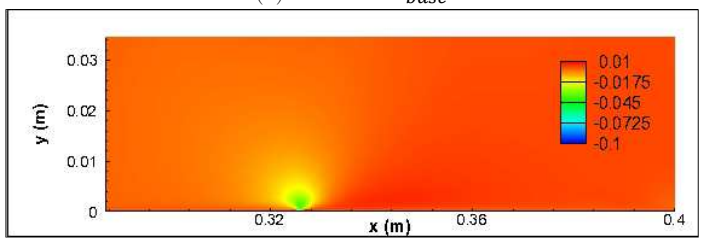

(b) AWC. $v - v_{base}$

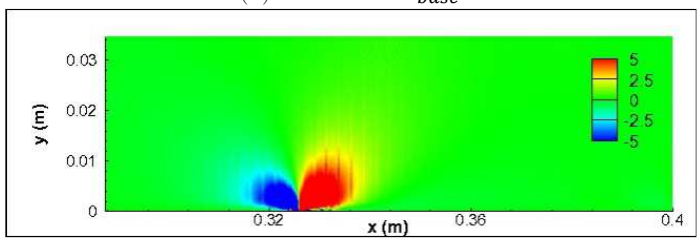

(c)CA. $\frac{\partial(v-v_{base})}{\partial x}$

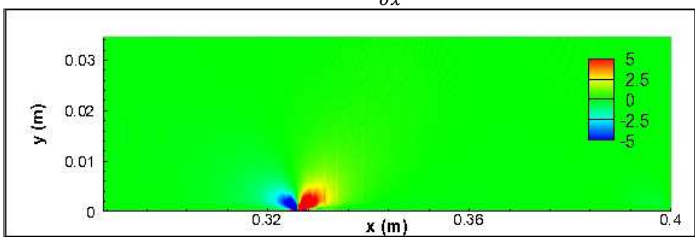

(d)AWC. $\frac{\partial(v-v_{base})}{\partial x}$

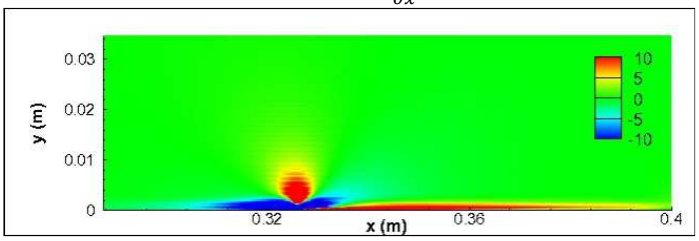

(e)CA. $\frac{\partial(v-v_{base})}{\partial y}$

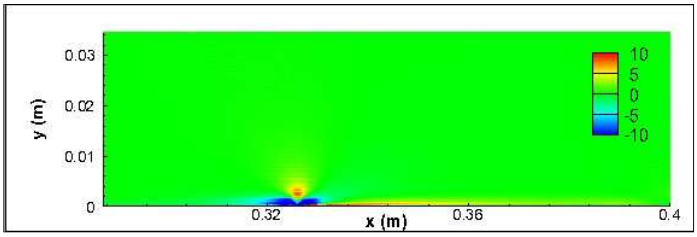

(f)AWC. $\frac{\partial(v-v_{base})}{\partial y}$

Figure 7.13: Downstream effect comparison between Continuous Actuation (CA) and Active wave cancellation (AWC). Contour maps show results of the time averaged wall jet, derivatives in x and y direction for the wall normal velocity component.

7.2.4. Linear Stability Analysis

Numerical results from DNS simulations of the flow over a flat plate influenced by a plasma actuator are analyzed using the linear stability theory. Disturbances are artificially excited at the point $x = 0.225$ m, and the plasma actuator is positioned at $x = 0.225$ m. Two operational modes are considered: Continuous operation with 20 % and 80 % of Power 1 and cycle operation using 20 % of Power 1 as amplitude of the applied body force. The averaged velocity profiles in several locations are used as input for the Orr-Sommerfeld equations. The growth rates of the excited disturbances are compared to the normalized TS wave amplitudes computed by DNS.

Figure 7.14-a shows results for linear stability analysis of continuous actuation with 20 % of Power 1. Downstream the excitation point, flow disturbances develop into TS waves at a distance about 0.03 m. The disturbances reach the values in perfect agreement with the theory up to the plasma actuator position. Downstream the actuator location, the amplitude reduction is very smooth due to the low power applied. The slight wave attenuation promoted by the effect of the actuator is also predicted by the stability theory.

The use of higher power with continuous actuation is compared to the stability theory in Figure 7.14-b. The stronger wave attenuation is predicted by the stability equations by an accentuated area of lower values for the N factors. The boundary layer stabilization effect promoted by a plasma actuator is in agreement with the stability analysis, because similar magnitudes are expected for the wave amplitude values. The higher the power, the lower are the growth rates, providing lower TS waves amplitudes.

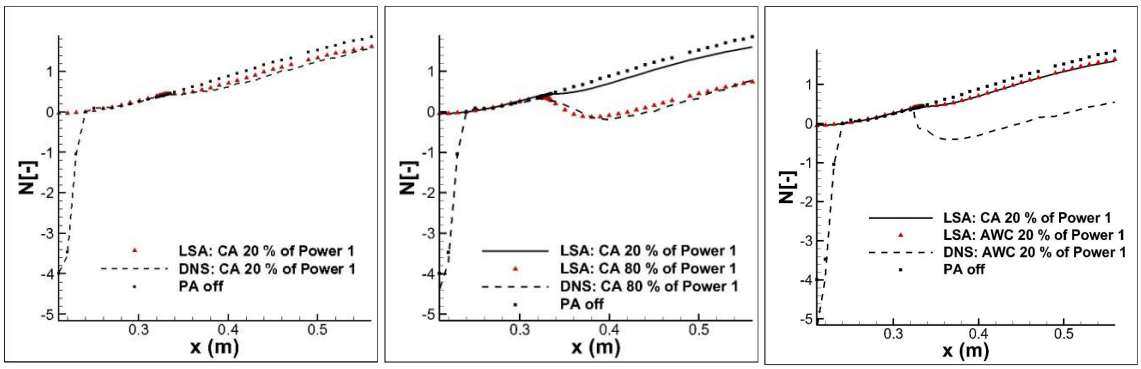

(a) (b) (c)

Figure 7.14: Linear stability analysis (LSA) of two techniques for flow control: boundary layer stabilization produced by continuous actuation (CA) and active wave cancellation (AWC) produced by cycle actuation. DNS results are compared with the theoretical non-dimensionalized growth rates. (a) Low forcing applied in continuous mode. (b) Low and high forcing applied in continuous mode. (c) Low forcing applied in continuous and cycle operational modes.

For an actuator which is operated in cycle mode, the mechanisms which are involved to produce a reduction of the flow disturbances are very different. The stability analysis for such cases is not able to predict the complete wave cancellation process. Figure 7.14-c shows the N factors resulting from the stability equations which indicate only a small reduction of the TS waves. The wave reduction which is predicted by the stability analysis for the cycle operation of the plasma actuator with amplitude 20 % of Power 1 is equivalent to the N factor values found for continuous actuation also using 20 % of Power 1. This important fact indicates that the active wave cancellation process also implies boundary layer stabilization to some degree, which is equivalent to the averaged value of power applied in continuous mode.

Active wave cancellation is a more efficient tool, in terms of power saving, for localized TS wave amplitude reduction. But using only this technique, the flow properties are not strongly modified downstream the actuator position. The boundary layer stabilization phenomenon is directly proportional to the averaged amount of momentum which is added to the flow. Such as the shape factor, the stability properties of a boundary layer flow are sensitive only to averaged quantities. Small and instantaneous profile modifications have a high influence on the velocity fluctuations and may interact with them. These changes alter very few quantities of the flow stability properties.

Using the DNS results, the stability analysis is also used to compute the unstable regions along the flat plate flow for several frequencies. In Figure 7.15, the area between the lines represents the positions in x direction where a certain frequency is amplified.

For the uncontrolled case with the plasma actuator off, a continuous and curved unstable region occupies the whole analyzed domain. Frequencies between 120 and 450 Hz should be amplified in different positions if no control is applied.

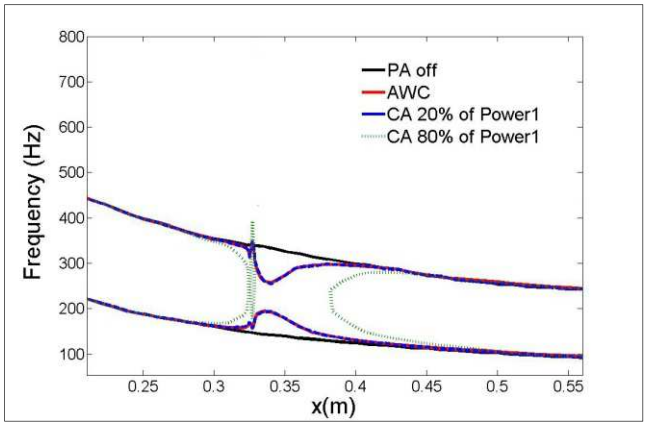

Figure 7.15: Critical values for the frequency amplification, for several operational modes.

The unstable regions evaluated for cycle operation of a plasma actuator coincide with the same results for continuous actuation using low power. These two lines are superimposed in the graphic of Figure 7.15. Likewise the growth rates quantities in Figures 7.14, the unstable regions are also only sensitive to time averaged quantities. For these two cases, the unstable region becomes narrow right at the actuator position. This indicates a reduction of the growth rates and the local stabilization of some frequency modes in the region surrounding the actuator. Further downstream, the unstable region is reestablished following the same values as for the uncontrolled case.

High power applied continuously to the actuator produces stronger modifications in the stability which divides the unstable region in two parts. Immediately after the actuator location, no frequency mode is found to be unstable. About 0.05 m downstream the actuator position, the unstable region is restored and modes around 280 Hz start being amplified once more. The use of 80 % of Power 1 is enough to provide a completely stable region for a few centimeters, where no frequency mode is able to be amplified. At this point is it useful to emphasize this characteristic as the main advantage of the use of continuous actuation. For active wave cancellation the stabilization effect is very small. Even the amplitudes are strongly reduced; the waves keep growing at the same rates. Continuous actuation promotes boundary layer stabilization by breaking the unstable region for a certain distance downstream the actuator position.

The higher the power applied to the actuator, the longer is the separation between the two sections where frequencies can be amplified. A very high power applied to the actuator can separate the unstable regions until a point where the residual disturbances completely vanish before reaching the next critical values. Figure 7.16 shows the linear stability diagram for Power 3 applied in continuous mode to the actuator in a 16 m/s flow. The strong forcing added to the boundary layer provides a completely stable region until the end of the computational domain.

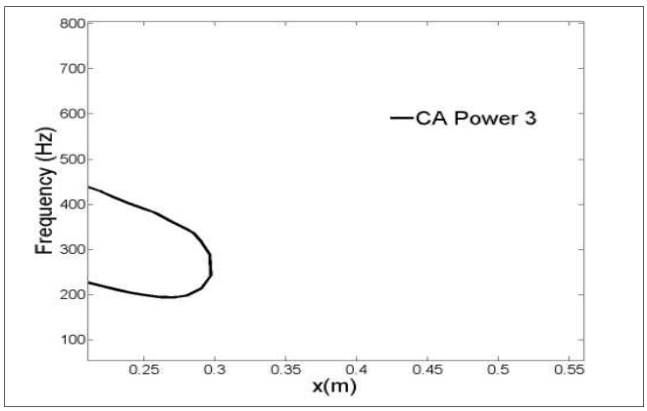

Figure 7.16: Critical values for the frequency amplification for Power 3 applied in continuous mode.

7.3. Summary of cycle actuation techniques

Active wave cancellation is promoted by a periodic force applied to the plasma actuator. When the control parameters amplitude and phase shift are correctly chosen, the wave amplitude reduction for this technique needs much lower energy consumption.

In comparison with continuous actuation, active wave cancellation happens right at the plasma actuator location. While, for continuous actuation, the wave attenuation is smoother and distributed along a certain distance downstream the actuator.

For cycle operation of the plasma actuator, only small modifications of the flow stability occur, due to the low amount of power which is used with this technique. In cycle operation, TS waves return to grow at an upstream position and with higher growth rates as in the similar case using continuous actuation. The stability modifications promoted by cycle operation of the actuator are equivalent to the modifications promoted by the averaged amount of power applied in continuous mode.

From the comparisons of both techniques, one can conclude that the main advantage of using continuous actuations is the fact of having a more stable boundary layer profile for a longer distance downstream the actuator. On the contrary, for cycle actuation, the main advantage is to have an immediate effect of wave reduction with lower power consumption at the actuator location.

8. Combined effects for flow control purposes

In this chapter, the knowledge acquired by the previous investigations of boundary layer stabilization and active wave cancellation is applied to formulate a new technique of plasma actuator operation. The performance of an actuator on the attenuation of Tollmien-Schlichting waves can be highly increased though the combination of effects in a hybrid approach. The studies aim to quantify the maximal reached efficiency and provide the full understanding of the physical effects which are involved.

Test cases use only one actuator (at PA1) which is operated in several modes with different power supply, and it is positioned at x = 0.325 m. The freestream velocity is 16 m/s and Tollmien-Schlichting waves are artificially excited at $x = 0.225$ m.

8.1. The hypothetical case

As previously discussed, when an actuator is operated in continuous mode, the velocity profile modifications can promote strong changes in the stability properties of a boundary layer flow. Such changes, when correctly applied, alter the amplification or attenuation of disturbances which are present in the flow field. On the other hand, for an actuator which is operated in cycle mode, the active wave cancellation process consists merely of a dynamic superposition of velocity fluctuations. However, within the active wave cancellation process, stabilization is also involved. From the linear stability analysis conducted in the previous chapter, it was found that the boundary layer stabilization effect promoted by an actuator in cycle mode is equivalent to the same effect of an actuator in continuous mode operated with the averaged value of power source.

To achieve results which can provide a purely active wave cancellation effect, a hypothetical test case is proposed, using negative values for the body force. The new power distribution, with a zero averaged value, aims to produce a reduction of the flow disturbances without producing any residual change in the averaged velocity profiles. In

this manner, the amplitude reduction of the TS waves and its further development downstream the actuator position is an effect completely free of changes in the stability properties of a flow.

The suggestion of an actuator which is operated with negative forces is possible only using numerical simulations. The current experimental configuration of the plasma actuator using two electrodes would not be able to provide a zero-net power supply by physical limitations. Nevertheless, the direct numerical simulations can provide very interesting information and contribute to the advancements in flow control sciences.

Figure 8.1-a shows the power distribution of the proposed hypothetical case (Hyp) with a null averaged power supply used for pure wave cancellation, compared with the real case of active wave cancellation (AWC) and the averaged value of power from AWC applied in continuous mode (CA). The numerical results for the TS wave amplitudes are shown in Figure 8.1-b, for a boundary layer flow influenced by an actuator operated in the three different modes.

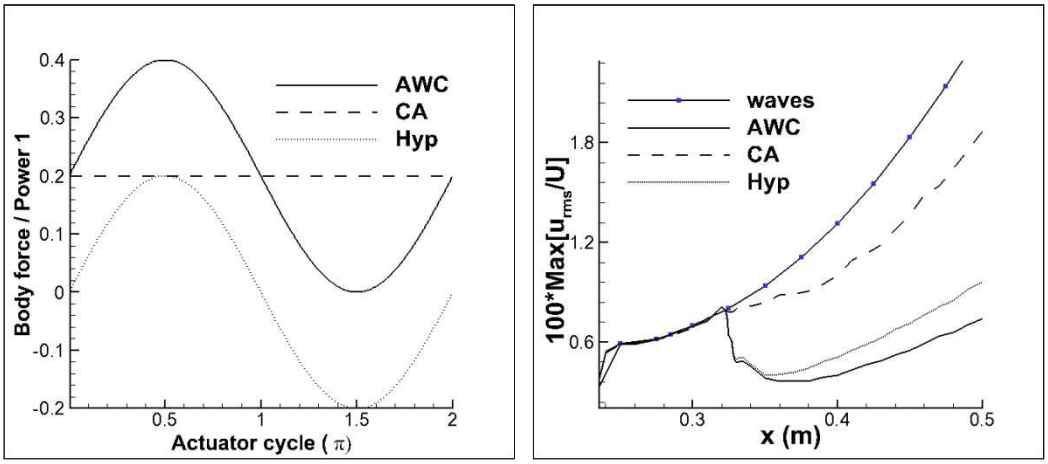

(a) (b)

Figure 8.1: The hypothetical case compared with the real case of active wave cancellation and continuous actuation. (a) Power supply. (b) Maximal amplitudes of the flow disturbances.

Rather poor wave attenuation is reached for the continuous mode operation of the plasma actuator, due to the low force which is employed. The same amount of power employed in cycle mode (AWC), with a correct adjustment of the control parameters, provides the lowest wave amplitude results. In comparison, the hypothetical case (Hyp), provides somewhat higher wave amplitudes than compared to the AWC. The results for Hyp show the pure effect of active wave cancellation without any boundary layer stabilization.

The quantification of the wave attenuation rates (in percentage) of these three last cases in Figure 8.1 is presented in Table 8.1, for several x locations. The hypothetical case shows cancellation rates at the actuator location with values close to the values found for active wave cancellation. A few centimeters downstream, at $x = 0.350$ m, the results between Hyp and AWC are still quite close. At $x = 0.380$ m, the rates for CA start to become more significant, and the rates for Hyp are lower than the ones found for AWC. This indicates that the absence of a continuous part for the hypothetical case is manifested only about 0.05 m downstream the actuator position. The active wave cancellation process is most responsible for reduction of the TS wave at the actuator location and in the region immediately downstream to it.

Further downstream, the rates for the hypothetical case have values about 10 % lower than the rates found for active wave cancellation. The pure continuous case has rates higher than 20 %. The real effect of active wave cancellation (AWC) is then not a simple sum of both effects of wave amplitude reduction found in CA and Hyp cases, but a complex combination of them.

x (m)	AWC	CA	Hyp
0.325	19.15	2.79	18.49
0.350	59.15	10.71	57.03
0.380	68.22	21.27	61.83
0.400	69.32	23.43	61.27
0.500	70.16	24.82	61.23

Table 8.1: Wave attenuation rates in several locations for three different approaches.

The shape factor is also evaluated for the hypothetical case as means of validation. Results are presented in Figure 8.2-a. Active wave cancellation and continuous actuation show similar values for the shape factor over the entire domain. For these two cases, the actuator produces a small negative peak in the shape factor values which is reestablished downstream. The hypothetical case, with null averaged force does not produce any modification in the shape factor values. Thus, the effect produced by the hypothetical case in wave amplitude reduction is purely a superposition of fluctuations.

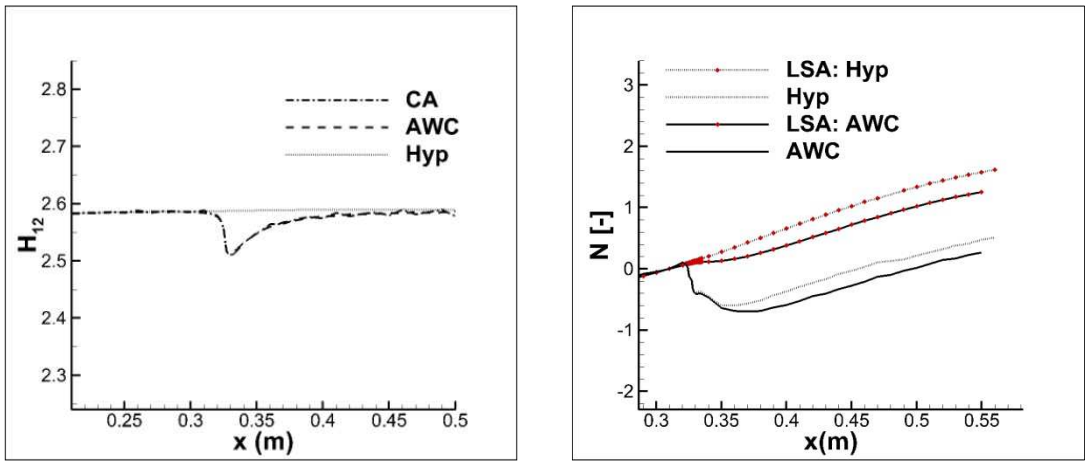

Figure 8.2: Analyze of the hypothetical case. (a) Shape factor influence. (b) Linear stability.

Linear Stability Analysis is also conducted to analyze the boundary layer stabilization effect promoted by the hypothetical case. Figure 8.2-b shows results for the maximal disturbances extracted from the DNS simulations compared with the N factor evaluated with LSA. No stability modifications were found in the hypothetical case. In contrast, for the AWC case a small portion of boundary layer stabilization is found right after the actuator location.

The previous cases use TS wave artificial excitation with a two-dimensional amplitude of A2D = 550. For the following special case, several other disturbances are excited using different amplitudes (A2D =400, 300, 210 and 130). The development of such waves with smaller amplitude is compared to the development of a wave excited at A2D = 550 after passing an actuator which is operated in null averaged mode (Hyp). Results can be seen in Figure 8.3.

The different amplitude disturbances are excited at the same frequency of 220 Hz. The smaller waves develop downstream with natural amplification rates, and are not influenced by any actuator. The downstream amplitude is proportional to the initial amplitude of excitation.

For TS waves excited with A2D = 210, a very good agreement of the maximal amplitude of the disturbances is reached downstream at x = 0.40 m with the results of the hypothetical case. The coincident values after the actuation indicate once more that the pure active wave cancellation does not promote additional modification in the boundary layer stability. Waves have their amplitude reduced due to the superposition of fluctuations. These waves return to grow a few centimeters downstream after the zone of influence of the actuator with the same rates as any disturbance would have when excited with a smaller amplitude.

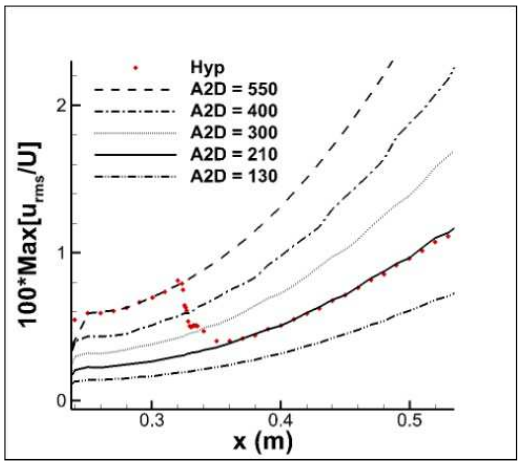

Figure 8.3: Development of Tollmien-Schlichting waves is compared to influence of an actuator which operated in hypothetical mode, with pure wave cancellation effect.

8.2. Hybrid approach

Starting from the point that real active wave cancellation process itself is already a combination of effects involving a small portion of pure wave attenuation, the idea of increasing the boundary layer stabilization gives rise to a new technique: the hybrid approach.

For a constant increase of pure continuous power applied to the actuator the wave attenuation rates increase until a certain location downstream the actuator position, Figure 8.4-a.

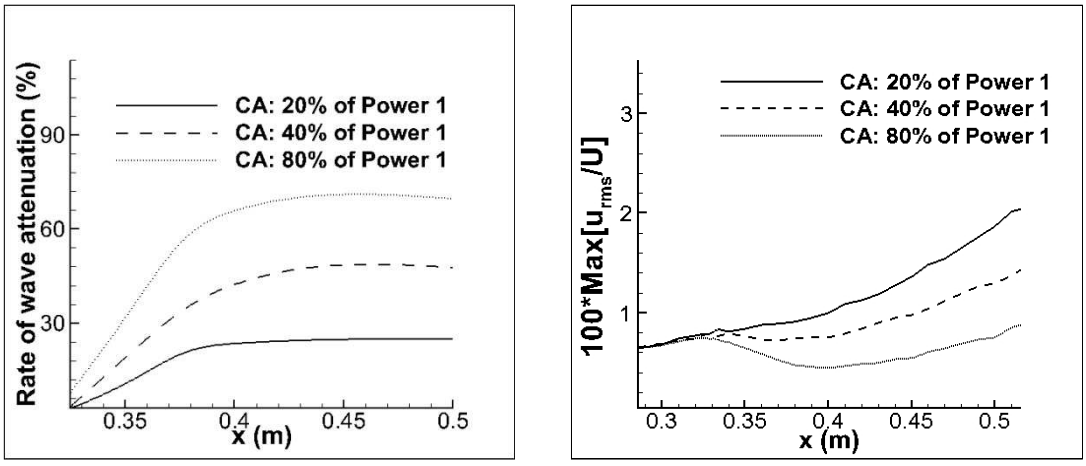

(a) (b)

Figure 8.4: (a) Rates of wave attenuation. (b) Maximal amplitude of disturbances for three different values of force applied to the actuator.

Further downstream of the actuator position, the rates of wave attenuation remain almost constant. Maximal amplitudes of the TS waves obtained with different magnitudes of boundary layer stabilization are also plotted in Figure 8.4-b. The rates of wave attenuation are not directly proportional to the amount of power which is applied in a constant mode to the actuator. A similar behavior is expected for hybrid operation of the plasma actuator.

Based on that, the first hybrid test cases utilize a small shift in the power supply, given by 10% and 20 % of Power 1 applied in continuous mode over the sinusoidal power distribution used for AWC, Figure 8.5-a. Results for the maximal amplitudes of the TS waves are shown in Figure 8.5-b, compared with the pure continuous actuation using 20 % of Power 1 and active wave cancellation with cycle operation and 20 % of Power 1 used as power amplitude.

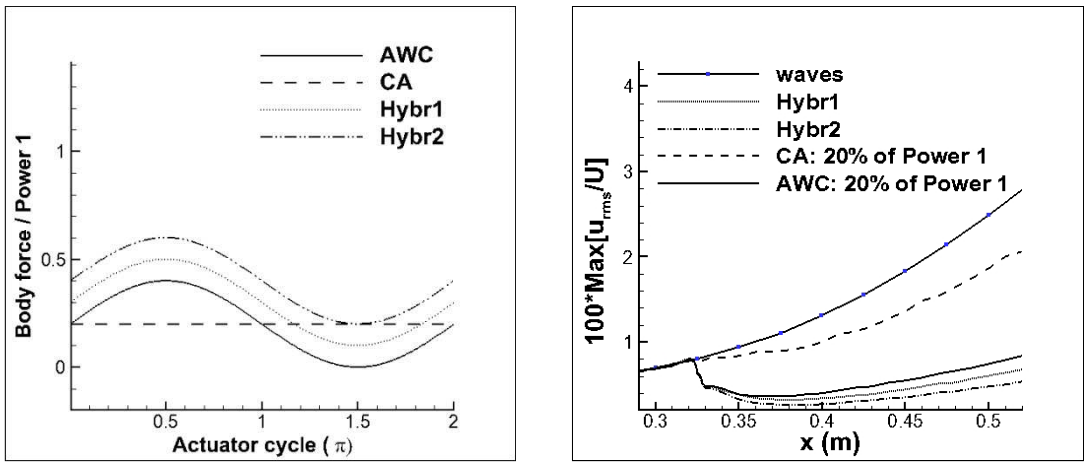

(a) (b)

Figure 8.5: Hybrid technique, combination of boundary layer stabilization and active wave cancellation. Hybr1: AWC (20 % of Power 1) + CA (10 % of Power 1). Hybr2: AWC (20 % of Power 1) + CA (20 % of Power 1). (a) Power supply used for the first hybrid tests. (b) Maximal amplitudes of disturbances.

The addition of a small continuous part also produces a small reduction of the wave amplitudes compared to the standard cycle operation of a plasma actuator. Table 8.2 provides a quantification of these rates.

A small increasing of the averaged power supply (10 % of Power 1) produces results in wave reduction about 5 % better than only cycle operation downstream the actuator. Further increase of power (20 % of Power 1) also produces an improvement of about 5 %. For low power added to cycle operation the effects obtained in wave attenuation seem to be linear and proportional to the shift of power supply. Though, the

improvement of the cancellation rates in the hybrid cases is still not equivalent to the rates of pure continuous actuation with 20 % of Power 1. Also, for Hybr2, better rates are reached already at the actuator position, while for Hybr1, small modifications only have a significant magnitude at more downstream positions.

The difference of a continuous quota of power between AWC and Hyp, as well as with Hybr2 and AWC, provides in both cases an improvement of about 10 %. The improvement of the wave amplitude reduction reached for Hybr2 is about 10 % better than the rates of AWC. Similarly, the rates amplitude reduction evaluated for AWC in relation to the hypothetical case, commented in the previous section, are also about 10 % better. In principle, it appears that the linear relation found for low power added in continuous to the cycle actuator remains independent of the direction in which the force is applied.

x(m)	CA	AWC	Hybr1	Hybr2
0.325	2.79	19.15	19.19	21.44
0.350	10.71	59.15	58.63	65.02
0.380	21.27	68.22	72.51	77.65
0.400	23.43	69.32	73.86	79.20
0.500	24.82	70.16	75.41	80.68

Table 8.2: Rates of TS wave amplitude reduction for low continuous power added to cycle actuation, hybrid technique.

What seems to be a linear relation for low power applied in continuous mode over a cycle mode of operation of the actuator for the amplitude reduction rates; is now tested in the following cases for a high power applied in continuous mode.

A new hybrid case uses now 100 % of Power 1 as continuous part (shift), in addition to the standard cycle operation used in AWC, as illustrated in Figure 8.6-a. For such a high shift of power, it is important to emphasize the re-optimization of the phase shift applied to the sinusoidal portion of power supply. The boundary layer stabilization promoted by continuous actuation modifies the TS waves speed and wave length immediately downstream the actuator position. These changes also interfere at the phase angle of the periodic velocity fluctuations. A wrong value of the phase shift can lead to wrong quantification of the wave stabilizing effects of the plasma actuator. However, the wave amplitude is kept at the same value for a better comparison of the hybrid effects.

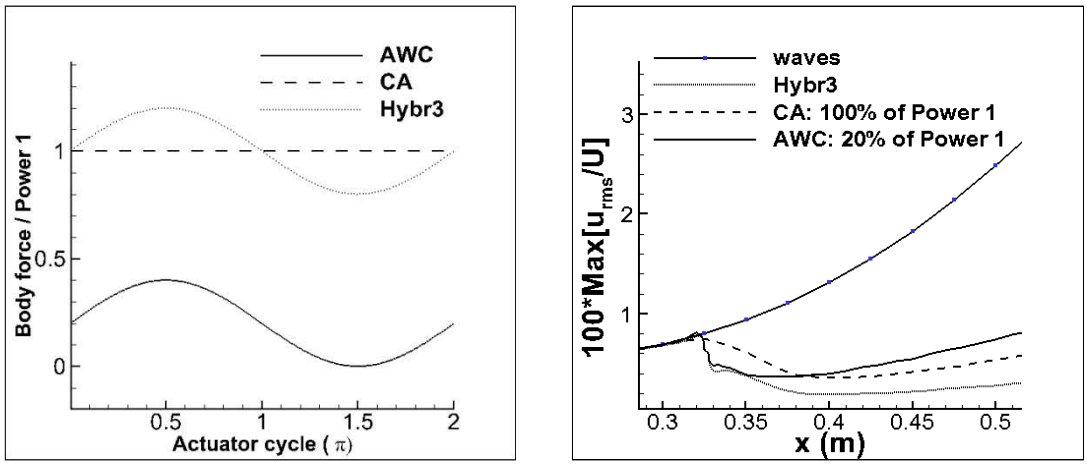

Figure 8.6: Hybrid technique with high continuous power applied. Hybr3: AWC (20 % of Power 1) + CA (100 % of Power 1). (a) Power magnitude illustration. (b) Maximal amplitude of the TS waves.

Significant reduction of the maximal amplitude of the flow disturbances can be seen in Figure 8.6-b. High continuous power provided the boundary layer stabilization downstream the actuator position.

Using Hybr3, at the distance between $x = 0.325$ m and x 0.350 m, most of the active wave cancelation occurs. Downstream $x = 0.350$ m, an additional reduction of the wave amplitude follows until approximately $x = 0.400$ m. Downstream, the Hybr3 curve is found almost in parallel with the curve of continuous actuation (CA). In Figure 8.6-b, the TS waves return to grow in Hybr3 with a different angle of inclination from AWC, but similar to CA.

The greatest advantage of the hybrid approach is that for the same averaged value of force applied in two techniques (CA with 100 % of Power 1 and Hybr3) significant improvement in wave reduction can be achieved by simple sinusoidal modulation of small amplitude. The combination of active wave cancellation and boundary layer stabilization provides high reduction of the wave amplitude right at the actuator position and also boundary layer stabilization further downstream.

Table 8.3 compares the rates of wave amplitude reduction of the different approaches. A high continuous part added to the cycle operation of the actuator provides an improvement of the wave attenuation rates which is lower than 20 %. The linearity between continuous addition of power and amplitude reduction rates, verified in previous cases, is only valid for very low power applied to the actuator, but not for Hybr3.

x(m)	AWC	CA	Hybr3
0.325	19.15	7.66	18.67
0.350	59.15	35.00	59.96
0.380	68.22	66.30	81.70
0.400	69.32	72.93	85.76
0.500	70.16	78.30	88.62

Table 8.3: Rates of wave amplitude reduction for a hybrid case with high continuous power supply (100 % of Power 1).

The effect of a sinusoidal modulation of power from the hybrid approach is verified comparing different hybrid power distributions, Figure 8.7-a. The respective reduction of the wave amplitude is shown in Figure 8.7-b.

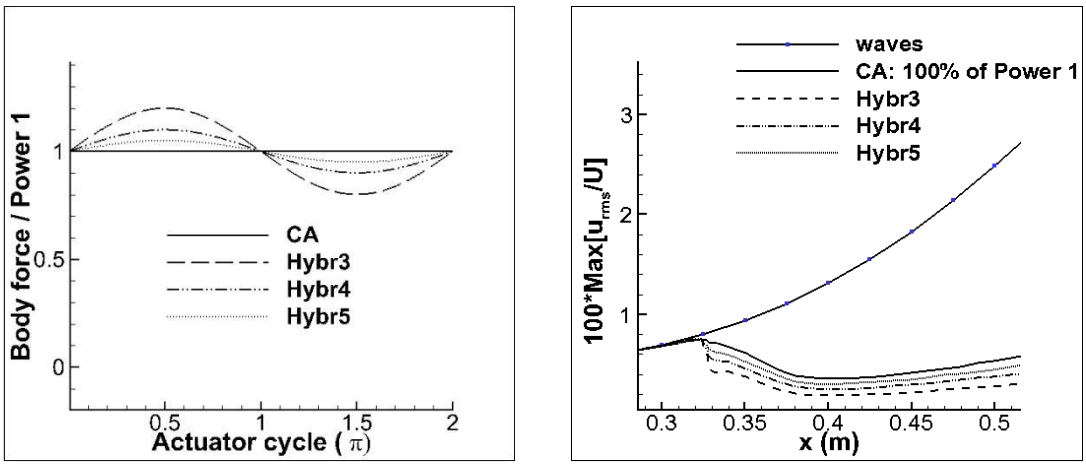

(a) (b)

Figure 8.7: Influence of the amplitude of power modulation. Hybr3: AWC (20 % of Power 1) + CA (100 % of Power 1), Hybr4: AWC (10 % of Power 1) + CA (100 % of Power 1), Hybr5: AWC (5 % of Power 1) + CA (100 % of Power 1). (a) Power supply. (b) Maximal amplitudes of the disturbances.

The amount of power modulation indicates that a corresponding reduction of the wave amplitudes occurs. For higher power modulation (Hybr3), the wave amplitudes are smaller closer to the actuator position. In all hybrid cases, the inclination angle of the maximal disturbances in Figure 8.7-b is correspondent to the angles of continuous actuation. As for Hybr3, Hybr4 and Hybr5 the averaged value of power is the same, the stability properties are also expected to be similar.

As a last comparison, the linear stability of Hybr3 case is analyzed. Figure 8.8 shows results for the N factors normalized and maximal wave amplitudes normalized. The N factor values evaluated for CA are similar to the values obtained with Hybr3. But the

corresponding reduction of the wave amplitude obtained by the hybrid technique is obviously higher.

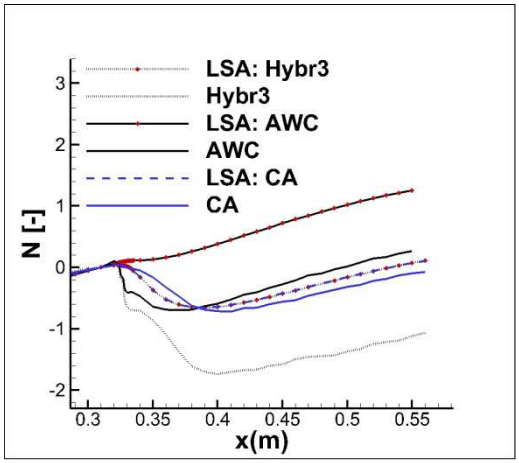

Figure 8.8: Linear stability analysis of the hybrid approach compared with continuous actuation and cycle operational mode.

8.3. Summary of flow control techniques using plasma actuators

A hypothetical case with null averaged power distribution was used to provide a quantitative analysis and the separation of both methods (active wave cancellation and boundary layer stabilization) inside the cycle operation technique. The hypothetical case provides pure active wave cancellation results with no modifications in the shape factor values or stability properties of the flow.

The addition of a continuous part to the cycle operation of the plasma actuator provided a great improvement of the wave reduction rates. By using a small modulation of power applied to a continuous distribution, the wave amplitude is reduced right at the actuator location, but stabilization effects remain at downstream positions. This approach combines the advantages of both techniques and provides a very promising new method of power application to a plasma actuator used in boundary layer flow control.

9. Conclusions

In the present work, a new approach was used for numerical simulation of the fluid mechanic effects of a plasma actuator in a boundary layer flow. The body force evaluated from experimental data (Particle Image Velocimetry) was added to the Navier-Stokes equations as a source term in a finite-volume solver, the *inhouse* code FASTEST. The base flow, with artificially excited Tollmien-Schlhting waves, was submitted to a detailed process of validation and verification to ensure a good precision of the current investigations. The numerical setup, together with the precisely evaluated body force, were able to provide good quantitative analysis of the plasma actuator effects and answer some of the many remaining questions regarding this topic inside the field of flow control sciences.

Numerical studies included the investigation of arrays of actuators, different power supply, continuous and cycle operation of the plasma actuators. The main insights are going to be recapped in the following sections.

9.1. Quantitative analysis of the plasma actuator aerodynamic effects

The numerical investigation of the boundary layer flow influenced by an actuator which operates in continuous mode showed an elongation of the Tollmien-Schlichting waves after passing the accelerated fluid area. This effect is more accentuated for high power applied to the actuator and it is accomplished to an increasing of the wave convective speed and the spatial wave length.

Plasma actuators in continuous mode also modify the stability proprieties of a flow according to the magnitude of power supply. The relation of power applied to the actuator and boundary layer stabilization is not a linear relation. High forcing can provide the breakdown of the unstable region and promote the damping of all frequency

modes in a certain extension near the actuator location. Further downstream, the stability proprieties of the flow are once more reestablished.

In a certain extension, the actuator position along the x direction does not influence the effects of wave attenuation promoted by continuous actuation. The drop of the shape factor promoted remains the same until a distance about $x = 0.475$ m. From this location and further downstream, the influence of the plasma actuator is slightly weaker, even the rates of wave attenuation remain similar related to the non-controlled case.

This independency of the x position is also verified in arrays of actuators. The values found for the wave amplitudes downstream are independent of the power distribution over the array. However, a decreasing distribution of power has the advantage of holding the wave amplitudes at a low value along the extension of the array.

For arrays of actuators, the effect of wave attenuation is cumulative. The use of an additional actuator with the same power supply provides the same rates of wave attenuation applied to a smaller wave, which was already attenuated.

Due to the modifications of the boundary layer velocity profile and increasing of the flow stability, the effect of wave attenuation is verified for all frequencies, not only a single one.

In cycle operation of the plasma actuator, the effect of wave cancellation is concentrated in one specific dominant frequency. Also, active wave cancellation is a localized phenomenon, which occurs right at the actuator position until a distance about 0.025 m downstream. Further downstream, the TS waves return to grow without strong modifications of the stability.

On the other hand, continuous actuation promotes boundary layer stabilization and it is a more power consuming technique. The same values for TS wave amplitude can be reached downstream the actuator with much lower values for cycle operation of the actuator, than compared to continuous actuation. But the boundary layer stabilization effects are more distributed downstream, for a longer extension, not localized. Also, the shape factor modifications are strong for continuous mode. Further downstream, the waves are amplified with different growth rates, due to the high amount of momentum which is inserted to the flow.

9.2. Combined effect for wave cancellation

Linear stability analysis reveals that the standard cycle operation of a plasma actuator, active wave cancellation (AWC), has a cumulative continuous effect which causes small residual boundary layer stabilization. This stabilizing effect is equivalent to the averaged value of the power supply which is applied in sinusoidal mode to the actuator.

The suggestion of a numerical experiment of a hypothetical case with a zero averaged value of power supply supports the quantification of each one of the mechanisms which are involved. The improvements in wave amplitude reduction of AWC in relation to the hypothetical case are equivalent to a further addition of power, in case of small quantities for continuous actuation.

From this point, the idea of a hybrid approach which uses combined techniques is presented as an innovative and very promising method. A certain modulation of power supply is applied to the continuous mode operation of a plasma actuator. The averaged amount of power remains the same. Consequently, the modifications in the shape factor, wall friction and stability remain the same as for the continuous case. But a significant improvement can be found for reduction of the wave amplitudes.

The hybrid approach combines the best effects of both techniques, providing wave cancellation right at the actuator location and also extended boundary layer stabilization. Further downstream, the waves return to be amplified with modified growth rates. The combined effect is not a superposition of wave cancellation rates, but an interaction of the two different mechanisms.

9.3. Concluding remarks and future work

The new methodology for plasma actuator numerical simulation was successfully implemented to the numerical solver. The DNS results provided useful information in a quantitative analysis of Tollmien-Schlichting wave amplitude reduction. The knowledge which was acquired in this simplified case of the flow passing a flat plate can be applied to other more complex problems, for example, the flow passing a real airplane wing.

Some of the results presented in this work were already successfully applied in experimental investigations inside the same research field. The investigation of the

operational parameters which is here presented influenced other research works and clarified some issues concerning the wave attenuation process.

The numerical simulation of aerodynamic plasma actuator effects was an interdisciplinary project which involved the participation of different research groups and departments. The complexity of the problem demanded several views emanating from distinguished areas of knowledge. All together in synergy, the different points of view formed new concepts. These concepts contributed for reaching fully comprehension of some questions which remaining unsolved until now.

As a complementary future work, three-dimensional numerical investigations could be used to verify the spanwise influence of high power applied to the plasma actuator over the Tollmien-Schlichting waves. Numerical simulations with different geometrical configurations involving spanwise oriented plasma actuators for transition control is also a very interesting topic. The knowledge acquired with simple continuous and cycle actuation can also be applied for promoting vortex generation with arrays of actuators.

Bibliography

[Alb11] T. Albrecht. *Zur Transition an einer ebenen Platte und deren Beeinflussung durch elektromagnetische Kräfte*. PhD Thesis. TU Dresden, Germany, 2011.

[AMMGG07] T. Albrecht, H. Metzkes, G. Mutschke, R. Grundmann and G. Geberth. Tollmien-Schlichting wave cancellation using an oscillating Lorentz force. *Advances in Turbulence XI*, Spring Proceedings Physics, 117:218-220, 2007.

[AWGMS11] T. Albrecht, T. Weier, G. Gerbeth, H. Metzkes, and J. Stiller. A method to estimate the planar, instantaneous body force distribution from velocity field measurements. *Physics of Fluids*, 23, 021702, 2011.

[AG06] M. Amitay and A. Glezer. Aerodynamic flow control using synthetic Jet Actuators. *Control of Fluid Flow*, 43-76, 2006.

[And99] P. Andersson. Modelling *of Boundary Layer Stability*. Ph.D thesis, KTH Stockholm, 1999.

[BT10] K. Barckmann and C. Tropea. Dielectric barrier discharge plasmas for flow control at high mach numbers. *5th Flow Control Conference*, Chicago, 2010.

[Bla08] H. Blasius: Grenzschichten in Flüssigkeiten mit kleiner Reibung. Z. *Math. Phys*, 56, 1-37, 1908.

[Bla01] J. Blazek. *Computational fluid dynamics: principles and*

applications. Elsevier, 2001.

[CWG07] C. Cierpka, T. Weier and G. Gerbeth. Electromagnetic control of separated flows using periodic excitation with different wave forms. *Active Flow Control* - Notes on Numerical Fluid Mechanics and Multidisciplinary Design, 95:27-41, 2007.

[CWG08] C. Cierpka, T. Weier and G. Gerbeth. Evolution of Vortex structures in an electromagnetically excited separated flow. *Exp. Fluids*, 45: 943-953, 2008.

[CEW10] T. C. Corke, C. L. Enloe and S. P. Wilkinson. Dielectric barrier discharge plasma actuators for flow control. *Ann. Rev. Fluid Mechanics*, 42:5050-29, 2010.

[De04] O. Debliquy. *Pseudo-spectral methods applied to hydronamics and magnetohydrodynamic turbulence*. Doc. Sc. Thesis, Université Libre de Bruxelles, Bruxelles, 2004.

[Duc12] Duchmann A. *Boundary-Layer stabilization with Dielectric Barrier Discharger Plasmas for Free-Flight Application*. Dissertation, TU Darmstadt, 2012.

[DRQKT10] A. Duchmann, A. Reeh, R. Quadros, J. Kriegseis, C. Tropea. Linear stability analysis of manipulated boundary-layer flows using plasma actuators. Seventh *IUTAM Symposium on Laminar-Turbulent Transition*, IUTAM Book Series; 18: 153-158, 2010.

[FAS05] Technische Universität Darmstadt Fachgebiet Numerische Berechnungsverfahren im Maschinenbau. FASTEST User Manual, 2005.

[FP02] J. H. Ferziger and M. Peric. *Computational methods for fluid dynamics*. Springer, 2002.

[FB05] J. Fransson and L. Brandt. Experimental study of the stabilization of Tollmien-Schlichting waves by finite amplitude streaks. *Physic of Fluids*, 17: 054110, 2005.

[FCG05] A. Frieman, A. Chirokov, and A. Gutsol. Non-thermal Atmospheric pressure discharges. *Journal of Physics D: Applied Physics*, 38(2):R1, 2005.

[Gol11] M. Goldhammer. The next decade in commercial aircraft aerodynamics – A Boeing perspective. *Aerodays*, Madrid, 2011.

[GH89] M. E. Goldstein and L. S. Hultren. Boundary-layer receptivity to long-wave free-stream disturbances. *Ann. Rev. Mech.*, 21: 137-66, 1989.

[GLS99] W. Gropp, E. Lusk and A. Skjellum. *Using MPI, 2nd edition: Portable parallel programming with the message-passing interface*. Massachssets Institute of Technology, 1999.

[Gru08] S. Grundmann. *Transition control using Dielectric Barrier Discharger actuators*. PhD Thesis, Technische Universität Darmstadt, 2008

[GSE10] S. Grundmann, E. L. Sayles and J. K. Eaton. Sensitivity of an asymmetric 3D diffuser to plasma-actuator induced inlet condition perturbations. *Exp. Fluids*, 50(1): 217-231, 2010.

[GT07] S. Grundmann and C: Tropea. Experimental transition delay using glow-discharge plasma actuators. *Exp. Fluids*, 42: 653-657, (2007).

[Hin07] M. Hinze. Control of weakly conductive fluids by near wall Lorentz forces. *GAMM-Mitt.* 30(1): 149-158, 2007.

[HZ08] X. Huang and X. Zhang. Streamwise and spanwise plasma actuators for flow-induced cavity noise control. *Physics of Fluids*, 20(3), 037101, 2008.

[JS08] B. Jayaraman and W. Shyy. Modeling of dielectric barrier discharge-induced fluid dynamics and heat transfer. *Progress in Aerospace Sciences*, 44:139-191, 2008.

[JL09] X. Jiang and C. H. Lai. *Numerical Techniques for Direct and Large-Eddy simulations*. Taylor and Francis, 2009.

[Kol41] A. Kolmogorov. *Dissipation of energy in locally isotropic turbulence.* Dokl. Akad. Nauk. SSSR, 31:99-101, 1941 (reprinted in Royal Society, London, 434:9-13).

[Kri11] J. Kriegseis. *Performance characterization and quantification of dielectric barrier dis-charge plasma actuators*. Dr.-Ing. Dissertation, TU Darmstadt, 2011.

[KGT11] J. Kriegseis, S. Grundmann and C. Tropea. Power comsumption, discharge capacitance and light emission as measures for thrust production of dielectric barrier discharge plasma actuators. *J. Appl. Phys.*, 110, 013305, 2011.

[KMGT11] J. Kriegseis, B. Möller, S. Grundmann and C. Tropea. Capacitance and power consumption quantification of dielectric barrier discharge (DBD) plasma actuators. *Journal of Electrostatics,* 69(4):302-312, 2011.

[LD06] Y. Lifshitz and D. Degani. Continuing nonlinear growth of Tollmien-Schlichting waves. *Physics of Fluids*, **19**, 088106 (2007).

[MKMJSGT11] I. Maden, J. Kriegseis, R. Maduta, S. Jakirlic, C. Schwarz, S. Grundmann, and C. Tropea. Derivation of a Plasma-Actuator Model Utilizing Quiescent-Air PIV Data. *Proceedings of the 20th Annual Conference of the CFD Society of Canada*. Alberta, Canada, 2012.

[MK10] R. Messing and M. Kloker. Investigation of suction for laminar flow control of three-dimensional boundary-layers. *J. Fluid Mech.*, 658:117-147, 2010.

[NCO08] R. C. Nelson, T. C. Corke and H. Othman. A smart wind turbine blade using distributed plasma actuators for improved performance. *American Institute of Aeronautics and Astronautics (AIAA)*, 46th Aerospace Sciences Meeting, 1312, Reno, 2008.

[Pat80] V. S. Patankar. *Numerical heat transfer and fluid flow*. Taylor and Francis. 1980.

[Pow06] M.J.D. Powell. The NEWUOA software for unconstrained optimization without derivatives. *in Large-Scale Optimization*, editors G. Di Pillo and M. Roma, Springer (New York), pp. 255–297, 2006.

[Pow08] M.J.D. Powell. Developments of NEWUOA for minimization without derivatives. *IMA J. Numer. Anal.*, Vol. 28, pp. 649–664, 2008.

[Pow09] M. J. D. Powel. The BOBYQA algorithm for bound restrict constrained optimization without derivatives (Report No. DAMTP 2009/NA06). Center for Mathematical Sciences, University of Cambridge, UK, 2009.

[Qua09] R. Quadros. *Numerical optimization of boundary-layer control using dielectric barrier discharge plasma actuators.* Dr. rer. nat. Dissertation, TU Darmstadt, 2009.

[QGTEU09] R. S. de Quadros, S. Grundmann, C. Tropea, J. Elsemüller, and S. Ulbrich. Numerical optimization of DBD plasma actuator operating parameters for active wave cancellation using sinusoidal modulation. *Proceedings of the Sixth International Symposium on Turbulence and Shear Flow Phenomena*, Seoul, Korea, 2009.

[RF95] U. Rist and H. Fasel. Direct numerical simulation of controlled transition in a flat plate boundary-layer. *J. Fluid Mech.* 298: 211-248, 1995.

[RG10] I. Romm and D. Greenblat. Subcritical pipe flow transition control using dielectric barrier discharge plasma actuators. *Conference in Active Flow Control*, Berlin, 2010.

[Rot2003] J. R. Roth. Aerodynamic flow acceleration using paraelectric and peristaltic electrohydrodynamic effects of a One Atmosphere Uniform Glow Discharge Plasma. *Phys. Plasmas* 10, 2117, 2003.

[SRK02] W. S. Saric, H. L. Reed and E. J. Kerschen. Boundary-layer receptivity to freestream disturbances. *Annu. Rev. Fluid Mech.* 34:291-319, 2002.

[Sch06] M. Schäfer. *Computational Engineering – Introduction to numerical methods*. Springer, 2006.

[SÖ10] P. Schlatter and R. Örlü. Assessment of direct numerical simulation data of turbulent boundary layers. *J. Fluid Mech.* 659:116-126, 2010.

[Sch82] Schlichting H. *Boundary-Layer Theory*. 7th ed., New York, USA, McGraw-Hill, 1979.

[SH01] P. Schmid and D. Henningson. Stability and transition in shear flows. *Applied Mathematical Sciences*, 142, Springer Verlag, Berlin, 2001. ISBN 0387989854, 2001.

[SLMOM10] M. Schneider, A. Likhanskii, S. Macheret, D. Opaits and D. Miles. State-of-the-art high-fidelity DBD plasma simulations. In *AFOSR DBD Plasma Actuator Workshop*, February 2010, Gainesville, 2010.

[SAA09] R. Sosa, J. D'Adamo and G. Artana. Circular cylinder drag

reduction by three-electrode plasma actuator. X Meeting on Recent Advances in the Physics of Fluids and their applications. *Journal of Physics*: Conference Series, 166, 012015, 2009.

[Squ33] H. B. Squire. On the stability of three dimensional distribution of viscous fluid between parallel walls. *Proc. Roy. Soc. London*, A 142: 621-628, 1933.

[Sto68] H. Stone. Iterative solution of implicit approximations of multidimensional partial differential equations. *SIAM Journal on Numerical Analysis*, 5(3):530-558, 1968.

[Tor09] E. F. Toro. *Riemann solvers and numerical methods for fluid dynamics.* Springer, 2009.

[Vie11] D. Vieira, A. Duchmann, M. Schäfer and S. Grundmann. Numerical simulation of boundary layer stabilization using plasma actuators. *Proceedings of the European Congress on Computational Methods in Applied Sciences and Engineering (ECCOMAS 2012)*, Vienna, 2012.

[WK02] P. Wassermann and M. Kloker. Mechanisms and passive control of crossflow-vortex-induced transition in a three-dimensional boundary layer. *J. Fluid Mech.*, 456:49-84, 2002.

[WAG11] T. Weier, T. Albrecht and G. Gerbeth. The electromagnetically forced flow over a backward-facing step. *Proceedings of the Seventh International Symposium on Turbulence and Shear Flow Phenomena (TSFP-7)*, Canada, 2007.

[WGMLL03] T. Weier, G. Gerbeth, G. Mustschke, O. Lielausis and G. Lammers. Control of Flow Separation Using Electromagnetic Forces. *Flow, Turbulence and Combustion*, 71: 5-17, 2003.

[WSG07] T. Weier, V. Shatrov and G. Gerbeth. Flow *Control and Propulsion in Poor Conductors. Magnetohydrodynamics: Historical Evolution and Trends, by S. Molokov, R. Moreau and H. K. Moffatt.* ISBN-13 978-1-4020-4832-6 (HB). Published by Springer, Dordrecht, The Netherlands, 295, 2007.

[Whi74] F. M. White. *Viscous Fluid Flow*. McGraw-Hill, New York, 1974.

[Wil09] B. Wilke. *Aerodynamische Strömungssteuerung mittels dielektrischen Barriereentladungs-Plasmaaktuatoren*. PhD Thesis, Technische Universität Darmstadt, DLR Göttingen, 2009.

Nomenclature

Important characters and symbols

Greek Symbols

α	. . . . .	Spatial wave number [m^{-1}].
β	. . . . .	Complex frequency [-].
β_r	. . . . .	Circular wave number [-].
β_i	. . . . .	Amplification factor of the disturbance (complex).
δ	. . . . .	Boundary layer thickness [m].
δ_{99}	. . . . .	Distance from the flat plate [m] for $u = 0.99U$,
δ_1	. . . . .	Displacement thickness [m].
δ_2	. . . . .	Momentum thickness [m].
ε	. . . . .	Average rate of energy dissipation per unit mass [J/Kg].
η	. . . . .	Blasius similarity variable [-].
ϕ	. . . . .	General transport variable [-].
θ	. . . . .	Phase angle between TS wave excitation and actuator [°].
κ	. . . . .	Kolmogorov length scale [m].
λ	. . . . .	Wave length of the disturbance, $\lambda = 2\pi/\alpha$.
μ	. . . . .	Dynamic viscosity [Pa.s].
ρ	. . . . .	Fluid density [Kg/m^3].
τ_{wall}	. . . . .	Wall shear stress [Pa]
φ	. . . . .	Amplitude of velocity fluctuations in a stream function [$m\ s^{-1}$].
ψ	. . . . .	Stream function of a velocity field [m^2s^{-1}].
Ω_k	. . . . .	Criteria for numerical stability of BOBYQA [-].

Letters

A	. . . . .	Amplitude of power oscillation of the plasma actuator [-].
A_{2D}	. . . . .	Two dimensional amplitude of disturbance excitation [-].
A_{3D}	. . . . .	Three-dimensional amplitude of disturbance excitation [-]. []
$A1$	. . . . .	TS wave amplitude for the non controlled case [-].
$A2$	. . . . .	TS wave amplitude for the actuated case [-].
A_{L1}	. . . . .	Amplitude of the disturbance [-].
A_{L0}	. . . . .	Initial amplitude of the disturbance at the neutral point [-].
a_i, b_i	. . . . .	Bounds for BOBYQA optimization.
c	. . . . .	Wave parameter for stability analysis [-].
c_f	. . . . .	Skin friction coefficient [-].
c_i	. . . . .	Wave amplification parameter [-].
c_r	. . . . .	Wave propagation speed [-].
H_{12}	. . . . .	Shape factor [-].
F	. . . . .	Objective function for BOBYQA optimization.
F_s	. . . . .	Periodic force applied in the plasma actuator [N/m^2].
FD	. . . . .	Tollmien-Schlichting body force excitation [Pa/m^2].
F_{PIV}	. . . . .	Force field evaluated from PIV measurements [Pa/m^2].
F_s	. . . . .	Periodic actuation body force [Pa/m^2].
f	. . . . .	Tollmien-Schlichting wave frequency [Hz].
f_i	. . . . .	External body force [N/m^2].
f_x	. . . . .	Plasma actuator body force distribuition in x direction [Pa/m^2].
f_y	. . . . .	Plasma actuator body force distribuition in y direction [Pa/m^2].
h	. . . . .	Increment size for the same direction [m].
hi		Domain height [m].
L	. . . . .	Characteristic length in any direction [m].
L_z	. . . . .	Characteristic length in spanwise direction [m].
N	. . . . .	Number of discretized points along a given direction [-].
n	. . . . .	General direction [-].
n_z	. . . . .	Wave periodicity in spanwise direction [m].
PA1	. . . . .	Actuator position at x = 0.325 m.
PA2	. . . . .	Actuator position at x = 0.375 m.

PA3	. . . . .	Actuator position at x = 0.425 m.
PA4	. . . . .	Actuator position at x = 0.475 m.
PA5	. . . . .	Actuator position at x = 0.525 m.
p	. . . . .	Pressure [Pa].
Q_k	. . . . .	Approximation for the objective function.
R	. . . . .	Rate of TS wave cancellation [-].
Re	. . . . .	Reynolds number [-].
Re_{turb}	. . . . .	Turbulent Reynolds number [-].
r_{max}	. . . . .	Radios of TS wave excitation [m].
t	. . . . .	Time [s].
t_η	. . . . .	Kolmogorov time scale [s].
U	. . . . .	Freestream velocity [m/s].
U_{conv}	. . . . .	Independent velocity for convective outlet [m/s].
$\boldsymbol{u}$	. . . . .	Velocity vector with the components u, v, and w [m/s].
u	. . . . .	Velocity component in the wall parallel direction [m/s].
u'	. . . . .	Velocity fluctuation in wall parallel direction [m/s].
u_η	. . . . .	Kolmogorov velocity scale [m/s].
u_{rms}	. . . . .	Squared mean of velocity fluctuations in x direction [m/s].
v	. . . . .	Velocity component in the wall normal direction [m/s].
v'	. . . . .	Velocity fluctuation in wall normal direction [m/s].
v_a	. . . . .	Function of quantities for 2D TS wave excitation [-].
v_r	. . . . .	Function of quantities for TS wave excitation [-].
v_s	. . . . .	Function of quantities for 3D TS wave excitation [-].
w	. . . . .	Velocity component in spanwise direction [m/s].
w'	. . . . .	Velocity fluctuation in spanwise direction [m/s].
x	. . . . .	Wall parallel coordinate [m].
x_{d0}	. . . . .	Initial reference for TS wave excitation [m].
x_{d1}	. . . . .	Final reference for TS wave excitation [m].
y	. . . . .	Wall normal coordinate [m].
y_d	. . . . .	Central point for TS wave excitation in y direction [m].
$\mathrm{Z_k}$	. . . . .	Matriz of variables for optimization [-].
z	. . . . .	Spanwise coordinate [m].

Abbreviations

BOBYQA	. . . . .	Bound Optimization BY Quadratic Adaptation.
DNS	. . . . .	Direct Numerical simulations.
LSA	. . . . .	Linear Stability analysis.
PA	. . . . .	Plasma actuator.
PIV	. . . . .	Particle Image Velocimetry.
TS	. . . . .	Tollmien-Schlichting.

List of Figures

List of Tables

Débora Gleice da Silva Del Rio Vieira

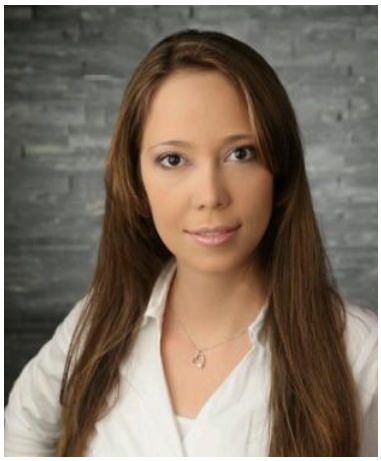

Address: Liebfrauenstraße, 91
64289 Darmstadt
Germany
Date of Birth: January, 29th, 1985.
Place of Birth: Ilha Solteira, SP, Brazil.
Phone: + 49 1515-0249-776
E-mail: deboragleicedelrio@gmail.com

EDUCATION

Dr.-Ing. in Mechanical Engineerig
Technische Universität Darmstadt, Hessen, Germany.
Graduate School of Computational Engineering
From December 2009 to April 2013
Thesis title: Numerical Simulations of Plasma Actuator Aerodynamic Effects.

Master of Science in Mechanical Engineering
UNESP – São Paulo State University, Sao Paulo State, Brazil.
From: August 2007 to November 2009
Theme: Numerical simulations using an Immersed Boundary Methodology and the Virtual Physical Model for biomechanical applications involving fluid structure interaction. The Navier-Stokes equations were resolved by Finite Volume Method. The computational code was developed in FORTRAN 95.

Lester Pearson International
Dalhousie University, Nova Scotia, Canada.
From March 2009 to September 2009.
Research activities: Numerical simulations of the flow over turbine blades using Finite Element and Immersed Boundary Methods with adaptive grids.

Mechanical Engineering Degree
UNESP – São Paulo State University, Sao Paulo State, Brazil.
From March, 2003 to July, 2007

High School
Colégio Euclides da Cunha – Sao Paulo State, Brazil.
Completed in December 2002